Department of Neuroscience and Biomedical Engineering

The role of basal phosphodiesterase activity in the regulation of mouse rod photoresponses

Teemu Turunen

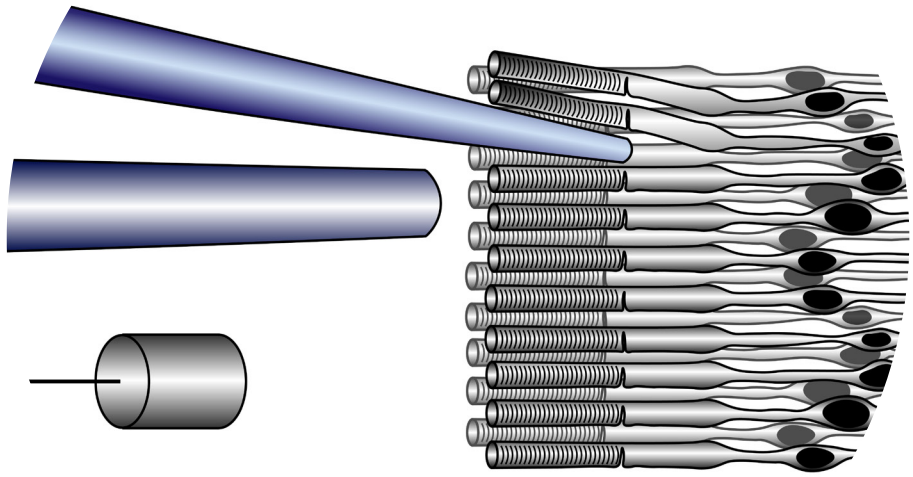

Aalto University

DOCTORAL DISSERTATIONS

Aalto University publication series
DOCTORAL DISSERTATIONS 58/2020

The role of basal phosphodiesterase activity in the regulation of mouse rod photoresponses

Teemu Turunen

A doctoral dissertation completed for the degree of Doctor of Science (Technology) to be defended, with the permission of the Aalto University School of Science, at an examination held at the auditorium F239 of the school on the 18th of September 2020 at 9am. The examination is publicly available via remote connection, https://aalto.zoom.us/j/68208502401

Aalto University
School of Science
Department of Neuroscience and Biomedical Engineering

Supervising professors
Professor Ari Koskelainen
Aalto University, Finland

Thesis advisors
Professor Ari Koskelainen
Aalto University, Finland

Preliminary examiners
Professor emeritus Kristian Donner
University of Helsinki, Finland

Professor Alapakkam Sampath
University of California, Los Angeles, USA

Opponents
Professor Marie Burns
University of California, Davis, USA

Aalto University publication series
DOCTORAL DISSERTATIONS 58/2020

ISBN 978-952-60-3832-2 (printed)
ISBN 978-952-60-3833-9 (pdf)
ISSN 1799-4934 (printed)
ISSN 1799-4942 (pdf)
http://urn.fi/URN:ISBN:978-952-60-3833-9

Unigrafia Oy
Helsinki 2020

Finland

Printed matter
4041-0619

Aalto University

Abstract

Aalto University, P.O. Box 11000, FI-00076 Aalto www.aalto.fi

Author
Teemu Turunen

Name of the doctoral dissertation
The role of basal phosphodiesterase activity in the regulation of mouse rod photoresponses

Publisher School of Science

Unit Department of Neuroscience and Biomedical Engineering

Series Aalto University publication series DOCTORAL DISSERTATIONS 58/2020

Field of research Engineering Physics, Biomedical Engineering

Manuscript submitted 17 April 2020 **Date of the defence** 18 September 2020

Permission for public defence granted (date) 16 June 2020 **Language** English

☐ **Monograph** ☒ **Article dissertation** ☐ **Essay dissertation**

Abstract

Phosphodiesterase-6 (PDE6) is an enzyme catalyzing the hydrolysis of cyclic guanosine monophosphate (cGMP), a second messenger molecule participating in a vast number of biological processes. Vertebrate photoreceptor cells react to light through a phototransduction cascade, where the activation of PDE6 leads to a decrease in the intracellular cGMP concentration and closure of cation channels in the photoreceptor outer segment plasma membrane. The channel closure causes a decrease in the intracellular calcium concentration, providing photoreceptor cells with negative feedback for light-induced sensitivity regulation, i.e., light adaptation, via calcium sensor proteins.

In rod photoreceptor cells, the calcium sensors guanylate cyclase-activating proteins (GCAPs) and recoverin are the dominant mediators of light adaptation. In publication I of this thesis, a novel source of calcium-mediated light adaptation was discovered in rods by recording transretinal *ex vivo* electroretinography (TERG) across dark-adapted isolated mouse retinas. The focus of the rest of the thesis work was to characterize this novel calcium-dependent sensitivity regulation mechanism with the leading hypothesis that the regulation might originate from the calcium-mediated control of the basal PDE6 activity (β_{dark}). To test the hypothesis, novel paradigms and methods were developed for the determination of β_{dark}.

In publication II, a device for the simultaneous recording of TERG and local ERG across the photoreceptor outer segment layer (LERG-OS) was developed to obtain quantitative information on rod phototransduction. The work demonstrated that the TERG recordings, although affected by signal components from photoreceptor inner segments, correspond well with those registered by LERG-OS.

These *ex vivo* ERG methods, TERG and LERG-OS, enabled the quantitative investigation of PDE6 and its inhibition in the living retina. Traditionally, PDE6 inhibitors have been examined using biochemically activated purified PDE6 molecules. In publication III of this thesis, a new method was developed to quantify the inhibition constants for PDE6 inhibitors acting on the naturally occurring light-activated and spontaneously activated forms of PDE6. According to the results, the inhibition constants of different PDE inhibitors can vary substantially against these two PDE6 forms. In publication IV, the inhibition constants were utilized for cGMP clamp experiments, a novel paradigm which allowed the determination of β_{dark} in wild type mouse rods for the first time. In publication V, the methods, together with mathematical modeling of photoresponses, were used to investigate the calcium-mediated light adaptation mechanisms in knockout mice lacking the dominant GCAPs- and recoverin-mediated adaptation pathways. It was found that β_{dark} increases by ~ 20 – 30% when rod extracellular calcium concentration is reduced below its normal physiological range. This finding introduces a novel mechanism contributing to rod light adaptation and to the functional regulation of PDE enzymes.

Keywords calcium, electroretinography, light adaptation, phosphodiesterase, photoreceptor

ISBN (printed) 978-952-60-3832-2 **ISBN (pdf)** 978-952-60-3833-9

ISSN (printed) 1799-4934 **ISSN (pdf)** 1799-4942

Location of publisher Helsinki **Location of printing** Helsinki **Year** 2020

Pages 204 **urn** http://urn.fi/URN:ISBN:978-952-60-3833-9

Tekijä
Teemu Turunen

Väitöskirjan nimi
Fosfodiesteraasin tausta-aktiivisuuden vaikutus hiiren sauvasolujen valovasteiden säädössä

Julkaisija Perustieteiden korkeakoulu

Yksikkö Neurotieteen ja lääketieteellisen tekniikan laitos

Sarja Aalto University publication series DOCTORAL DISSERTATIONS 58/2020

Tutkimusala Teknillinen fysiikka, lääketieteellinen tekniikka

Käsikirjoituksen pvm 17.04.2020 **Väitöspäivä** 18.09.2020

Väittelyluvan myöntämispäivä 16.06.2020 **Kieli** Englanti

☐ **Monografia** ☒ **Artikkeliväitöskirja** ☐ **Esseeväitöskirja**

Tiivistelmä

Fosfodiesteraasi-6 (PDE6) -entsyymi hydrolysoi syklistä guanosiinimonofosfaattia (cGMP), joka toimii toisiolähettinä monissa solujen viestintäketjuissa. Selkärankaisten näköaistinsolut reagoivat valoon fototransduktiokaskadin välityksellä, missä PDE6:n aktivaatio johtaa solunsisäisen cGMP:n pitoisuuden laskuun ja näköaistinsolujen ulkojäsenten solukalvon kationikanavien sulkeutumiseen. Tämän seurauksena solun sisäinen kalsiumionikonsentraatio laskee, mikä toimii negatiivisena takaisinkytkentänä näköaistinsolujen herkkyyden säädössä, eli toisin sanoen valoadaptaatiossa, kalsiumia sitovien proteiinien kautta.

Kalsiumia sitovat guanylaattisyklaasia aktivoivat proteiinit (GCAPs) ja rekoveriiniproteiinit vastaavat pääosin näköaistinsolujen valoadaptaatiosta. Väitöskirjan ensimmäisessä osatyössä sauvatyypin näköaistinsoluista löydettiin uusi kalsiumvälitteinen valoadaptaatiomekanismi hyödyntäen hiirten eristetyistä verkkokalvoista rekisteröitävää transretinaalista *ex vivo* elektroretinografiaa (TERG). Väitöskirjatyön loppuosio keskittyi löydetyn mekanismin karakterisointiin. Päähypoteesina oli, että herkkyyden säätö voisi olla seurausta PDE6-entsyymin tausta-aktiivisuuden (β_{dark}) kalsiumvälitteisestä muutoksesta. Hypoteesin testaukseen kehitettiin lähestymistapoja ja menetelmiä, joiden avulla β_{dark} pystyttiin määrittämään.

Väitöskirjan toisessa osatyössä kehitettiin laitteisto, jolla pystyttiin rekisteröimään ERG-signaalia samanaikaisesti koko verkkokalvon yli sekä paikallisesti näköaistinsolujen ulkojäsenkerroksen yli (LERG-OS) mahdollistaen fototransduktion kvantitatiivisen tutkimuksen. Työssä osoitettiin, että vaikka näköaistinsolujen sisäjäsenissä syntyvät signaalikomponentit kytkeytyvät TERG-signaaliin, tekniikalla rekisteröidyt valovasteet vastaavat hyvin LERG-OS-tekniikalla kerättyjä valovasteita.

Nämä *ex vivo* ERG -menetelmät mahdollistivat PDE6:n ja sen inhibition kvantitatiivisen tutkimuksen elävissä verkkokalvoissa. Yleensä PDE6-inhibiittoreita tutkitaan käyttäen biokemiallisesti aktivoituja puhdistettuja PDE6-molekyylejä. Väitöskirjan kolmannessa osatyössä kehitettiin menetelmä, jolla PDE6-inhibiittorien inhibitiovakio voitiin määrittää luonnollisesti esiintyviä, valo- tai tausta-aktivoituneita olomuotoja kohti. Työssä huomattiin, että eri inhibiittorien inhibitiovakiot voivat vaihdella suuresti näiden olomuotojen välillä. Väitöskirjan neljännessä osatyössä inhibitiovakioita hyödynnettiin uudessa cGMP clamp -menetelmässä, joka mahdollisti ensimmäistä kertaa PDE6 tausta-aktiivisuuden määrityksen villityypin hiirten sauvasoluista. Väitöskirjan viidennessä osatyössä kehitettyjä menetelmiä ja matemaattista näköaistinsolujen valovasteiden mallinnusta käytettiin kalsiumvälitteisen valoadaptaation tutkimiseen poistogeenisellä hiirimallilla, jossa GCAPs- ja rekoveriinivälitteinen valoadaptaatio oli estetty. Työssä näytettiin, että β_{dark} kasvaa ~ 20 – 30%, kun sauvasolujen soluvälitilan kalsiumionitaso lasketaan alle sen normaalin fysiologisen alueen. Löytö lisää uuden mekanismin sauvasolujen valoadaptaation ja PDE-entsyymien toiminnallisen säätelyn tuntemukseen.

Avainsanat elektroretinografia, fosfodiesteraasi, kalsium, näköaistinsolu, valoadaptaatio

ISBN (painettu) 978-952-60-3832-2 **ISBN (pdf)** 978-952-60-3833-9

ISSN (painettu) 1799-4934 **ISSN (pdf)** 1799-4942

Julkaisupaikka Helsinki **Painopaikka** Helsinki **Vuosi** 2020

Sivumäärä 204 **urn** http://urn.fi/URN:ISBN:978-952-60-3833-9

Acknowledgments

Now that my doctoral thesis is finished, I want to thank those accompanying me along the journey. I express my sincere gratitude towards my supervisor Prof. Ari Koskelainen who introduced me to the field of electrophysiology through the inspiring research projects and the kind-hearted attitude towards all of his students. Even if being buried with other tasks, he was always available to help with my research, and further, he gave me the possibility and the needed time to derive my own solutions. I want to thank Prof. emer. Kristian Donner, a mentor and one of my idols in science. His in-depth knowledge in the field of physiology and biophysics never stops impressing me. Also, thanks to Prof. emer. Kristian Donner and to Prof. Alapakkam Sampath for helping me to improve this manuscript as my thesis pre-examiners. I am grateful for Prof. Marie Burns, who kindly took the time to act as the opponent in the defense. I want to express my gratitude towards the Department of Neuroscience and Biomedical Engineering and Aalto University School of Science together with the funders of this work, International Doctoral Programme in Biomedical Engineering and Medical Physics, Finnish Cultural Foundation, Oscar Öflunds Stiftelse, and Silmä- ja kudospankkisäätiö for making the thesis possible.

I am extremely grateful to Dr. Marja Pitkänen to whom I am missing the words to thank enough. We have shared a decade as colleagues and even longer as friends. The struggles with my thesis have always been bearable since we have faced them together. Marja's endless support and companionship are something I cherish above this thesis.

I was privileged to join the group with young talented scientists Asst. Prof. Frans Vinberg, Dr. Hanna Heikkinen, Adj. Prof. Soile Nymark, who taught me to conduct electrophysiological experiments and shared their expertise on retina and photoreceptors. The possibility to closely follow the evolution of their career has been a key motivator for me throughout the thesis work.

I am grateful for my close colleagues and friends in the department. Most special thanks to Mooud Amirkavei, whose full-hearted attitude towards new challenges has been truly inspiring to follow. Many thanks to Ossi Kaikkonen, whom I consider as one of the most talented hands-on engineer I know. Thanks to Jani Tirronen for sharing his expertise and joining us on a project transforming a scientific discovery into a real-life application. I would also like to thank the former members of the Cellular Biophysics group, Satu Pallasaho, Anni Antikainen, Rauli Albert, and Piia Saarinen. It has been a pleasure to work with them. I am grateful for Assoc. Prof. Petri Ala-Laurila and his group for their company and numerous discussions related to vision among the other things. Thanks especially for my big brother Tuomas Turunen who I accidentally tricked to start a Ph.D. project in Petri's lab. I am grateful for the friendly

atmosphere and the company of the many fellow students I have learned to know at the department.

Meetings, conferences, and collaborations have introduced me to the vast community of vision researchers who deserve my thankfulness. I especially want to show my gratitude towards late Dr. Victor Govardovskii, Dr. Misha Firsov, and Dr. Luba Astakhova for welcoming me to their laboratory and sharing their skills on suction electrode recording. My sincere thanks to Magnus Lindström for organizing the Annual Visionarium meetings in Tvärminne. The meeting is a model example for sharing novel findings and networking with other scientists in the most relaxing and welcoming atmosphere possible.

My warmest thanks to my friends for providing the needed balance for the solitary thesis work and making sure that I do not forget myself to the dark lab for too long. My deepest gratitude to my family, who have always provided me everything I needed and more. Lastly, thanks to Katri for all your love, support, and patience. I am lucky our paths crossed.

Espoo, August 17th, 2020

"You certainly usually find something, if you look, but it is not always quite the something you were after."

— J.R.R. Tolkien, The Hobbit, or There and Back Again

Contents

List of Abbreviations and Symbols

α	The rate of cGMP synthesis
α_{dark}	The rate of cGMP synthesis in darkness
A	Amplification constant
ADP	Adenosine diphosphate
AMP	Adenosine monophosphate
APB	DL-2-amino-4-phosphonobutyric acid
ATP	Adenosine triphosphate
ATPase	A class of enzymes that catalyze the decomposition of ATP into ADP
β	Rate of cGMP hydrolysis
β_{dark}	Basal phosphodiesterase-6 activity
β_{light}	Light-induced phosphodiesterase-6 activity.
β_{sub}	The average hydrolytic rate for one activated phosphodiesterase-6 subunit
B_{cGMP}	Cyclic guanosine monophosphate buffer capacity in rod outer segments
BK	A class of Ca^{2+}-gated potassium channels
c_{GE}	Coupling coefficient for phosphodiesterase-6 activation by transducin
C57BL/6Jrcc	A strain of black laboratory mice
cAMP	Cyclic adenosine monophosphate
cGMP	Cyclic guanosine monophosphate
$[cGMP]$	Cyclic guanosine monophosphate concentration
$[cGMP]_{dark}$	Cyclic guanosine monophosphate concentration in darkness
CNG	Cyclic nucleotide-gated
CO_2	Carbon dioxide
E4021	A phosphodiesterase inhibitor

EDTA	Ethylenediaminetetraacetic acid
EGTA	Ethylene glycol tetraacetic acid
ERG	Electroretinography
γ-subunit	γ-subunit of phosphodiesterase-6
G^*_{dark}	The average rate of spontaneous transducin activations·rod^{-1}s^{-1}
GAFa, GAFb	The regulatory domains of phosphodiesterase-6
GAP	GTPase accelerating protein complex
GARP2	Glutamic acid-rich protein-2
Gβ5	Member of GTPase accelerating protein complex
GC	Guanylate cyclase
GCAP	Guanylate cyclase-activating protein
GDP	Guanosine diphosphate
GMP	Guanosine monophosphate
GRK	G-protein-coupled receptor kinase
Gt_α	α-subunit of transducin
GTP	Guanosine triphosphate
HCN1	Hyperpolarization-activated cation channel 1
HEPES	4-(2-hydroxyethyl)-1-piperazineethanesulfonic acid
IBMX	3-isobutyl-1-methylxanthine
J_{cG}	Current through cyclic nucleotide-gated channels
$J_{cG,max}$	Maximal current through cyclic nucleotide-gated channels
J_{dark}	Circulating current through the cyclic nucleotide-gated channels in darkness.
k_{cat}	The maximal catalytic rate of the phosphodiesterase-6 dimer
k_f	The rate of phosphodiesterase-6 and cyclic guanosine monophosphate encounters
k_{li}	Diffusion-limited phosphodiesterase-6 hydrolytic activity
k_{PDE}	The rate constant for phosphodiesterase-6 deactivation
k_r	The rate of the dissociation of phosphodiesterase-6 cyclic guanosine monophosphate complex

k_R	The rate constant for rhodopsin deactivation
K_{cGMP}	The cyclic guanosine monophosphate concentration leading to a half-maximal cyclic nucleotide-gated channel opening.
K_D	Dissosiation constant
K_I	Inhibition constant
$K_{I,dark}$	Inhibition constant against spontaneously activated phosphodiesterase-6
$K_{I,light}$	Inhibition constant against light-activated phosphodiesterase-6
$K_{I,trypsin}$	Inhibition constant against trypsin-activated phosphodiesterase-6
K_M	Michaelis constant
K_x	Class of voltage-gated potassium channels
LERG	Local electroretinography
LERG-OS	Local electroretinography recorded across the photoreceptor outer segment layer
LERG-PR	Local electroretinography recorded across the photoreceptor layer
mRNA	Messenger ribonucleic acid
n_{cGMP}	The Hill coefficient for cyclic nucleotide-gated channel activation
N_A	Avogadro's number
$N_{cGMP/comp.}$	Number of cGMP molecules in one rod disk compartment
NCKX	$Na^+/Ca^{2+}K^+$ exchanger
NCKX1	$Na^+/Ca^{2+}K^+$ exchanger 1 found in the rod outer segments
PDE	Phosphodiesterase
PDE5	Phosphodiesterase-5
PDE6	Phosphodiesterase-6
$PDE6^*_{dark}$	The average rate of spontaneous phosphodiesterase-6 activations·$rod^{-1}s^{-1}$
PI, PII, PIII	The components of the retinal light response as recorded by electroretinography
PID	Proportional-integral-derivative
PMCA	Ca^{2+} transport protein in the plasma membrane
$r(t)$	The time course of the electroretinography signal (the retinal light response)
r_{max}	Maximal amplitude of the electroretinography signal

$r_{max,control}$	Maximal amplitude of the electroretinography signal in control conditions
$r_{max,I}$	Maximal amplitude of the electroretinography signal in the presence of a PDE6 inhibitor
R*	The number of activated rhodopsin molecules
R9AP	Member of GTPase accelerating protein complex
RGS	Regulator of G-protein signaling
RGS9	Member of GTPase accelerating protein complex
ROS	Rod outer segment
SOC	Store-operated Ca^{2+} channel
τ_{PDE}	The average lifetime of activated phosphodiesterase-6
τ_R	The average lifetime of activated rhodopsin
t_d	The combined time delay from recording equipment and phototransduction
t_{RGE}	Time delay from rhodopsin activation to the activation of phosphodiesterase-6
TERG	Transretinal electroretinography
TRMP	Family of transient receptor potential ion channels
Φ	Number of rhodopsin isomerizations caused by a pulse of light
Φ_{dark}	The average rate of spontaneous rhodopsin isomerizations·$rod^{-1}s^{-1}$
Φ_{BG}	The rate of rhodopsin activations by a background light
ν_{RG}	The rate at which rhodopsin activates transducin
ν_{RE}	The rate at which rhodopsin activates phosphodiesterase-6
V_{cyto}	Rod outer segment cytoplasmic volume

List of Publications

This doctoral dissertation consists of a summary and of the following publications, which are referred to in the text by their Roman numerals.

I. Vinberg F, Turunen TT, Heikkinen H, Pitkänen M and Koskelainen A (2015). A novel Ca^{2+} feedback mechanism extends the operating range of mammalian rods to brighter light. *Journal of General Physiology*, vol. 146, no. 4, p. 307-21.

II. Turunen TT & Koskelainen A (2017). Transretinal ERG in Studying Mouse Rod Phototransduction: Comparison With Local ERG Across the Rod Outer Segments. *Investigative Ophthalmology & Visual Science*, vol. 58**,** p. 6133–6145.

III. Turunen TT & Koskelainen A (2018). Electrophysiological determination of phosphodiesterase-6 inhibitor inhibition constants in intact mouse retina*. Toxicology and Applied Pharmacology*, vol. 345 p. 57–65.

IV. Turunen TT & Koskelainen A (2019). Determination of basal phosphodiesterase activity in mouse rod photoreceptors with cGMP clamp. *Scientic reports*, vol. 9(1):1183.

V. Turunen TT & Koskelainen A. Calcium modulates basal phosphodiesterase activity in mouse rod photoreceptors. 42 pages, submitted, 3/2020.

Author's Contribution

Publication I: A novel Ca^{2+} feedback mechanism extends the operating range of mammalian rods to brighter light.

The author performed the experiments together with the first author. The author participated in data analysis and preparing the manuscript.

Publication II: Transretinal ERG in Studying Mouse Rod Phototransduction: Comparison With Local ERG Across the Rod Outer Segments.

The author designed and developed the device for the experiments, planned and conducted the experiments, and analyzed the data. The author wrote the manuscript and finalized it together with the co-author.

Publication III: Electrophysiological determination of phosphodiesterase-6 inhibitor inhibition constants in intact mouse retina.

The author formulated the research question and the theory behind the methodology. The author designed and conducted the experiments, and analyzed the data. The author wrote the manuscript and finalized it together with the co-author.

Publication IV: Determination of basal phosphodiesterase activity in mouse rod photoreceptors with cGMP clamp.

The author and the co-author developed the ideas. The author designed and conducted the experiments, performed the data analysis, and wrote the manuscript. The manuscript was finalized together with the co-author.

Publication V: Calcium modulates basal phosphodiesterase activity in mouse rod photoreceptors.

The author and the co-author developed the ideas. The author designed and conducted the experiments, performed the data analysis, and wrote the first draft of the manuscript. The manuscript was edited and finalized together with the co-author.

1. Introduction

The retina converts the information in incoming light into electrical signals in neurons, processes it, and transmits a pattern of pre-processed signals to the brain, where the visual percept is formed. The first steps in the formation of the neural image take place at the distal side of the retina, in photoreceptor cells. These cells can be divided into rods and cones. Rods are responsible for dim-light vision, and cones are used for fast signaling in daylight and for color discrimination. Together these photoreceptor cells enable vision in different illuminations covering a 10^{12}-fold range, which includes dim starlight and goes beyond the light levels experienced during bright winter days. (Stockman & Sharpe, 2006)

The rod system can function over 10^{7}-fold range of illuminations, while the dynamic range of a single mammalian rod covers around three to four orders of magnitude (Stockman & Sharpe, 2006; Grimes *et al.*, 2018). Rods extend their dynamic range by regulating their sensitivity to light via calcium sensor proteins. Light absorption by rhodopsin in rod outer segments activates a powerful biochemical amplification cascade, phototransduction, where the activation of the phosphodiesterase-6 (PDE6) enzyme leads to a vast increase in cGMP hydrolysis, decrease in the intracellular cGMP concertation and closure of cyclic nucleotide-gated (CNG) cation channels in the plasma membrane. Upon channel closure, sodium and calcium influx through the channels ceases, while the extrusion of calcium by sodium/calcium-potassium exchangers continues. The resulting decline in the intracellular calcium concentration provides calcium sensor proteins with negative feedback to mediate the rod sensitivity regulation and adaptation to changing illuminations. (for reviews, see, e.g., Pugh & Lamb, 2000; Fu & Yau, 2007)

Rods have three acknowledged calcium-mediated light adaptation mechanisms. Guanylate cyclase-activating proteins (GCAPs) control the activity of cGMP-synthesizing guanylate cyclase (Mendez *et al.*, 2001). Recoverin controls the lifetime of activated rhodopsin (Chen *et al.*, 1995, 2015; Zang & Neuhauss, 2018), and calmodulin modulates the affinity of cGMP to CNG channels (Hsu & Molday, 1993). A great deal of the studies on photoreceptor light adaptation mechanisms has been conducted with amphibian photoreceptors, where the effects of specific feedback mechanisms are well described (Koch, 1994; Pugh *et al.*, 1999; Nikonov *et al.*, 2000). In mammalian rods, GCAPs are considered to have a dominant role in light adaptation, but even without GCAPs, some adaptation persists (Mendez *et al.*, 2001; Burns *et al.*, 2002). The role of calmodulin, on the other hand, is considered only minor (Chen *et al.*, 2010*c*), and the role of recoverin is still controversial.

The first part of this thesis showed that the fast, subsecond-timescale, light adaptation is entirely mediated by calcium ions in mouse rods. Additionally, the study quantified the magnitude of GCAPs and recoverin-mediated sensitivity regulation and found that recoverin plays a

crucial role in mouse rod light adaptation. However, some calcium-mediated regulation remained even in the absence of GCAPs and recoverin. The rest of the thesis delved into characterizing the novel modulation with the leading hypothesis that it arises from the calcium-mediated control of basal PDE6 activity (β_{dark}), one of the fundamental factors setting the photoreceptor sensitivity.

The study was conducted by recording extracellular light-induced field potential changes with transretinal *ex vivo* electroretinography (TERG) from dark-adapted isolated mouse retinas. In TERG, the photoreceptor component of the ERG signal can be extracted by pharmacologically blocking the synaptic transmission from photoreceptors to second-order neurons. TERG can be used to investigate phototransduction, but the signal components arising from the operation of voltage-gated ion channels in the rod inner segments are known to modify the signal (Vinberg *et al.*, 2009). Therefore, a technique was developed for simultaneous recording of TERG and local ERG across the photoreceptor outer segment layer (LERG-OS). This method enables quantitative investigation of the phototransduction mechanisms in the intact living retina together with pharmacological manipulation of photoreceptor cells. The study demonstrated that TERG signals correspond well to those registered by local ERG and that the combination of TERG and LERG-OS techniques offers a versatile tool in the study of both phototransduction and retinal function.

PDE6 is almost solely expressed in photoreceptors, and the *ex vivo* ERG methods permitted quantitative study of PDE6 activity and its inhibition. PDE6 inhibitors are traditionally examined using purified PDE6 molecules that are biochemically activated. These treatments change the structure of the PDE6 molecule and might affect its properties. In this thesis, experimental paradigms were developed to quantify the inhibition constants for PDE6 inhibitors acting on the light-activated and spontaneously active forms of PDE6 in their natural environment, the living retina. The work demonstrated that the inhibition constants against light-activated, spontaneously activated, and biochemically activated forms of PDE6 can differ substantially. This finding questions the application of solely biochemically activated PDE6, e.g., in the investigation of novel PDE inhibitor drugs with possible adverse effects.

The determined inhibition constant values and the developed LERG-OS technique were employed in a novel cGMP clamp paradigm to determine the value for β_{dark}. In the cGMP clamp procedure, the PDE6 inhibitor-induced decrease in the basal PDE6 activity is counterbalanced by increasing the PDE6 activity with light. Thereby the LERG-OS signal, and thus, the intracellular cGMP concentration, remain clamped to their dark values. This method allowed the determination of β_{dark} in wild type mouse rods for the first time. In addition, it enabled the demonstration that the absence of GCAPs or recoverin in genetically manipulated mouse rods does not affect β_{dark}. To examine the modulation of β_{dark}, the rod extracellular calcium concentration was lowered to $\sim$ 20 nM, mimicking the effect of intense background light. The experiments revealed that the basal PDE6 activity can increase by $\sim$ 20 – 30% in mice lacking GCAPs and recoverin proteins when the calcium level decreases. This new mechanism supplements our current understanding of rod light adaptation and the functional regulation of PDE enzymes.

2. Mammalian rod photoreceptors

2.1 Structure

Vertebrate vision begins in the rod and cone photoreceptor cells. Rods are extremely sensitive to light, and they are responsible for our vision at low light levels. Cones are 30 – 1000 times less sensitive to light than rods, and they are responsible for daylight vision (Nikonov *et al.*, 2006; Naarendorp *et al.*, 2010; Koenig & Hofer, 2011; Korenbrot, 2012; Vinberg *et al.*, 2014; Ingram *et al.*, 2016). Further, the comparison of the bioelectrical signals from different cone types enables color vision in many vertebrate species (Rodieck, 1999). Both photoreceptor types reside in a layer in the distal part of the retina, and in most mammals, the retina is dominated by rods (Peichl, 2005; Kim *et al.*, 2016). In the human retina, cones are densely packed in the macular region of the central retina where rods are absent, and rods dominate in the retinal periphery (Osterberg, 1935; Curcio *et al.*, 1990). In mice, the rod photoreceptors dominate the whole retina, while cones are rather evenly distributed across the retina, constituting 1/30 of the total population of 5 to 7 million photoreceptors (Carter-Dawson & Lavail, 1979; Jeon *et al.*, 1998; Donatien & Jeffery, 2002; Ortin-Martinez *et al.*, 2014). This thesis concentrates mainly on rods.

A photoreceptor cell consists of three parts: an outer segment, an inner segment, and a synaptic terminal. The outer segment is pointing towards the back of the eye, and it contains the light-capturing pigment molecules and the machinery for converting photon information into a bioelectrical signal. In rod photoreceptors, the photon-capturing molecules are located in disk membranes that occupy 70% from the volume of the murine rod outer segment and around 50% of amphibian outer segment volume. The rest is filled with cytoplasm. (Peet, 2004; Nickell *et al.*, 2007) An average mouse rod outer segment has ca. 1.4 µm diameter and 24 µm length (Liang *et al.*, 2004; Rakshit *et al.*, 2017). On average, it contains 810 discs dividing the outer segment space into somewhat isolated compartments (Carter-Dawson & Lavail, 1979; Liang *et al.*, 2004). Correspondingly, a mouse cone outer segment diameter is 1.2 µm and length 13 µm, but instead of separate discs, there are invaginations of the plasma membrane (Carter-Dawson & Lavail, 1979; Mustafi *et al.*, 2009). In both photoreceptor types, the outer segment is connected to the inner segment by a narrow cilium. The inner segment holds the cell organelles and the nucleus. A thin axon connects the inner segment to the synaptic terminal, which transmits the signals generated by the photoreceptors to horizontal and bipolar cells by modulating glutamate release into the synaptic cleft (see, e.g., Thoreson, 2007). The length of the whole rod photoreceptor cell in the murine retina is close to 100 µm (Hagins *et al.*, 1970). Rods are densely packed to a hexagonal arrangement to maximize the probability of photon capture. The average rod density in mouse retinas is about 437,000 cells/mm^2 (Jeon *et al.*, 1998). Fig. 1 illustrates the structure of rod and cone photoreceptors.

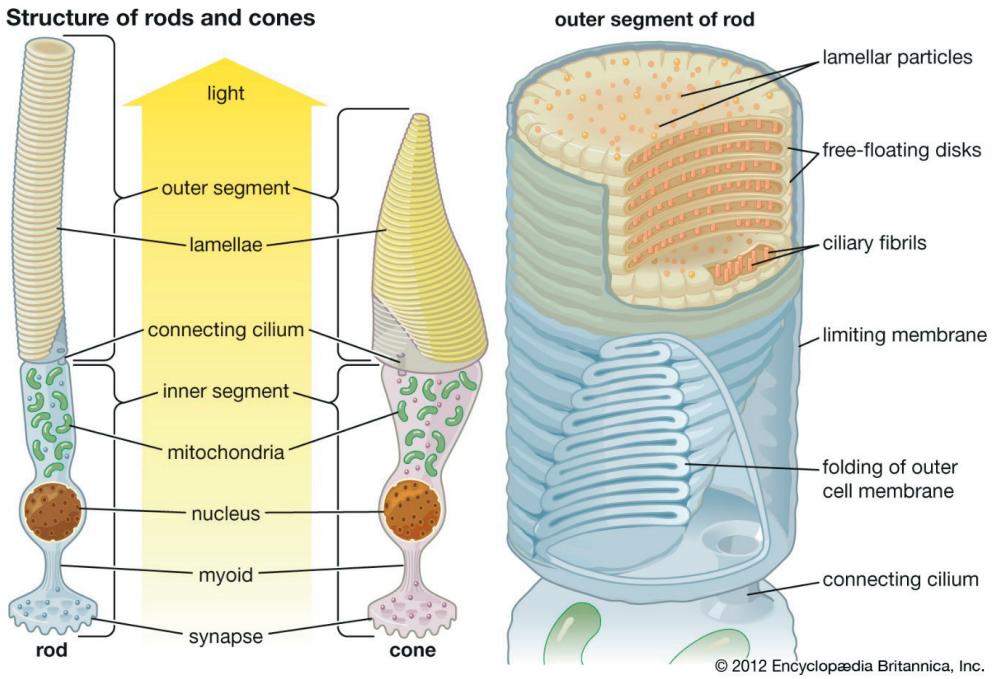

Figure 1. Structure of rod and cone photoreceptor cells. By courtesy of Encyclopædia Britannica, Inc., copyright 2012; used with permission.

2.2 Ionic mechanisms in rods

Fig. 2 illustrates the main ionic mechanisms controlling the membrane currents in rod photoreceptors. In darkness, photoreceptors maintain ionic gradients between the intracellular and extracellular space and a cation current flowing from the photoreceptor inner segment to the outer segment, which is controlled by ion pumps, exchangers, and channels unevenly distributed along the length of the photoreceptor. This cation current in darkness is often referred to as the circulating dark current. Maintaining the circulating current is highly energy consuming, taking around 60% of the total energy consumption of the vertebrate photoreceptor (Okawa *et al.*, 2008). The resting potential of a rod photoreceptor is near -35 mV in darkness, which is relatively depolarized compared with that of a typical neuron. Upon light exposure, rods can hyperpolarize below -60 mV. (Baylor & Nunn, 1986; Cangiano *et al.*, 2012)

The cyclic nucleotide-gated (CNG) channels are the only functional ion channels in the photoreceptor outer segment, and they serve as the sink for the circulating current. The channels are tetrameric complexes penetrating the photoreceptor cell membrane, consisting of three CNGA1 subunits and one CNGB1 subunit in rods, and three CNGA3 subunits and one CNGB3-subunit in cones (Kaupp & Seifert, 2002). CNG channels are nonselective cation channels, and the inward current flowing through the channels in photoreceptors is mostly carried by sodium and calcium ions. Ca^{2+} carries 10 to 20% of the channel current in rods and around 30% in cones (Nakatani & Yau, 1988*a*; Ohyama *et al.*, 2000). In photoreceptors, the cyclic nucleotide ligand that modulates the open probability of the channel is cGMP, and therefore they

are commonly referred to as cGMP-gated channels. The light-induced reduction in the cGMP concentration (see Section 3.3 for details) causes the closure of these channels and hyperpolarization of the cell membrane, which transmits the information from the captured light to the photoreceptor synaptic terminal. The intracellular cGMP concentration keeping half of the channels open, K_{cGMP}, has been determined to be close to 80 µM in human rods (Dhallan *et al.*, 1992), 165 µM in bovine rods (Quandt *et al.*, 1991), around 40 µM in striped bass and brown anole lizard rods (Savchenko *et al.*, 1997; Rebrik & Korenbrot, 1998) and around 30 µM in salamander rods (Nikonov *et al.*, 2000). The cytoplasmic cGMP concentration $[cGMP]$ in rods is estimated to be less than 4 µM in rods (Cobbs & Pugh, 1985; Yau & Nakatani, 1985; Yau & Baylor, 1989; Pugh & Lamb, 1990; Caruso *et al.*, 2005; Gross *et al.*, 2012*a*) and the Hill coefficient for channel activation, n_{cGMP}, around 3 (Pugh & Lamb, 2000; Gross *et al.*, 2012*a*; Lamb & Kraft, 2016). The ratio of open channels follows the Hill equation

$$\frac{Channels\ open}{Channels\ total} = \frac{[cGMP\ ]^{n_{cGMP}}}{[cGMP\ ]^{n_{cGMP}} + {K_{cGMP}}^{n_{cGMP}}} \approx \left(\frac{[cGMP\ ]}{K_{cGMP}}\right)^{n_{cGMP}}, \qquad (1)$$

where the approximation holds when ${K_{cGMP}}^{n_{cGMP}} \gg [cGMP\ ]^{n_{cGMP}}$. Considering the K_{cGMP} estimate of 30 µM and $[cGMP]$ of 4 µM, less than 1% of the CNG channels are concurrently open in darkness. Towards larger K_{cGMP} estimates, the fraction of open channels decreases further.

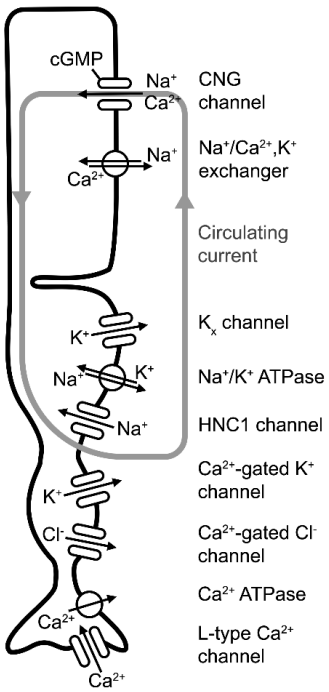

Figure 2. Ion transport mechanisms in rod photoreceptors. The CNG channels in the outer segments function as the sinks for the circulating current, while multiple channels in the rod inner segment act as the source for the current.

The rod outer segment contains $Na^+/Ca^{2+}K^+$ exchangers (NCKX), which extrude calcium ions using the driving force from the sodium and potassium ion gradients. They transport one calcium and one potassium ion out of the cell for every four sodium ions transported into the

cell. The maximal circulating dark current in mouse rods is at least 20 pA (Okawa *et al.*, 2008). If Ca^{2+} carries 15% of this current, it means that over 9.4 million Ca^{2+} ions pass through the CNG channels of a rod outer segment every second. The intracellular free calcium concentration in mouse rods is close to 250 nM in darkness (Woodruff *et al.*, 2002). In the ca. 11 fl mouse rod outer segment cytoplasmic volume, this means that there are 1700 free Ca^{2+} ions in the outer segment. Hence, the calcium exchangers remove the whole store of free calcium in every 0.2 ms, which is among the fastest turnover rates in known biological systems (Rodieck, 1999). After the absorption of light and the closure of CNG channels, the influx of calcium decreases, while the extrusion of calcium through the exchangers continues. Under rod saturating light, the cytoplasmic calcium concentration declines fast to below 20 nM due to the rapid turnover of calcium ions (Woodruff *et al.*, 2002). Decreased intracellular Ca^{2+} concentration serves as an essential feedback signal for the mechanisms of light adaptation, which accelerate the rod recovery to the dark state (reviewed, e.g., in Fu & Yau, 2007; Koch & Dell'Orco, 2015; Vinberg *et al.*, 2018*a*). Many biochemical studies have shown that the NCKX1 exchanger is the primary calcium transporter in the rod outer segments (Schnetkamp, 1986; Cook & Kaupp, 1988; Reid *et al.*, 1990; Reilander *et al.*, 1992). However, a recent study demonstrates that knocking out NCKX1 exchanger does not entirely abolish calcium extrusion from mouse rods, suggesting the existence of a parallel mechanism for calcium extrusion (Vinberg *et al.*, 2015*b*).

The photoreceptor inner segment and the synaptic terminal contain a diverse selection of ion channels and pumps whose main ionic mechanisms have been identified and characterized. However, the distribution of the channels along the photoreceptor length and their function in shaping the rod membrane potential still requires examination. Na^+/K^+ ATPase maintains the sodium and potassium ion gradients across the cell membrane required for circulating the dark current and for the functioning of the photoreceptor. The ion pump extrudes three sodium ions and intrudes two potassium ions with the energy received from the hydrolysis of one adenosine triphosphate (ATP) molecule. A mouse rod photoreceptor consumes around 10^8 ATP molecules per second in darkness. 60% of this is used for Na^+ and K^+ pumping (Okawa *et al.*, 2008). The high need for energy is also reflected in the distribution of mitochondria, as the photoreceptor inner segments contain 55 – 65% of all the mitochondria in the retina (Medrano & Fox, 1995; Kooragayala *et al.*, 2015).

The inflow of sodium in rod outer segments is balanced by the outflow of potassium supplied by the Na^+/K^+ ATPase through K^+ channels in the rod inner segment. Two main types of K^+ channels are expressed in photoreceptors: voltage-gated K^+ channels and Ca^{2+}-gated K^+ channels (Van Hook *et al.*, 2019). The voltage-gated K^+ channels were first characterized in salamander rods. The reversal potential of the channels was shown to correspond to the equilibrium potential of K^+, -75 mV (Beech & Barnes, 1989). These channels were named K_x channels. The voltage-gated K^+ channels reach their maximal conductance at ca. -30 mV and activate at membrane potentials higher than -60 mV (Molday & Kaupp, 2000). The current flowing out through the voltage-gated K^+ channels and in through the CNG channels are the main factors that set the resting membrane potential of rod photoreceptors in darkness. When the CNG channels close, the membrane potential hyperpolarizes towards the equilibrium potential of K^+. A recent study in primate rods showed that the K_x current might not be caused by single channel type but arises from the action of voltage-gated $K_v2.1$ channels and heteromeric $K_v2/K_v8.2$ channels found in the inner segment (Gayet-Primo *et al.*, 2018). Among Ca^{2+}-gated

K^+ channels, BK channels are thought to be the most relevant in photoreceptors, and they are distributed along the whole inner segment region of salamander rods (Pelucchi *et al.*, 2008). The BK channels have large conductance and fast gating kinetics. The channels are open at membrane potentials of ca. -30 to +40 mV, and they are thought to contribute to the setting of the membrane potential in darkness. An increase in the cytoplasmic Ca^{2+} concentration activates the channels, and they can balance the depolarizing effect caused by the inflow of Ca^{2+} through the L-type calcium channels. (Moriondo *et al.*, 2001) There is also evidence that BK channels modulate mouse retinal signaling, but most likely at the level of bipolar and amacrine cells (Nemargut *et al.*, 2009; Tanimoto *et al.*, 2012).

Hyperpolarization-activated cation channels have been found along the whole inner segment of rod photoreceptors, but the channel densities are still unknown (Demontis *et al.*, 2002; Knop *et al.*, 2008). These HCN1 channels are closed in darkness and activate at membrane potentials below -50 mV, reaching maximal conductance at a membrane potential of -90 mV (Fain *et al.*, 1978; Bader *et al.*, 1982; Demontis *et al.*, 2002; Kawai *et al.*, 2002). HCN1 channels pass potassium and sodium ions, and their reversal potential is near -30 mV. The physiological function of HCN1 channels is to modulate the voltage response of rods by restricting strong hyperpolarizations caused by a bright light (Seeliger *et al.*, 2011). When the membrane potential starts to hyperpolarize, HCN1 channels open and let sodium ions flow into the cell. The Na^+ inflow shifts the membrane towards a new, more depolarized state. The gating of the HCN1 channels is quite slow, which creates a "nose" like appearance to the voltage responses of a rod to bright flashes (Baylor *et al.*, 1984*a*). HCN1 channels speed up the recovery of rod membrane potential after illumination and prevent saturation of the rod system (Sothilingam *et al.*, 2016). In addition, the operation of these channels reduces the hyperpolarization of cones through rod-cone gap junction connections and prevents the saturation of the retinal network through rods. This is an important feedback mechanism improving cone vision in mesopic light conditions (Seeliger *et al.*, 2011).

The release of glutamate into the photoreceptor synaptic cleft is regulated by the intracellular calcium concentration in the photoreceptor synaptic terminal. The inflow of Ca^{2+} through voltage-gated L-type calcium channels and the extrusion of Ca^{2+} through Ca^{2+} ATPase (PMCA) control the calcium concentration in the synaptic terminals (see, e.g., Krizaj & Copenhagen, 2002). There are three types of voltage-sensitive Ca^{2+} channels in the retina: Ca_V 1.2, Ca_V 1.3, and Ca_V 1.4. The Ca_V 1.4 L-type calcium channels are found exclusively in the photoreceptor synaptic terminals, and they are the primary Ca^{2+} channels responsible for the calcium control of glutamate release (Baumann *et al.*, 2004). Recently, also Ca_V 1.3 type channels have been shown to contribute to the regulation of the photoreceptor and retinal light responses together with synaptic plasticity (Shi *et al.*, 2017). In amphibian photoreceptors, the L-type Ca^{2+} channels activate near a membrane potential of -40 mV, reach their maximal conductance at 0 mV, and inactivate at +50 mV. (Bader *et al.*, 1982; Corey *et al.*, 1984; Rieke & Schwartz, 1994) Hence, the calcium channels close already at voltages very near the photoreceptor resting potential in darkness, although the photoreceptors can hyperpolarize close to -60 mV during a light response (Baylor & Nunn, 1986; Della Santina *et al.*, 2012; Cangiano *et al.*, 2012). This suggests that the amphibian rod synapse can transmit only small deviations in membrane potential to the post-synaptic terminals. Later studies with freshly isolated pig rod photoreceptors, however, have demonstrated that L-type Ca^{2+} channels start to activate already around -60 mV

and reach their maximal conductance between -20 to -30 mV (Cia *et al.*, 2005), which corresponds more closely to the dynamic range of the rod voltage response. There are also other channels participating in the regulation of the inner segment calcium concentration. The store-operated Ca^{2+} channels (SOC) open in response to the depletion of calcium ions from the endoplasmic reticulum and provide a mechanism for reacting to an extensive reduction in intracellular Ca^{2+} concentration. (Molnar *et al.*, 2012) Furthermore, CNG channels have been found in the cone synaptic terminal, where they allow the inflow of Ca^{2+} into cells. The channels may help the cone synapses to broaden the operational range and mediate nitric oxide-induced glutamate release (Savchenko *et al.*, 1997; Barnes & Kelly, 2002).

The Ca^{2+}-gated chloride channels offer a passage for chloride anions. In mouse photoreceptors, these channels are expressed in the synaptic region (Stöhr *et al.*, 2009). The equilibrium potential for chloride has been determined to be around -20 mV in salamander rods (Thoreson *et al.*, 2002) and -46 mV in salamander cones (Thoreson & Bryson, 2004), which is near to or slightly more depolarized than the resting potential of the photoreceptor cell. Hence, the chloride flow produces an inward current (an efflux of Cl^-) in physiological conditions. Activation of the channel by Ca^{2+} increases the Cl^- conductance, and the Cl^- current is thought to inhibit Ca^{2+} inflow, providing a feedback mechanism that limits excess glutamate release (Thoreson *et al.*, 2003; Dauner *et al.*, 2013; Van Hook *et al.*, 2019).

2.3 The response of photoreceptors to light

Photoreceptors respond to light through a biochemical cascade, phototransduction, where the activation of a rhodopsin molecule by photon absorption leads to increased hydrolysis of cGMP by phosphodiesterase-6 (PDE6) enzymes in the rod disk membranes. The decrement in the cytoplasmic cGMP concentration evokes the unbinding of cGMP from the CNG channels and channel closure. The decrease in the Na^+ and Ca^{2+} flow through CNG channels (decrease in the circulating current) and continuing efflux of K^+ through the potassium channels in the inner segments drive the membrane potential towards the equilibrium potential for potassium. This hyperpolarization is transmitted to the synaptic terminal, where it causes the closure of L-type calcium channels and a decline in Ca^{2+} influx. The decrease in the synaptic calcium concentration reduces the glutamate release into the synaptic cleft, which serves as a message of the incoming light to the bipolar and horizontal cells. After the photoresponse onset and the propagation of the signal to the inner retina, phototransduction molecules deactivate, and cGMP concentration returns to its dark concentration. The following sections explore in more detail cGMP homeostasis, photoresponse onset and recovery, and the calcium-mediated feedback mechanisms, which enhance photoreceptor recovery after the photoresponse.

2.3.1 cGMP homeostasis

The homeostasis of cGMP is maintained by continuous synthesis and hydrolysis of cGMP even in darkness. The well-balanced cGMP level offers a non-fluctuating signal baseline for reliable detection of photons in an environment where thermal energy continuously causes stochastic activations of molecules involved in phototransduction. The synthesis of cGMP is carried out by guanylate cyclase, which converts guanosine triphosphate (GTP) to cGMP. The hydrolysis

of cGMP to guanosine monophosphate (GMP) is catalyzed by PDE6, which has high basal activity in darkness.

cGMP synthesis by guanylate cyclase

Mammalian photoreceptor outer segments express two forms of membrane-bound guanylate cyclases: ROS-GC1 and ROS-GC2. Rods express both forms, while cones express only ROS-GC1 (Yang *et al.*, 1999; Baehr *et al.*, 2007; Helten *et al.*, 2007). ROS-GC1 is 25-fold more common than ROS-GC2 in the bovine retina (Helten *et al.*, 2007) and 4 times more common in mouse photoreceptors (Peshenko *et al.*, 2011). The maximal guanylate cyclase activity has been estimated to be 600 μMs^{-1} in (Peshenko *et al.*, 2011) and 149 μMs^{-1} in (Makino *et al.*, 2008) for mouse rods. Guanylate cyclase-activating proteins (GCAPs) control the activity of guanylate cyclases by sensing changes in intracellular calcium concentrations (see Section 3.3.4). The guanylate cyclase activity in darkness is ca. 8 – 14-fold smaller than the maximal activity (Burns *et al.*, 2002; Olshevskaya *et al.*, 2004; Peshenko *et al.*, 2011; Gross *et al.*, 2012*a*). Despite the high rate of continuous cGMP synthesis consuming high-energy GTP molecules, the process takes only a small share of the total energy consumption of photoreceptors. Makino et al. calculated the maximal rate of cGMP synthesis to be $1.6 \cdot 10^6$ cGMP molecules·$rod^{-1}s^{-1}$, which correspond approximately to a rate of $1.7 \cdot 10^5$ cGMP molecules·$rod^{-1}s^{-1}$ in darkness (Makino *et al.*, 2008). Slightly higher estimates were proposed in (Okawa *et al.*, 2008) by calculating that the guanylate cyclase activity determined by Makino et al. (2008) at 30 °C would double at mouse body temperature (38 – 39 °C). The total ATP consumption in rods is estimated to be around 10^8 ATP/s in darkness and less than $2.5 \cdot 10^7$ ATP/s in bright light (Okawa *et al.*, 2008). Since the energy content of ATP and GTP are similar, the synthesis of cGMP takes only 0.2 – 0.4% of the total energy consumption of rods in darkness and 6 – 13% in bright light, where the guanylate cyclase activity reaches its maximum, and the circulating current is diminished.

cGMP hydrolysis by basal phosphodiesterase-6 activity

In rods, the basal cGMP hydrolysis in darkness results from spontaneous PDE6 activations due to thermal energy. This is probably caused by momentary fluctuations in the inhibitory PDE6γ-subunit binding to the catalytic site of the PDE6 body (for more details, see Section 4.1). A small part of the basal PDE6 activity is also caused by thermal activations of rhodopsin molecules, which are identical to the rhodopsin activations caused by photon absorptions (Rieke & Baylor, 1998). These two phenomena are thought to produce the dark noise in photoreceptors, which refers to the thermal fluctuation in the number of open CNG channels causing fluctuations in the circulating current (Baylor *et al.*, 1980; Rieke & Baylor, 1996). The spontaneous closings and openings of CNG channels also give a small contribution to this dark noise, but at higher frequencies than the rod light response (Reingruber *et al.*, 2015). In dark-adapted toad rods, 1 out of 5000 PDE6 molecules was estimated to be spontaneously active at a given moment (Rieke & Baylor, 1996) and in mouse rods, roughly 1 out of 1000 (Reingruber *et al.*, 2013). The value corresponds to one spontaneously active PDE6 molecule per one compartment in the mouse rod outer segment at a time (Reingruber *et al.*, 2013). For rods, this is considered to be close to the optimal basal activity because, with lower activity, the cGMP concentration would increase momentarily in some compartments and spontaneous PDE6 activation would cause a large change in the cGMP concentration near that compartment, which again would lead to high fluctuations in the open CNG channels. The resulting increase in the

dark noise would hamper the discrimination of single-photon responses from the fluctuating baseline. A single active PDE6 molecule in each compartment would provide, on average, a steady rate of cGMP hydrolysis in the whole photoreceptor cell. With higher basal activity, on the other hand, the light-activity needed to overcome the threshold level for photon detection set by the basal activity would be higher. Hence, more light-activated PDE6 molecules would be needed to induce a detectable signal (for review, see Reingruber *et al.*, 2015). The basal PDE6 activity estimates vary from 0.1 s^{-1} to 1.5 s^{-1} in toad rods (Rieke & Baylor, 1996; Whitlock & Lamb, 1999; Hamer *et al.*, 2003), from 0.49 to 3.4 s^{-1} in frog rods (Astakhova *et al.*, 2008, 2012) and from 1.2 to 2.8 s^{-1} in salamander rods (Hodgkin & Nunn, 1988; Cobbs, 1991; Nikonov *et al.*, 2000). For mouse rods, the basal PDE6 activity has been estimated to be ca. 4 s^{-1} in GCAPs$^{-/-}$ background (Gross *et al.*, 2012*a*).

In a steady-state, cGMP synthesis and hydrolysis are in balance.

$$\alpha = \beta \cdot [cGMP], \quad (2)$$

where α is the rate of cGMP synthesis, β the rate of cGMP hydrolysis, and $[cGMP]$ is the cytoplasmic cGMP concentration (Pugh & Lamb, 2000). In rod subsaturating light conditions, the synthesis rate is determined only by the rate of guanylate cyclase activity, as a sufficient supply of GTP is considered to be available for the conversion (Biernbaum & Bownds, 1985; Wimberg *et al.*, 2018). The hydrolysis depends on both free cGMP concentration and the basal PDE6 activity. The factor β defines the turnover rate of cGMP in a steady-state. For example, in mouse rods in darkness, assuming the basal PDE6 activity to be ~ 4 s^{-1}, the free cGMP pool is renewed approximately every 250 ms (Gross *et al.*, 2012*a*). From a cGMP synthesis rate of 16.7 μMs^{-1} and hydrolysis rate of 4 s^{-1}, the size of the free cGMP pool in darkness can be calculated to be near 4 µM (Gross *et al.*, 2012*a*), which is close to previous estimates of 2 – 4 µM (Cobbs & Pugh, 1985; Yau & Nakatani, 1985; Yau & Baylor, 1989; Pugh & Lamb, 1990; Cote & Brunnock, 1993; Caruso *et al.*, 2005). The turnover rate of cGMP is one of the main factors setting the kinetics of photoresponse recovery. Hence, basal PDE6 activity is of key importance in setting the absolute threshold for rod light sensitivity and temporal resolution.

2.3.2 Photon absorption and phototransduction

Phototransduction is one of the most thoroughly examined biochemical signaling cascades in vertebrates. Fig. 3 illustrates the molecules involved in phototransduction and their interactions. Several book chapters and review articles describe the phototransduction steps. A detailed description can be read, e.g., in Chapter 8 of the book "The First Steps in Seeing" by R.W. Rodieck (Rodieck, 1999). For highly quantitative analysis, see also (Pugh & Lamb, 2000) and for latest updates to phototransduction, see the reviews by (Fu & Yau, 2007; Gross *et al.*, 2015; Koch & Dell'Orco, 2015; Reingruber *et al.*, 2015).

Phototransduction begins with photon absorption in a class of G-protein coupled receptors, visual rhodopsins, protein molecules that are densely packed in the disk membranes of rod outer segments. In cones, these light-capturing molecules are packed in the invaginations of the plasma membrane. The surface density of rhodopsin is ca. 25,000 molecules/μm^2 (Liebman *et al.*, 1987; Nickell *et al.*, 2007), and rhodopsin occupies 25% of the disk membrane surface area (Liebman *et al.*, 1987). The total number of rhodopsin in mammalian rods is close to $5 \cdot 10^7$ molecules·rod^{-1} (Nathans, 1992). Rhodopsin has previously been thought to diffuse

freely in the disk membrane in monomeric conformation (Cone, 1972; Poo & Cone, 1973, 1974; Liebman & Entine, 1974). Present knowledge, however, supports the view that rhodopsin is oligomerized to densely packed paracrystalline lattice arrangements where it forms long tracks of dimers working as platforms for signal propagation (Fotiadis *et al.*, 2003, 2004; Govardovskii *et al.*, 2009; Gunkel *et al.*, 2015). Rhodopsin is composed of two parts: the apoprotein opsin and the covalently bound, light-absorbing prosthetic group, the chromophore. In mammals, the chromophore is vitamin A1 aldehyde, retinal, while many amphibian and fish species have vitamin A2 derived didehydroretinal (Crescitelli, 1958; Bridges *et al.*, 1984; Amora *et al.*, 2008; Enright *et al.*, 2015). Photon absorption causes isomerization of retinal from the 11-*cis* to the all-*trans* configuration. The isomerization triggers a sequence of very fast conformational changes in the opsin protein, converting the rhodopsin to its active form, metarhodopsin II within a few milliseconds (reviewed in Okada *et al.*, 2001).

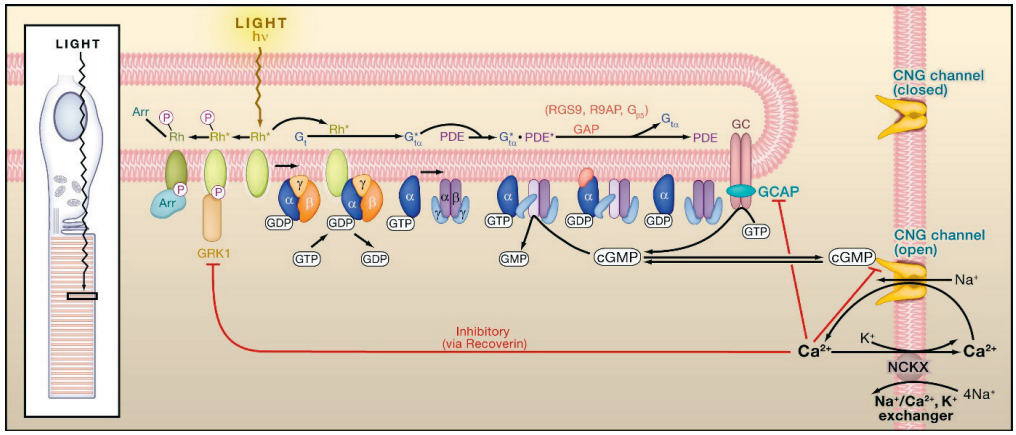

Figure 3. Phototransduction proceeds through the following steps: Step 1: Absorption of photon and isomerization of rhodopsin. Step 2: Activated rhodopsin catalyzes the exchange of GDP to GTP in the photoreceptor G-protein called transducin, which it encounters in the disk membrane. Step 3: The α-subunit of activated transducin detaches from the transducin βγ-body. Step 4: The transducin α-subunit binds to PDE6, and the complex starts to hydrolyze cGMP with a rate limited by aquatic diffusion. Step 5: The drop in the cytoplasmic cGMP concentration leads to closure of CNG channels in the rod outer segment plasma membrane and a decrease in the circulating current. Phosphorylation of rhodopsin by rhodopsin kinase (GRK1) and binding of arrestin terminates the activity of rhodopsin, while the GAP-complex mediates the deactivation PDE6. Calcium sensor proteins boost the recovery of photoreceptors after photoresponse: recoverin controls the activity of rhodopsin kinase, GCAPs activate guanylate cyclase, and calmodulin regulates the affinity of cGMP to CNG channels. Reprinted from (Yau & Hardie, 2009), with permission from Elsevier.

The activated rhodopsin can bind to G-protein, transducin, catalyzing the exchange of GDP to GTP on the transducin α-subunit (Gt_α). The amount of transducin is one-tenth of the amount of rhodopsin in frog rods (Hamm & Bownds, 1986). The amount translates to approximately $5{\cdot}10^6$ transducins in the mammalian rod outer segment, assuming the same proportion to both species. The estimated rates at which rhodopsin activates transducins vary profoundly in the literature, between 300 – 1300 s^{-1} (Leskov *et al.*, 2000; Heck & Hofmann, 2001; Gross *et al.*, 2012*a*; Lamb *et al.*, 2018). If rhodopsin deactivation is assumed to follow first-order reaction kinetics and the average active lifetime of rhodopsin is around 40 ms (Gross & Burns,

2010), one activated rhodopsin can activate 10 to 50 transducins in the mammalian rod before it deactivates (Reingruber *et al.*, 2015; Yue *et al.*, 2019).

The exchange of GDP to GTP on Gt_α releases the α-subunit from the G-protein βγ-complex. The activated Gt_α binds to one of the $2{\cdot}10^5$ PDE6 molecules in the mammalian rod outer segment (Hamm & Bownds, 1986; Cote & Brunnock, 1993; Dumke *et al.*, 1994; Pentia *et al.*, 2006; Nickell *et al.*, 2007). The rod PDE6 is composed of two catalytic subunits, α and β, and two inhibitory γ-subunits (Baehr *et al.*, 1979; Hurley & Stryer, 1982). Gt_α binds to one of the PDE6γ-subunits, displacing it, and revealing the active site of the catalytic subunit (Wensel & Stryer, 1990; Granovsky & Artemyev, 2001*a*). A widely accepted hypothesis is that one Gt_α can activate approximately one PDE6 catalytic subunit (Leskov *et al.*, 2000; Burns & Pugh, 2009). Hence, the absorption of one photon leads to the activation of 10 – 50 PDE6 subunits. The average lifetime of the light-activated PDE6 is considered to be close to 200 ms in mouse rods (Nikonov *et al.*, 2006; Chen *et al.*, 2010*b*; Azevedo & Rieke, 2011; Sakurai *et al.*, 2011*b*; Gross *et al.*, 2012*b*; Woodruff *et al.*, 2014; Sarfare *et al.*, 2014). Many studies have questioned the hypothesis proposing that the 1 : 1 binding of transducin to one PDE6-subunit would lead to activation of the concerned subunit (Melia *et al.*, 2000; Norton *et al.*, 2000; Qureshi *et al.*, 2015, 2018; Lamb *et al.*, 2018). In addition, some studies argue that the activation of PDE6 by transducin would induce a lower catalytic activity of the enzyme compared to the chemical activation of PDE6 by limited trypsin proteolysis, which completely detaches the inhibitory γ-subunits from the PDE6αβ-body (Whalen *et al.*, 1990; Melia *et al.*, 2000; Norton *et al.*, 2000; Liu *et al.*, 2009). (see Section 4.1.2).

2.3.3 Photoresponse recovery

Timely recovery of photoreceptor cells is crucial so they can rapidly respond to subsequent photons and changes in the background illumination. The recovery of a photoreceptor cell from a photon-initiated response includes the deactivation of the activated rhodopsin, the deactivation of the Gt_αPDE6 complex, and the restoration of the cGMP concentration. These deactivation processes set the time course of photoresponses.

Rhodopsin deactivation mechanisms

Two proteins participate in the termination of the rhodopsin activity: rhodopsin kinase and arrestin (see Fig. 3). Rhodopsin kinase in rod photoreceptors is the first discovered member of the G-protein-coupled receptor kinases (GRKs). Hence, it is known as GRK1 (Palczewski & Benovic, 1991; Palczewski, 1997; Maeda *et al.*, 2003). Rhodopsin kinase can phosphorylate sequentially six to seven serine and threonine residues at the C terminus of rhodopsin. The phosphorylation of rhodopsin has been found to gradually decrease rhodopsin activity and increase the probability of arrestin binding to rhodopsin. Arrestin fully terminates rhodopsin activity and rate-limits the rhodopsin deactivation process, at least in mouse rods. (Wilden *et al.*, 1986; Xu *et al.*, 1997; Gibson *et al.*, 2000; Mendez *et al.*, 2000; Arshavsky, 2002; Hamer *et al.*, 2003; Doan *et al.*, 2006; Vishnivetskiy *et al.*, 2007; Gross *et al.*, 2012*b*; Berry *et al.*, 2016) This multistep quenching of rhodopsin activity and the increased probability for arrestin binding with each phosphorylation step can explain the high reproducibility of rod single-photon responses (Mendez *et al.*, 2000; Hamer *et al.*, 2003; Doan *et al.*, 2006). However, this acknowl-

edged model has been challenged by Lamb and Kraft, who argue that rhodopsin activity remains high and drops to a lower level only after several phosphorylation steps before a complete termination of activity by arrestin binding to low-activity rhodopsin (Lamb & Kraft, 2016).

After the phosphorylation of rhodopsin and the binding of arrestin, the inactivated rhodopsin dissociates to opsin and *all-trans*-retinal. To regenerate rhodopsin to its dark-adapted form and to restore the rod sensitivity, rhodopsin has to be dephosphorylated and arrestin decoupled from rhodopsin. Additionally, the *all-trans*-retinal has to be isomerized into the functional *11-cis* form. This is accomplished in the visual cycle, a process where the chromophore is transported to the retinal pigment epithelium, enzymatically isomerized, returned to the outer segments, and coupled with dephosphorylated opsin. (see e.g. Lamb & Pugh, 2004; Lee *et al.*, 2010; Reuter, 2011; Saari, 2012)

PDE6 deactivation mechanisms

Hydrolysis of the GTP, bound to transducin during light-activation, deactivates the $Gt_{\alpha}PDE6$ complex. Gt_{α} has some GTPase activity by itself, but the hydrolysis is profoundly accelerated by a GTPase accelerating protein (GAP) complex (see, e.g., Arshavsky & Wensel, 2013). There are three members in the GAP complex: RGS9, Gβ5, and R9AP. At least 11 different RGS coding mRNAs are expressed in the retina, but only RGS9 is enriched in photoreceptor outer segments (He *et al.*, 1998). RGS9 has high GAP activity. The protein forms a tight complex with Gβ5 (Makino *et al.*, 1999; Cheever *et al.*, 2008). The soluble complex of RGS9 and Gβ5 can be purified from cells (He *et al.*, 2000*b*), although for its proper function, the complex has to be bound to the rod disk membranes. This action is accomplished by a third factor, R9AP anchoring protein (Hu & Wensel, 2002). The GAP complex can significantly increase the GTPase efficacy of transducin. However, its affinity to transducin is low (Skiba *et al.*, 2000). The effective deactivation of $Gt_{\alpha}PDE6$ is enabled by the PDE6γ-subunit, which enhances the affinity of transducin to the GAP complex by more than 15-fold. Additionally, this mechanism ensures that activated transducin is not unnecessarily deactivated before its binding to PDE6. (Angleson & Wensel, 1994; Skiba *et al.*, 2000).

All the GAP complex proteins are necessary for the timely recovery of photoresponses. The transgenic animals that lack RGS9, Gβ5, or R9AP show identically delayed recovery of photoresponses with a negligible change in the activation phase (Chen *et al.*, 2000; Krispel *et al.*, 2003; Keresztes *et al.*, 2004). The incidence of the components in the GAP complex is highly dependent on each other. The RGS9 knockout does not have detectable Gβ5 in their photoreceptors and vice versa, while both have a normal level of R9AP. R9AP knockouts, on the other hand, suffer from a severe depletion of both RGS9 and Gβ5 in their photoreceptors (Chen *et al.*, 2000, 2003; Keresztes *et al.*, 2004). Interestingly, the overexpression of R9AP causes a profound increase in the expression level of the whole GAP complex, unlike the overexpression of RGS9 or Gβ5 (Chen *et al.*, 2003; Krispel *et al.*, 2006). Krispel et al. utilized this phenomenon to show that the overexpression of the GAP complex accelerates rod photoresponse recovery drastically while the overexpression of GRK1 has no significant effect (Krispel *et al.*, 2006). This finding attests that PDE6 deactivation is the rate-limiting factor in rod photoresponse recovery (Krispel *et al.*, 2006; Invergo *et al.*, 2013). Additionally, the overexpression of the PDE6γ-subunit has been shown to accelerate the rod response recovery independently of the GAP complex, which suggests that the inhibitory sites on PDEαβ body are accessible for excess PDE6γ-subunits after the activation of the PDE6 molecule by transducin

(Tsang *et al.*, 2006). The deactivation of $Gt_{\alpha}PDE6$, where Gt_{α} dissociates from PDE6, is a single-step stochastic process while rhodopsin deactivation proceeds through multiple steps. The reproducibility of single-photon responses, in the case of PDE6 deactivation, is secured by the activation of 10 – 50 PDE6 subunits per one rhodopsin activation, which provides the necessary averaging of the activated PDE6 lifetime.

2.3.4 Calcium-mediated feedback mechanisms

In dark-adapted conditions, rods can respond to single photons, but their signaling starts to saturate already with flashes causing around 100 rhodopsin isomerization per rod (see, e.g., Baylor *et al.*, 1979*a*; Cobbs & Pugh, 1987; Long *et al.*, 2013; Reingruber *et al.*, 2013). Still, rods can function in conditions producing steady illumination of ca. 10^5 $R^*rod^{-1}s^{-1}$. (Adelson, 1982; Sharpe *et al.*, 1992; Naarendorp *et al.*, 2010) The expansion of the operation range is accomplished by accelerating the deactivation processes in phototransduction and speeding up the recovery of the cytoplasmic cGMP concentration in background illuminations (Pugh *et al.*, 1999). The number of hydrolyzed cGMP molecules resulting from rhodopsin activation is decreased mainly by shortening the lifetime of activated rhodopsin (Gorodovikova *et al.*, 1994; Chen *et al.*, 1995; Matthews & Fain, 2001; Makino *et al.*, 2004). However, later studies suggest that also the lifetime of activated PDE6 may be under modulation (Woodruff *et al.*, 2008; Chen *et al.*, 2012, 2015). Additionally, some evidence suggests that phototransduction amplification in amphibian rods might be reduced in background light when intracellular calcium level decreases (Lagnado & Baylor, 1994; Jones, 1995; Gray-Keller & Detwiler, 1996). However, these findings were questioned by Pugh et al. (1999), who suggested that the acceleration of response recovery might affect the response kinetics at earlier times than anticipated, leading to reduced phototransduction amplification estimations. The speeding of cGMP recovery is achieved by accelerating the cGMP synthesis rate of guanylate cyclase. This is considered as the dominant mechanism for fast light adaptation in rods (Koch & Stryer, 1988; Koutalos *et al.*, 1995*a*; Nikonov *et al.*, 2000; Mendez *et al.*, 2001; Burns *et al.*, 2002; Peshenko & Dizhoor, 2004). Additionally, the affinity of cGMP to CNG channels is under regulation, but particularly in mammalian rod photoreceptors, the contribution of this regulation to light adaptation is only modest (Hsu & Molday, 1993; Nikonov *et al.*, 2000; Chen *et al.*, 2010*c*). Intracellular Ca^{2+} concentration plays a decisive role in rod light adaptation (Matthews *et al.*, 1988; Nakatani & Yau, 1988*b*; Koutalos *et al.*, 1995*a*), as all the light adaptation mechanisms described above are mediated through calcium sensor proteins: recoverin, guanylate cyclase-activating proteins (GCAPs), and calmodulin, respectively (see Fig. 3). These calcium-sensitive mechanisms and their role in controlling photoreceptor sensitivity are discussed in detail in many reviews (see, e.g., Palczewski *et al.*, 2000; Nikonov *et al.*, 2000; Vinberg *et al.*, 2018*a*).

Guanylate cyclase-activating proteins

Guanylate cyclase-activating proteins (GCAPs) constitute a subfamily of neuronal calcium sensor proteins, which control the activity of membrane-bound guanylate cyclase. One to eight GCAPs isoforms exist in different vertebrate species (Koch & Dell'orco, 2013; Wen *et al.*, 2014). Mammalian rod photoreceptors contain two isoforms: GCAP1 and GCAP2, which both can activate the guanylate cyclases ROS-GC1 and ROS-GC2 independently. GCAP1 and GCAP2 increase the efficiency of ROS-GC1 28-fold and 13-fold, respectively, while they stimulate ROS-GC2 only 6-fold and 5-fold, respectively (Peshenko *et al.*, 2011). In darkness, when the calcium level is high, GCAPs bind calcium and do not activate guanylate cyclase. When light induces a

decline in the cytoplasmic calcium concentration, Ca^{2+} ions are released from GCAPs and replaced by Mg^{2+} (Dizhoor *et al.*, 2010). Mg^{2+}-bound GCAPs can activate guanylate cyclases and enhance the total synthesis rate of cGMP by 8 – 14-fold (Burns *et al.*, 2002; Olshevskaya *et al.*, 2004; Peshenko *et al.*, 2011; Gross *et al.*, 2012*a*). This mechanism accelerates photoresponse recovery and decreases the number of closed CNG channels in prolonged illumination (Mendez *et al.*, 2001; Burns *et al.*, 2002). GCAP1 has a lower affinity to Ca^{2+}, and it responds faster to the light-induced decline in cytoplasmic calcium. GCAP2, with higher affinity to Ca^{2+}, responds when calcium level continues to decline further and hence the role of GCAP2 is emphasized in bright light (Makino *et al.*, 2008, 2012; Wen *et al.*, 2014). Together, the GCAPs provide strong negative feedback that counterbalances light-induced changes in the cGMP level. Rods lacking both GCAPs produce 5-fold larger single-photon responses, and their light adaptation is severely compromised (Mendez *et al.*, 2001). Similar findings have also been made in cone photoreceptors lacking GCAPs (Sakurai *et al.*, 2011*a*; Vinberg *et al.*, 2018*b*). In addition, studies utilizing PDE6 inhibitors suggest that GCAPs-mediated feedback does not only work by activating guanylate cyclase in response to Ca^{2+} decreases, but can also respond to increases in cytoplasmic Ca^{2+} concentration above the dark-adapted level by inhibiting guanylate cyclase. PDE6 inhibitors elevate cGMP concentration by decreasing the basal cGMP hydrolysis rate. Both electrophysiological and biochemical studies have shown that the PDE6 inhibitor-induced elevation in cGMP concentration is profoundly increased if either calcium concentration is buffered to a steady level or GCAPs are knocked out (Zhang *et al.*, 2005; Tsang *et al.*, 2012). Both of these manipulations prevent GCAPs-mediated inhibition of guanylate cyclase.

Recoverin

Recoverin is a calcium sensor protein that modulates the activity of rhodopsin kinase, and hence, the lifetime of activated rhodopsin (Gorodovikova *et al.*, 1994; Chen *et al.*, 1995; Matthews & Fain, 2001; Makino *et al.*, 2004). The intracellular calcium level is high in darkness, and in these conditions, recoverin binds two calcium ions. The binding of Ca^{2+} to recoverin facilitates its binding to the disk membrane and inhibition of rhodopsin kinase, which leads to delayed phosphorylation and deactivation of rhodopsin. (Chen *et al.*, 1995; Senin *et al.*, 1995; Palczewski *et al.*, 2000) The decline of intracellular Ca^{2+} upon illumination causes recoverin to unbind from rhodopsin kinase, allowing efficient rhodopsin phosphorylation and deactivation.

Recoverin has been shown to contribute to the light-dependent acceleration of response recovery in mouse rods, but it seems to have little or no effect on the response amplitudes or initial time course of responses. Additionally, recoverin did not seem to have a role in rod light adaptation in several studies. (Makino *et al.*, 2004; Sampath *et al.*, 2005; Chen *et al.*, 2010*a*, 2010*b*, 2012). However, these experiments were conducted in the presence of the dominant GCAPs-mediated Ca^{2+} feedback mechanism, which might partially hide the smaller effects of recoverin. Moreover, recent experiments have suggested that besides the control of rhodopsin lifetime, recoverin might modulate the lifetime of activated PDE6 (Chen *et al.*, 2012, 2015; Morshedian *et al.*, 2018) and basal PDE6 activity (Morshedian *et al.*, 2018). However, biochemical evidence supporting the hypotheses are still lacking (Koch & Dell'Orco, 2015).

Calmodulin

The CNGB1-subunit of the CNG channel in rods contains a binding site for the calcium sensor protein calmodulin, which controls the affinity of cGMP to the CNG channels (Grunwald *et al.*, 1998; Weitz *et al.*, 1998). When the intracellular calcium level is high, calmodulin binds Ca^{2+} and occupies the binding site in the CNG channel. When calmodulin releases the bound Ca^{2+}, it unbinds from the CNG channel, which increases the affinity of cGMP to the channel. (Hsu & Molday, 1993; Nakatani *et al.*, 1995; Gordon *et al.*, 1995; Warren & Molday, 2002) This phenomenon could potentially serve as a light adaptation mechanism in photoreceptors. However, its effect in mammalian rods is considered only minor (Chen *et al.*, 2010*c*). Both electrophysiological and modeling studies with amphibian rods indicate a small contribution of calmodulin-mediated channel modulation to light adaptation in bright light (Koutalos *et al.*, 1995*b*, 1995*a*; Nikonov *et al.*, 2000). However, in a study with a mouse model lacking the calmodulin-binding site of CNG channels, the researchers found no contribution from the calmodulin pathway on sensitivity regulation of rod dim flash responses at different background light intensities, albeit preventing calmodulin binding to CNG channels did accelerate the recovery of saturated responses (Chen *et al.*, 2010*c*). A peculiar phenomenon involving calmodulin was noted by McKeown and Kraft, and Chen et al., when they showed that removal of the calmodulin-binding site potentiated the overshoot after step responses to intense background light in both in wild type (McKeown & Kraft, 2014) and $GCAPs^{-/-}$ mice (Chen *et al.*, 2010*c*). The direct mechanisms of calmodulin involvement remained unidentified, but it could be associated with changes in Ca^{2+} and Mg^{2+} homeostasis. Interestingly, a later investigation showed that this overshoot was abolished after knocking out recoverin (Morshedian *et al.*, 2018). Furthermore, a recent biochemical study suggests that rhodopsin kinase contains a separate binding site for calmodulin in addition to the binding site for recoverin. The study proposes that these two calcium sensor molecules work synergistically in a way that calmodulin complements the effect of recoverin and broadens the calcium range where the modulation of rhodopsin kinase takes place (Grigoriev *et al.*, 2012).

3. Phosphodiesterase-6 (PDE6)

The cyclic nucleotide phosphodiesterases (PDEs) comprise a superfamily of 11 regulatory enzymes (Bender & Beavo, 2006). Their function is to catalyze the hydrolysis of cyclic nucleotides, cyclic adenosine monophosphate (cAMP) and cyclic guanosine monophosphate (cGMP), to adenosine monophosphate (AMP) and guanosine monophosphate (GMP), respectively. PDE activity is found practically in every cell in the body, as PDEs control a broad range of cellular processes as well as a communication between the cells (see, e.g., (Soderling & Beavo, 2000; Conti & Beavo, 2007; Francis *et al.*, 2011*a*). Phosphodiesterase-6 (PDE6) appears primarily in photoreceptor outer segments, where it controls the cytoplasmic cGMP concentration and serves as an essential member of the phototransduction cascade converting the information of captured photons to a bioelectrical signal (see, e.g., Stryer, 1986; Zhang & Cote, 2005; Cote, 2006). This section concentrates mostly on rod PDE6 and its significance for rod signaling.

3.1 Structure and function

The rod PDE6 is composed of two active catalytic subunits, α and β, and two inhibitory γ-subunits, while the cone PDE6 is composed of two similar catalytic α'-subunits and two inhibitory γ'-subunits (Baehr *et al.*, 1979; Hurley & Stryer, 1982). Fig. 4 illustrates a model structure of PDE6 determined from cryo-electron microscopy experiments (Zhang *et al.*, 2015). The two catalytic subunits form a dimer (αβ in rods and α'α' in cones), and each subunit contains three structural domains: GAFa, GAFb, and the catalytic domain. Additionally, the hydrophobic C-terminal of PDE6 anchors the PDE6 to the rod disk membrane (Catty & Deterre, 1991). The relative PDE6 to rhodopsin ratio in rod disk membranes is near 1 : 300 in amphibian and mammalian photoreceptors (Hamm & Bownds, 1986; Cote & Brunnock, 1993; Dumke *et al.*, 1994; Pentia *et al.*, 2006). The total PDE6 concentration is approximately 30 μM in rod outer segments as calculated based on the 8.23 mM rhodopsin concentration in mouse rods (Nickell *et al.*, 2007), close to an earlier estimate of 22 μM for frog rods (Dumke *et al.*, 1994). The 30 μM PDE6 concentration implies $2 \cdot 10^5$ PDE6 molecules in one mouse rod and around 200 PDE6 molecules per rod disk membrane (Nickell *et al.*, 2007). PDE6 is mostly concentrated on the rim regions of the disks (Muradov *et al.*, 2009, 2010).

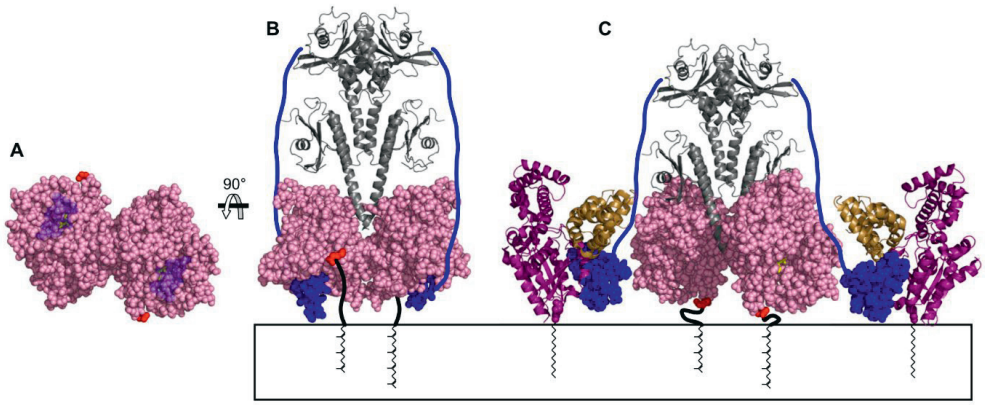

Figure 4. Model structure of the phosphodiesterase-6 enzyme and its interactions. The catalytic domains are expressed in pink, the GAF domains as gray, and the PDEγ-subunits are shown in blue. The C-terminal residues in the catalytic domain structure are highlighted with red color and the residues connecting PDE6 to the disk membrane with black color. A) Bottom view of the catalytic domains. B) A front view of the enzyme. C) A proposed model for the interaction of transducin Gt_{α}-subunit (purple) and PDE6. A fragment of RGS9 is shown in brown. This research was originally published in (Zhang *et al.*, 2015) © the American Society for Biochemistry and Molecular Biology.

The catalytic domains of mammalian phosphodiesterases are highly conserved and contain invariant catalytic site residues (Zhang *et al.*, 2004*b*; Conti, 2004). PDE family members share ca. 25% sequence identity within catalytic domains (Ke, 2004), and the closest relatives PDE5 and PDE6 share approximately 50% of the catalytic domain identity (Granovsky & Artemyev, 2001*a*). The catalytic domain contains two metal-binding motifs: one binding Zn^{2+} with high affinity and the other Mg^{2+} with lower affinity. They have a role in stabilizing the PDE6 structure in addition to the high importance for the cGMP catalysis (He *et al.*, 2000*a*; Ke, 2004). PDE6 hydrolyzes cGMP with a rate limited by the aquatic diffusion (Reingruber *et al.*, 2013). The catalytic activity surpasses that of PDE5 by 500-fold, but the reason for this difference is not yet well understood. The metal binding motifs in the catalytic region of PDEs are likely partially responsible for the difference since substituting two residues from the divalent metal binding region in PDE5 to their PDE6 counterpart increased the maximal catalytic activity of PDE5 by 10-fold (Granovsky & Artemyev, 2001a). The rate of cGMP hydrolysis v can be considered to follow the Michaelis-Menten kinetics

$$v = \frac{PDE6^{*} \cdot ½ k_{cat}[cGMP]}{K_M + [cGMP]}, \qquad (3)$$

where $PDE6^{*}$ denotes the number of activated PDE6 subunits, $[cGMP]$ the cytoplasmic cGMP concentration and K_M is the Michaelis constant signifying the cGMP concentration resulting in a half-maximal rate for cGMP hydrolysis. The estimates for the Michaelis constant K_M of the hydrolysis reaction range from 10 µM to 100 µM (Gillespie & Beavo, 1988; Dumke *et al.*, 1994; Granovsky *et al.*, 1998; D'Amours & Cote, 1999; Leskov *et al.*, 2000; Mou & Cote, 2001; Zhang *et al.*, 2008; Muradov *et al.*, 2010). The maximal catalytic rate of the PDE6 dimer, k_{cat}, lies around 5,000 s^{-1} (Dumke *et al.*, 1994; Mou & Cote, 2001; Muradov *et al.*, 2010). The multiplier ½ derives from the assumption that two PDE6 subunits of the dimer are equally active (Leskov *et al.*, 2000; Burns & Pugh, 2009). PDE6 is highly selective for cGMP. The maximal

catalytic activity for the hydrolysis of cAMP by PDE6 ($k_{cat} \approx 3000\ s^{-1}$) is of the same order as for cGMP but the K_M for cAMP is almost 100-fold larger than for cGMP.

The regulatory GAF domains contain allosteric cGMP-binding pockets, which regulate the affinity of γ-subunits for the catalytic domain (Zhang *et al.*, 2008). Four potential non-catalytic cGMP-binding sites exist in the PDE6 dimer. Two of the sites bind cGMP with high affinity, and these sites seem to be almost permanently occupied in physiological conditions. The binding of cGMP to the high-affinity sites increases the affinity of one γ-subunit for PDE6αβ catalytic domain by at least 10-fold, while the affinity of the other γ-subunit remains unaffected or even decreases slightly (D'Amours & Cote, 1999; Mou & Cote, 2001; Cote, 2006). Mutually, binding of γ-subunits to the PDE6 body increases the affinity of cGMP to the two high-affinity binding sites. In other words, the dissociation constants, K_D, for the two high-affinity binding sites shows positive cooperativity with the binding of γ-subunits. With γ-subunits bound, the dissociation constants are < 1 nM and 15 nM for the two cGMP-binding sites, and without γ-subunits, the dissociation constants increase to 60 nM and to > 1 μM, respectively (Gillespie & Beavo, 1989*a*; Cote *et al.*, 1994; Artemyev *et al.*, 1996; Mou *et al.*, 1999; Cote, 2006). Additionally, two low-affinity binding sites (K_D = 7 μM) have been localized to rod outer segments. The identity of the sites remain unknown but since no other cGMP binding proteins are found in sufficient amounts in rod outer segments, it is plausible that the binding sites in PDE6 account for the low-affinity binding (Cote & Brunnock, 1993; Zhang & Cote, 2005). The bound cGMP constitute roughly 90% of the total 60 μM cGMP concentration in the rod outer segments in the dark-adapted state (Cote *et al.*, 1984; Gillespie & Beavo, 1989*a*; Cote & Brunnock, 1993) and even during prolonged light adaptation, the total cGMP concentration can undergo a decrease of no more than roughly 50% (Cote *et al.*, 1984, 1986; Calvert *et al.*, 2002). In addition to cGMP binding, GAF domains control the dimerization of PDE6 into αβ form instead of αα or ββ (Artemyev *et al.*, 1996) and guide the localization of PDE6 to the photoreceptor outer segments (Cheguru *et al.*, 2014).

The concentration of the inhibitory PDE6 γ-subunits is equal to that of PDE6 catalytic units in rod outer segments (Norton *et al.*, 2000). γ-subunits are likely to exist natively unfolded in solution (Uversky *et al.*, 2002; Uversky, 2002; Cote, 2006) but when bound to PDE6, the γ-subunit extends linearly from the C-terminal to N-terminal of the PDE6αβ forming multiple interaction sites with both the GAF domains and with the catalytic domain (Guo *et al.*, 2006; Guo & Ruoho, 2008; Zhang *et al.*, 2015). Moreover, the γ-subunit has been observed to bind simultaneously to both PDE6α and PDE6β subunits (Guo *et al.*, 2005, 2006). The primary purpose of the γ-subunits is to block the access of cGMP to the C-terminal catalytic pockets and to relieve this blockage upon the binding of light-activated Gt_α to the γ-subunit (Wensel & Stryer, 1990; Granovsky & Artemyev, 2001*a*; Barren *et al.*, 2009). Additionally, the binding of the γ-subunit increases the affinity of cGMP for the non-catalytic cGMP binding sites and the affinity of the GAP complex for activated Gt_α, which leads to enhanced deactivation of Gt_αPDE6 complex (see Section 3.3.3). The multifunctional γ-subunit is also believed to have other tasks in many organs such as in the lungs (Tate *et al.*, 1998) and the brain (see, e.g., Guo & Ruoho, 2008).

3.1.1 The sources of basal PDE6 activity

The basal activity of PDE6 (β_{dark}) can originate from three main sources: spontaneous activations of rhodopsin, transducin, and PDE6 caused by thermal energy. In a steady-state, the contribution of these different sources to the basal PD6E activity can be calculated as follows:

Spontaneous rhodopsin isomerizations → $\beta_{dark} = \beta_{sub} \frac{\nu_{RE}}{k_{PDE} k_R} \Phi_{dark}$

Spontaneous transducin activations → $\beta_{dark} = \beta_{sub} c_{GE} G^*_{dark}$, (4)

Spontaneous PDE6 activations → $\beta_{dark} = \beta_{sub} PDE6^*_{dark}$

where Φ_{dark} is the average rate of spontaneous rhodopsin isomerizations·rod^{-1}s^{-1}, and G^*_{dark} and $PDE6^*_{dark}$ are the average number of activated transducin and PDE6 molecules·rod^{-1} at a given time, respectively. k_R and k_{PDE} are the rate constants for rhodopsin and PDE6 deactivation (The average lifetime of the activated molecules $\tau_i = \frac{1}{k_i}$). c_{GE} is the coupling coefficient for PDE6 activation by transducin. Usually, all transducins are assumed to bind PDE6 before their deactivation and, hence, c_{GE} is close to 1 (Lamb, 1994). $\nu_{RE} = \nu_{RG}\ c_{GE}$ is the rate by which rhodopsin activates PDE6, while ν_{RG} is the rate constant for transducin activation by activated rhodopsin. β_{sub} is the average hydrolytic rate for one activated PDE6 subunit. β_{dark} is estimated to be close to 1 s^{-1} in amphibian rods at room temperature (Hodgkin & Nunn, 1988; Cobbs, 1991; Rieke & Baylor, 1996; Whitlock & Lamb, 1999; Nikonov et al., 2000; Hamer et al., 2003; Astakhova et al., 2008, 2012) and 4 s^{-1} in mouse rods in 37 °C (Gross et al., 2012a).

Rhodopsin is an extremely stable molecule, and it activates thermally only once in several hundred years (Baylor *et al.*, 1984*b*). Still, because of the vast amount of rhodopsin molecules in rods, thermal isomerizations of rhodopsin occur at a rate of once per tens to hundreds of seconds per rod. The rate of rhodopsin isomerizations have been determined to be less than 1/200 s^{-1} in bullfrog rods (Donner *et al.*, 1990) but around 1/50 s^{-1} in toad rods both near 20 °C (Baylor *et al.*, 1980). In mammalian body temperature, the rate has been determined in monkey rods, 1/160 s^{-1} (Baylor *et al.*, 1984*b*), and in mouse rods, 1/100 s^{-1} (Burns *et al.*, 2002). If ν_{RE} is assumed to be 1000 s^{-1} in mammalian rod in body temperature (Heck & Hofmann, 2001; Lamb *et al.*, 2018), n_{cGMP} to be 3 (Pugh & Lamb, 2000) and β_{sub} to be 0.007 s^{-1} (Based on amplification constant of around 20 s^{-2} determined Papers IV and V, see Eq. 19), and the lifetimes of activated rhodopsin and PDE6 to be 40 ms and 200 ms, respectively, the rate of spontaneous cGMP hydrolysis caused by the thermal isomerizations of rhodopsin would be ca. 5·10^{-4} s^{-1} (calculated based on Eq. 4). Hence, spontaneous activations of rhodopsin most likely do not have a significant effect on the basal rate of cGMP hydrolysis.

In addition to spontaneous rhodopsin activation, the chromophore-free opsin is shown to activate PDE6 (and transducin) with a rate of 2·10^{-3} s^{-1}, around 10^6-to 10^7-fold lower than the activity of light-activated rhodopsin (Melia *et al.*, 1997). A similar conclusion was drawn from electrophysiological experiments with bleach adapted salamander rods where opsin was estimated to be 10^6 to 10^7 times less active than activated rhodopsin (Cornwall & Fain, 1994; Matthews *et al.*, 1996). In a recent study, the free opsin-to-rhodopsin ratio was estimated to be 1.5·10^{-4} in dark-adapted mammalian rod outer segments (Tian *et al.*, 2017). The estimate corresponds to around 7500 free opsin molecules in one mouse rod. With a rate of 2·10^{-3} s^{-1}

for PDE6 activation, this would lead to 15 PDE6 activations·s^{-1} corresponding to 5 simultaneously active PDE subunits in rod (200 ms lifetime of PDE6) or to a cGMP hydrolysis rate of 0.04 s^{-1} (see Eq. 4). Hence, free opsin is not expected to have a significant contribution to the basal PDE6 activity. However, a novel finding suggests that opsin exists in equilibrium with a predominant inactive state and a rare, highly active state. According to that study, free opsin might contribute to the discrete shot noise events in rods, generally considered to originate from the thermal activations of rhodopsin (Sato *et al.*, 2019).

Spontaneous GDP to GTP exchange in transducin extracted from bovine rods was determined to occur at a rate of 10^{-5} to $2{\cdot}10^{-4}$ s^{-1} (Fawzi & Northup, 1990; Ramdas *et al.*, 1991). The rate is 10^7 to 10^8-fold less than that caused by light-activated rhodopsin. Still, because there are $5{\cdot}10^6$ transducins in each mouse rod, 50 to 1000 spontaneous transducin activations·s^{-1} occur in a rod outer segment. With 200 ms average lifetime of active PDE6, the rate translates to 10 – 200 simultaneously active PDE6 molecules·rod^{-1} or to a cGMP hydrolysis rate of 0.07 – 1.4 s^{-1} (see Eq. 4). These values imply that the spontaneous activations of transducins could contribute to the total basal PDE6 activity. However, Rieke and Baylor (1996) showed that the complete removal of GTP in toad rods did not affect the dark noise originating from the fluctuations in the basal PDE6 activity (Rieke & Baylor, 1996). The finding questions the contribution of spontaneous activation of rhodopsin, opsin, and transducin to the basal rate of cGMP hydrolysis, at least in amphibian rods.

The spontaneous activation of PDE6 is believed to occur when thermal energy wiggles the γ-subunit and momentarily releases the inhibition of the active core of the PDE6 catalytic domain. The biochemical estimates for the dissociation constant of the γ-subunit from the catalytic domain differ profoundly. Some studies report different dissociation constants (K_D) for the two subunits as < 0.3 pM and 2 – 3 pM (Mou & Cote, 2001; Paglia *et al.*, 2002) and some report similar K_D for both subunits, from 10 to 80 pM (Wensel & Stryer, 1986; D'Amours & Cote, 1999; Muradov *et al.*, 2010). The fraction of active PDE6 subunits of the total 30 µM concentration of PDE6 dimers ($2{\cdot}10^5$ PDE6 dimers in one rod) can be calculated from the equation

$$\frac{[PDE6][\gamma]}{[PDE6\gamma]} = K_D. \qquad (5)$$

Considering the different K_D values for the two subunits, less than 1/ 10 000 of the high affinity (K_D < 0.3 pM) subunits and around 1/3200 of the lower affinity subunits (K_D = 3 pM) would be active at a given moment. Higher K_D estimates suggest that 1/2500 (K_D = 10 pM for both subunits) to 1/870 (K_D = 80 pM for both subunits) subunits are active at a given moment. These values would translate to around 80 – 460 active PDE6 subunits in mouse rod or to basal PDE6 activity of 0.6 to 3.2 s^{-1} with subunit activity β_{sub} = 0.007 s^{-1} (see Eq. 4). The dissociation constants were determined at room temperature and, thus, the values might even double in body temperature. Simulations by Reingruber et al. resulted in an estimate of around 700 spontaneously activated PDE6 molecules in a mouse rod at body temperature at any given moment (Reingruber *et al.*, 2013). With $\beta_{sub} \approx 0.007$ s^{-1}, this corresponds to $\beta_{dark} \approx 4.9$ s^{-1}, very close to the value 4 s^{-1} for β_{dark} determined earlier for mouse rods (Gross *et al.*, 2012*a*). In summary, the likely source of the basal rate of cGMP hydrolysis is the thermal activation of PDE6. However, both the spontaneous activity of transducin and free opsin could potentially contribute to β_{dark}.

3.1.2 PDE6 activation by light

After the GDP to GTP exchange catalyzed by activated rhodopsin, the free transducin alpha subunit Gt_α binds to the PDE6αβγγ holoenzyme via multiple interaction sites (Zhang *et al.*, 2012). The binding of the transducin Gt_α-subunit to the γ-subunit displaces the C-terminal of the γ-subunit, reveals the catalytic cGMP-binding site and activates the enzyme (Wensel & Stryer, 1990; Granovsky & Artemyev, 2001*a*) (see Fig. 4C). Transducin has also been shown to interact with the central region of the γ-subunit, where its binding lowers the cGMP affinity to the non-catalytic cGMP binding sites in GAF domains (Zhang *et al.*, 2012). During the light-activation of PDE6, γ-subunits stay attached to the GAF domains of the PDE6αβ body (Artemyev *et al.*, 1992). However, it is also hypothesized that this connection is maintained only when the high-affinity cGMP-binding sites are occupied. Unbinding of cGMP from the high-affinity site could lead to a decrease in the affinity of the γ-subunit to the PDE6 body, allowing the γ-subunit to break away from the PDE6-body along with the Gt_α-subunit (Yamazaki *et al.*, 1990; Arshavsky *et al.*, 1992). This effect might be involved in light adaptation during prolonged light exposures (Zhang *et al.*, 2008).

The catalytic activity of the α and β subunits of rod PDE6 have been found to be equal (Muradov *et al.*, 2010). According to the general view, the α and β subunits work independently. The binding of transducin to one γ-subunit can release half of the total catalytic power of the enzyme, and the binding of another transducin to the second γ-subunit releases the remaining half (Wensel & Stryer, 1990; Pugh & Lamb, 2000; Leskov *et al.*, 2000). However, multiple studies have concluded that only approximately half of the maximal catalytic activity of PDE6 can be achieved in physiological conditions with transducin activation (Whalen *et al.*, 1990; Melia *et al.*, 2000; Norton *et al.*, 2000; Liu *et al.*, 2009). Some studies argue that the binding of the first transducin releases the achievable potency of PDE6 and the binding of the second transducin might work only as a signal to enhance the deactivation of the PDE6 enzyme (Bruckert *et al.*, 1994; Melia *et al.*, 2000; Yamazaki *et al.*, 2002). Others have found that the binding of the first transducin results to only less than 5% activation of the enzyme and the binding of the second transducin is needed for effective catalysis (Norton *et al.*, 2000; Lamb *et al.*, 2018; Qureshi *et al.*, 2018). In the latter model, a high local concentration of activated transducin would be enough to form a cluster of PDE6 enzymes binding two transducins and cause effective hydrolysis of cGMP in the small compartment limited by rod disk membranes. Such a system would be beneficial by limiting significant PDE6 activation by spontaneously activated transducins filtering the transducin-mediated phototransduction noise (Norton *et al.*, 2000; Lamb *et al.*, 2018; Qureshi *et al.*, 2018). Overall, the scientific consensus between the models for PDE6 activation by transducin is yet to be found.

3.2 Inhibition of PDE6

The application of PDE inhibitors revealed that PDE6 has an essential function in controlling the photoreceptor response to light (Lipton *et al.*, 1977; Capovilla *et al.*, 1982, 1983) already before the identification of the cGMP-gated channels as the light-sensitive cationic channels in the rod outer segment plasma membrane (Fesenko *et al.*, 1985). Since then, PDE inhibitors have provided vast mechanistic insight on how the catalytic activity of PDE6 controls the absolute sensitivity, response kinetics, and dark noise of photoreceptors (Cervetto & McNaughton, 1986; Hodgkin & Nunn, 1988; Rieke & Baylor, 1996). As PDEs take part in almost

every regulatory system in the body, the therapeutic and scientific value of PDE inhibitors has long been recognized (Lugnier, 2006). PDE inhibitors are widely used for pharmacological treatments of disorders such as erectile dysfunction, congestive heart failure, and inflammatory airway disease (Essayan, 1999; Boswell-Smith *et al.*, 2006; Francis *et al.*, 2011*b*). However, PDE inhibitors suffer from poor specificity because of the structural similarity of the catalytic domains between PDE classes. Poor specificity has been reported to cause various side effects for PDE-targeted drugs, including hearing impairment and increased sensitivity to light (Boswell-Smith *et al.*, 2006; Kerr & Danesh-Meyer, 2009; Khan *et al.*, 2011; Azzouni & Abu samra, 2011). PDE6 is especially non-discriminant for different PDE inhibitors. Practically all so-called "specific" PDE inhibitor drugs inhibit PDE6 effectively in addition to their target PDE isoform (Zhang *et al.*, 2005). Hence, photoreceptors offer a valuable platform for examining the effects and isoform specificity of PDE inhibitors in a well-characterized model system.

PDE6 inhibitors are traditionally investigated together with trypsin-activated purified PDE6 (Wensel & Stryer, 1986; Catty & Deterre, 1991; Zhang *et al.*, 2005). In trypsin activation, the γ-subunits are degraded from the PDE6αβ, causing the permanent activation of the PDE6 enzyme that can be reversed only by the addition of substitutive γ-subunits (Wensel & Stryer, 1986). Furthermore, trypsin provokes the cleavage of the catalytic subunit C-terminal releasing the PDE6 from rod disk membranes and converting PDE6 to soluble form (Catty & Deterre, 1991). The mechanism of PDE6 inhibition has been investigated only with few inhibitors. Zaprinast, dipyridamole, and E4021 show classical competitive inhibition of trypsin activated PDE6 in biochemical studies (Gillespie & Beavo, 1989*b*; D'Amours *et al.*, 1999). Additionally, an electrophysiological study by Cobbs demonstrated that IBMX behaves as a competitive inhibitor of both light-activated and spontaneously active PDE6 (Cobbs, 1991). Zaprinast, dipyridamole, E4021, vardenafil, and sildenafil, but not IBMX, have also been found to stimulate the PDE6 holoenzyme activity with a high substrate and a low inhibitor concentration in addition to the regular competitive inhibition seen with higher inhibitor concentrations (Gillespie & Beavo, 1989*b*; D'Amours *et al.*, 1999; Zhang *et al.*, 2005). The phenomenon indicates that the inhibitor hinders the γ-subunit binding to the catalytic subunits more than it hinders the actual cGMP binding to the catalytic core, suggesting a complex competition between some inhibitors, cGMP and the γ-subunit for binding to the catalytic region.

The potency of inhibition of trypsin-activated PDE6 can exceed that of spontaneously active PDE6 (D'Amours *et al.*, 1999; Zhang *et al.*, 2005; Liu *et al.*, 2009). The inhibition constant of IBMX against spontaneously active PDE6 was found to be 3-fold larger than the inhibition constant against trypsin-activated PDE6. With vardenafil, the difference was over 11-fold and with E4021, as high as 40-fold. (D'Amours *et al.*, 1999; Zhang *et al.*, 2005) The difference in inhibiting trypsin-activated and spontaneously activated PDE6 can be largely explained by mutually exclusive competition between the γ-subunits and the PDE6 inhibitors. The inhibition constant determined from the trypsin-activated PDE6 represents the pure affinity of the inhibitor to the enzyme. In the spontaneously active state, the apparent inhibition constant reflects the combined effect of the inhibitor and the γ-subunit binding to the same active site. This interpretation is supported by the shared binding sites between the γ-subunit and PDE6 inhibitors. The γ-subunit has been shown to interact with multiple amino acid residues in the PDE6 catalytic domain, including Met759, Phe778, and Phe782, close to the active site, thereby closing the entrance of cGMP to the catalytic core (Granovsky & Artemyev, 2001*a*, 2001*b*; Cote, 2004). In molecular modeling, the PDE inhibitors zaprinast and sildenafil were demonstrated

to interact with Met759 and Phe778 in addition to the binding to the catalytic core, suggesting a direct competition from the same binding sites between the inhibitor and the γ-subunit (Simon *et al.*, 2006). Interestingly, in transducin-activated PDE6, only half of the subunits could be inhibited by vardenafil, and in spontaneously active PDE6, vardenafil could bind to only around 10% of the subunits (Liu *et al.*, 2009). These values correlated strongly with the percent of total hydrolytic activity of PDE6 in transducin-activated (38%) and spontaneously activated (∼10%) state compared to the fully active trypsin-activated PDE6 (100%) (Liu *et al.*, 2009). This implies that γ-subunit could completely block the binding of vardenafil to the catalytic region, letting vardenafil inhibit PDE6 only when the enzyme is active (Liu *et al.*, 2009). Overall, further investigations are needed in order to determine the mechanism of the interaction between transducin, the γ-subunit of PDE6, and different PDE6 inhibitors – research that can offer crucial knowledge when developing truly isoform-specific PDE inhibitors for a broad range of diseases (Maurice *et al.*, 2014; Ahmad *et al.*, 2015).

4. Aims of the study

The broad aim of this thesis was to investigate the calcium-mediated modulation of photoresponses of mouse rod photoreceptors. The first paper of the thesis quantified the effects of acknowledged calcium sensor proteins GCAPs and recoverin on mouse rod light adaptation but also discovered a new source of calcium-mediated modulation. The rest of the thesis delved into developing and utilizing methods to characterize the mechanism of this novel modulation. The specific aims were:

1. *To investigate the role of calcium and recoverin in the fast light adaptation in mice where the dominant GCAPs-mediated modulation is knocked out (Paper I).* Earlier data have shown that the mammalian rod light adaptation is dominated by calcium-dependent modulation of guanylate cyclase activity by GCAP1 and GCAP2. However, the contribution of other factors to mammalian rod light adaptation are not fully characterized. The goal of this work was to quantify the contribution of recoverin and other possible Ca^{2+}-feedback mechanisms in GCAPs-independent light adaptation of mammalian rod photoreceptors.

2. *To identify the applicability of transretinal ex vivo ERG in investigating the rod phototransduction cascade by comparing it to local ex vivo ERG recordings across the rod outer segment layer (Paper II).* Transretinal ERG (TERG) recorded *ex vivo* has been widely used in research on the phototransduction cascade because it enables examination of retinal function in the intact retina and pharmacological manipulation of retinal signaling. Phototransduction mechanisms are located in the outer segment of photoreceptors, and measuring the light-induced changes in the outer segment membrane current is the most powerful way of investigating phototransduction in intact cells. When the photoreceptor component of the TERG signal is pharmacologically isolated, the signal does arise mainly from the changes in the outer segment current, but components arising from the inner segment layer inevitably contribute to the recorded signal. This study aimed to clarify how consistently TERG reflects changes in the rod outer segment current signaling by comparing TERG to simultaneously recorded local ERG across the outer segment layer (LERG-OS). An additional aim was to develop the LERG-OS technique for further use in Papers III, IV, and V.

3. *To develop a method for the quantification of the inhibitory effect of phosphodiesterase-6 inhibitors against naturally activated forms of phosphodiesterase-6 in intact*

mouse retina (Paper III). The cyclic nucleotide phosphodiesterases in vertebrates hydrolyze the second messengers, cAMP and cGMP, and they are involved in practically every regulatory system in the body. Many of the PDE inhibitors are rather non-selective for different PDEs, and efficient quantitative methods to investigate the isoform-specificity of PDE inhibitors in natural environments are unavailable. Traditionally, the potency of PDE6 inhibitors is determined biochemically from purified PDE6, which is activated by trypsin. This treatment changes the structure of the enzyme and affects its interaction with the inhibitors. The study aimed to develop a method for determining the inhibition constant of PDE6 inhibitors against naturally occurring, light-activated and spontaneously activated forms of PDE6 inside intact photoreceptors in living retina. This knowledge was also crucial for achieving the aims of Papers IV and V.

4. *To develop an ex vivo ERG-based method for determining the basal PDE6 activity of rod photoreceptors (Paper IV).* The rate of spontaneous cGMP hydrolysis, i.e., the basal PDE6 activity (β_{dark}), sets the steady-state level and the turnover rate of cGMP. Hence, it is the main factor in setting the kinetics of photoresponse recovery, and the spatial propagation of cGMP concentration decrease during photoresponses. For amphibian photoreceptors, the determination of basal PDE6 activity is possible with a "3-isobutyl-1-methylxanthine (IBMX) jump" technique, but it is still not feasible with the more fragile mammalian photoreceptors. To date, there has been no means to determine the β_{dark} of wild-type mammalian photoreceptors. This work aimed to develop a method for the determination of β_{dark} in intact photoreceptors and determine for the first time the β_{dark} of wild-type mouse rod photoreceptors.

5. *To investigate whether calcium modulates the basal PDE6 activity in mouse rods and to quantify the effect of the possible modulation on rod sensitivity (Paper V).* Paper I discovered a new source of light adaptation in mouse rods, but the mechanism was unidentified. The novel light adaptation mechanism was found to be dependent on calcium but independent of GCAPs- or recoverin-mediated pathways. This work aimed to probe whether calcium modulates basal PDE6 activity and whether this modulation could explain the discovered new sensitivity regulation of mouse rod photoresponses.

5. Methods

5.1 *Ex vivo* electroretinography

Electroretinography (ERG) records light-induced changes in the extracellular field potentials generated in the retinal tissue. The spatial separation of ion influxes and effluxes through the cell membranes of retinal cells creates ion currents flowing in the resistive extracellular medium of the retina. The excitable cells in the retina are organized in highly structured and densely packaged layers, which leads to a high electrical resistivity of the extracellular space (Hagins *et al.*, 1970). High resistivity enables the generation of mass potential fields across the retina. The extracellular currents and potential differences within the retina are interconnected according to Ohms law

$$\Delta V(z,t) = \int r(z) i_z(z,t) dz \qquad (6)$$

where $r(z)$ is the resistivity (Ω·m) of the extracellular medium and $i_z(z,t)$ is the radial ionic current density (A/m^2). In a uniformly illuminated retina, the lateral ion currents cover less than 10% of the total currents in the photoreceptor layer of the retina (Penn & Hagins, 1969; Hagins *et al.*, 1970). In photoreceptors, the sinks of the circulating current lie in the photoreceptor outer segment layer and sources in the inner segment layer (Penn & Hagins, 1969; Hagins *et al.*, 1970). The absorption of light to the rod outer segments produces a change in the circulating current and a corresponding change in the extracellular voltage. The signal is synaptically transmitted to second- and third-order retinal neurons causing changes in their membrane currents, e.g., through glutamate receptor-mediated TRMP1 channel closure in bipolar cells (Koike *et al.*, 2010*a*, 2010*b*; Morgans *et al.*, 2010; Xu *et al.*, 2012). Many of these changes can be detected in the ERG recordings.

The ERG signal components are classified in two ways: based on the distinctive waveforms, which are separated in time, or based on the underlying signal components, which originate from different sources. The typical classification commonly used in clinical diagnostics, and in the study of retinal function, divides the ERG signal to the following waveforms: the a-wave is a fast waveform triggered soon after the light stimulus. The polarity of this component is often considered as negative because, in conventional corneal ERG recording, this component causes a negative shift in corneal recording electrode potential with respect to the potential of the reference electrode placed to a skin contact near the examined eye (Pugh *et al.*, 1998). The b-wave is a large-amplitude wave with positive polarity dominating the ERG signal after the fast a-wave. The slow positive c-wave peaks only after 2 to 10 s after the light stimulus onset. The d-wave is generated after the offset of the prolonged light stimulus. In addition to

these waves, oscillatory potentials superimpose with most of the b-wave (Wachtmeister, 1998). Fig. 5 presents the waveforms of the ERG signal.

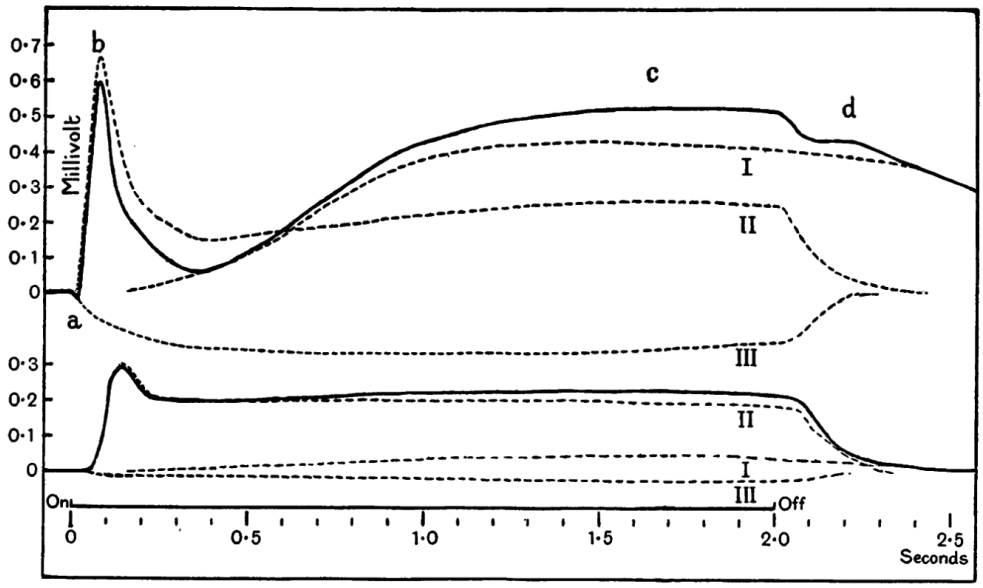

Figure 5. Cat ERG components (PI, PII, and PIII) and waveforms (a, b, c and d-waves) in response to a 2 s bright (above) and dim (below) light stimulus. Reprinted from (Granit, 1933) with permission from John Wiley & Sons, Inc.

When examining the sources of the ERG signal, it is practical to decompose the signal to its superimposed components. Ragnar Granit (Granit, 1933) dismantled the ERG signal to components based on their sensitivity to the depth of the anesthesia in a cat. The first signal component to disappear from the overall signal was termed PI, the second PII, and the last surviving component PIII. The PIII component was later divided into fast PIII and slow PIII based on the signal kinetics (Murakami & Kaneko, 1966; Sillman *et al.*, 1969). It is now known that these signal components originate in specific retinal layers. The PI component, which corresponds mainly to the ERG c-wave, originates from the changes in the extracellular potassium flux to retinal pigment epithelium due to light illumination (Steinberg *et al.*, 1970; Oakley, 1977). The PII component, comprising the central part of the b-wave, has been shown to arise from the function of bipolar cells (Pugh *et al.*, 1998). The fast PIII component is generated in the photoreceptors and the slow PIII in the Müller cells (Penn & Hagins, 1969; Oakley *et al.*, 1992; Pugh *et al.*, 1998). The ERG components are illustrated in Fig. 5. The photoreceptor component (fast PIII) in the ERG signal is mostly masked under the more prominent PI, PII, and slow PIII components. Consequently, an effective way to investigate the function of photoreceptors and phototransduction is to isolate the photoreceptor component from the mixed signal.

In our *ex vivo* methods, the ERG signals are registered from an isolated retina, which is kept alive in a specific sample holder. *Ex vivo* ERG allows the isolation of the photoreceptor component by two different means: pharmacologically in transretinal ERG, or spatially with local ERG. These techniques are discussed below.

5.1.1 Transretinal electroretinography

Transretinal ERG (TERG) is an *ex vivo* ERG technique where the ERG signal is registered across the whole retina with macroelectrodes placed on the distal and proximal sides of the isolated retina. The recording geometry is illustrated in Fig. 6A. A constant flow of nutrition solution perfuses the photoreceptor side of the retina, which also allows the delivery of drugs to the retina. The different cell types of the retina contribute to the TERG signal, and extraction of the photoreceptor signal is necessary when investigating phototransduction. This can be achieved by blocking the glutamatergic synaptic transmission from photoreceptors to bipolar cells, e.g., with glutamate receptor agonist aspartate or with glutamate receptor antagonist DL-2-amino-4-phosphonobutyric acid (APB) (Slaughter & Miller, 1981; Vinberg *et al.*, 2009, 2014). In addition, the component arising from Müller cells (slow PIII) can be abolished by blocking the potassium channels in the Müller cell membrane with $BaCl_2$ (Bolnick *et al.*, 1979; Nymark *et al.*, 2005). The remaining signal arises exclusively from photoreceptor cells. Fig. 6B introduces the TERG signal to varying light flash stimuli without blockers and Fig. 6C shows the isolated photoreceptor component of TERG (see also Fig. 3 in Paper II). The TERG technique provides unparalleled signal-to-noise ratio, stability, and maximal duration of experiments compared to the more widespread single-cell techniques, suction electrode recordings and patch-clamp. Hence, TERG has been routinely used to examine photoreceptor signaling and phototransduction (Nymark *et al.*, 2005; Heikkinen *et al.*, 2008; Palczewska *et al.*, 2014; Berry *et al.*, 2016; Vinberg *et al.*, 2017). However, despite the use of pharmacological isolation of the photoreceptor component from the TERG signal, imperfect pharmacological blocking or the presence of signal components originating in the photoreceptor inner segment region may shape the TERG signal. The changes in the extracellular voltage are proportional to the changes in the superimposed extracellular currents, and the cell membrane potential affects the extracellular voltage indirectly by modulating voltage-gated channel currents. The distribution, selectivity, and regulation of the voltage-gated ion channels in the inner segment and their contribution to the ERG signal are partly unknown, which complicates the quantitative interpretation of the TERG signal when the goal is to investigate the phototransduction. At least HCN1 channels located in the rod inner segment are thought to modify the photoreceptor component of the TERG signal (Vinberg *et al.*, 2009). Additionally, a transient capacitive component originating in the inner segment of rods seems to play a role in generating the "nose" like appearance in the leading edge of the TERG responses to intense flashes of light (Robson & Frishman, 2014).

5.1.2 Local electroretinography

In local electroretinography from isolated retinas, the extracellular voltage is recorded with microelectrodes whose tips are inserted to desired retinal depths (Fig. 6A). The current flowing through the rod outer segment CNG channels is independent of the membrane potential over the physiological range in salamander rods (Baylor & Nunn, 1986) and has only a subtle voltage dependence in pig rods (Cia *et al.*, 2005). Hence, accurate information on the changes in the intracellular cGMP concentration, and thus on the phototransduction cascade, can be obtained by recording light-induced changes in the circulating current. However, a recent study shows that the CNG channels in mouse cones have a small but clear current-voltage dependence in the physiological range of membrane potentials (Ingram *et al.*, 2020). Recording of the circulating current is most commonly realized with the suction electrode technique

where the inner or the outer segment of the photoreceptor is gently sucked into a glass pipette. The recording geometry forces the extracellular current flowing from the inner segment to the outer segment to pass through the recording electronics (Baylor *et al.*, 1979*b*). Since there are no other light-dependent current sinks or sources in the photoreceptor outer segments than the CNG channels, the extracellular voltage changes across the rod outer segment layer are practically directly proportional to the changes in the circulating current. The membrane capacitance of the outer segment functions as a low pass filter for the extracellular voltage signal with approximately 1 ms time constant. This may have a small effect on the leading edge of the responses to strong saturating flashes of light (Cideciyan & Jacobson, 1996; Smith & Lamb, 1997; Robson & Frishman, 2014). Overall, it is possible to get quantitative information about the phototransduction cascade by recording local ERG across the photoreceptor outer segment layer (LERG-OS) (Hagins *et al.*, 1970; Pugh *et al.*, 1998).

The relationship between the circulating current and the LERG-OS signal can be calculated based on Eq. 6. The extracellular current density in the photoreceptor layer is at its maximum near the cilium, and it decreases quite linearly towards the distal end of the outer segment (Hagins *et al.*, 1970). Hence, with 20 pA circulating dark current produced by a single rod and with a rod density of 437,000 rod/mm^2, the extracellular current density in the cilium region is 8.7 pA/µm^2. The average current density along the 24 µm length of the average photoreceptor outer segment is half of this, i.e., 4.4 pA/µm^2 (Hagins *et al.*, 1970; Liang *et al.*, 2004; Rakshit *et al.*, 2017). The resistivity along the photoreceptor outer segment layer has been determined to around 1 MΩ·µm for rat retina (Penn & Hagins, 1969; Hagins *et al.*, 1970), while a substantially larger value of ca. 20 MΩ·µm was determined from rabbit eyecup (Karwoski & Xu, 1999). Consequently, the voltage drop along the photoreceptor outer segment layer calculated with the above values would be close to 100 µV and 2 mV, respectively. The voltage drop should correspond to the maximal extracellular voltage change that can be induced with bright light closing all the CNG channels. The relationship of the outer segment current and voltage is further discussed in (Penn & Hagins, 1969; Hagins *et al.*, 1970; Arden, 1976; Pugh *et al.*, 1998) and in Paper II of this thesis.

When investigating phototransduction, LERG-OS recordings should provide good correspondence with the signals recorded by the suction electrode technique, but additionally, allow pharmacological manipulation of the retina. LERG-OS is free from the inner segment contributions to the recorded signal, which makes the quantitative analysis more trustworthy compared to TERG. On the other hand, the signal-to-noise ratio and the stability of the signal during the experiments are inferior with LERG-OS compared to TERG. Lower signal-to-noise ratios result mainly from the larger resistance of the recording electrode and the mechanical disturbance to the cells by the microelectrode inserted into the retina. Figs. 6D and E display flash responses recorded with local ERG across the whole photoreceptor layer and across the photoreceptor outer segment layer, respectively.

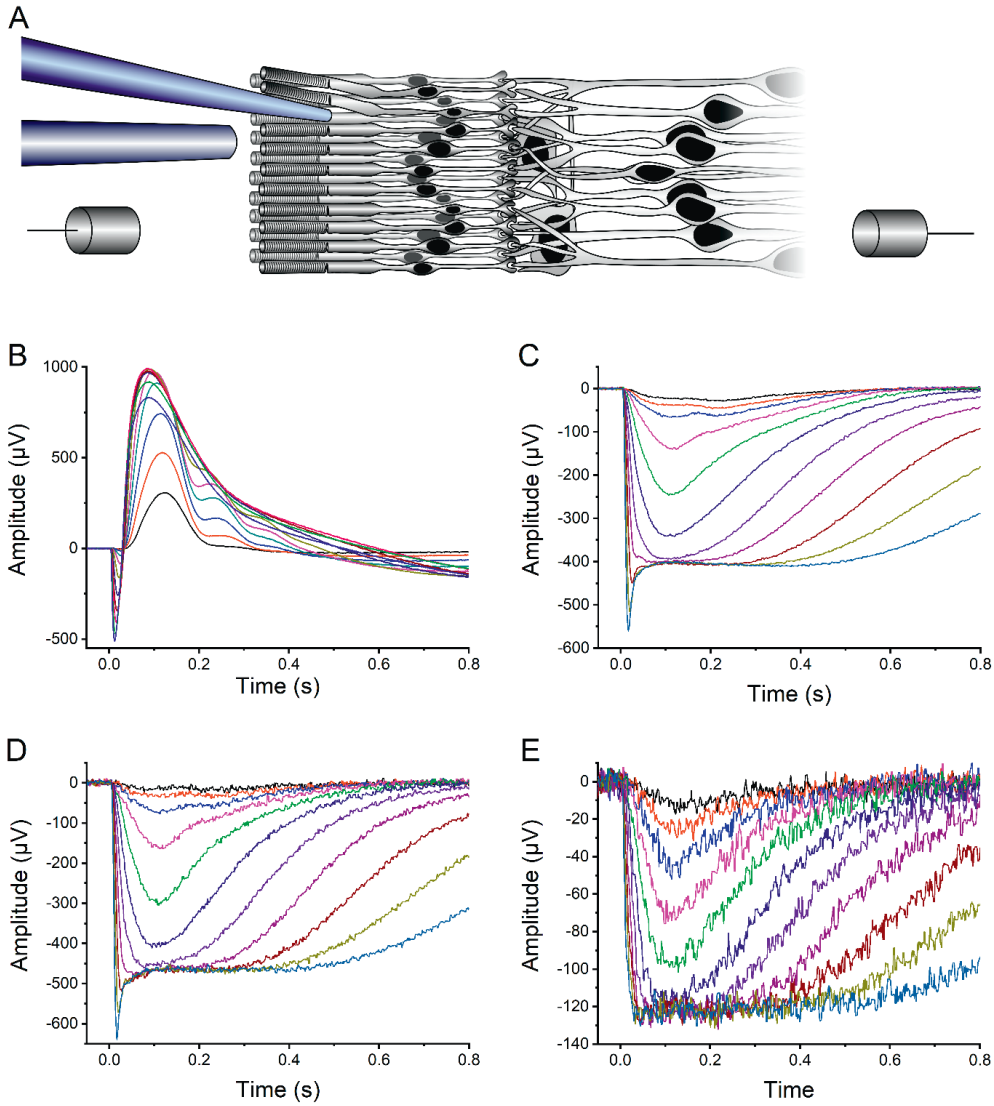

Figure 6. A) Recording geometries for two *ex vivo* ERG techniques: transretinal ERG (TERG) and local ERG (LERG). TERG was recorded with two macroelectrodes placed on both sides of the retina (gray cylinders). LERG was recorded across the desired retinal layers with two microelectrodes (blue pipettes). The figure shows the LERG-OS geometry where the recording electrode is placed near the proximal ends of the rod outer segments, and the reference electrode is left at the distal surface of the retina. The amacrine and ganglion cell layers are disregarded in the figure. B – E) Flash response families collected in different *ex vivo* ERG geometries with increasing response strengths covering the whole operation range of rods B) TERG response family without pharmacological blockers. C) Pharmacologically isolated photoreceptor response family recorded with TERG. D) Response family recorded by LERG across the photoreceptor layer (LERG-PR) E) LERG-OS response family.

5.2 Experimental methods

5.2.1 Ethical approval

The use and handling of the animals were in accordance with the Finland Animal Welfare Act 2006, guidelines of the Animal Experiment Board in Finland, and with the Directive 2010/63/EU of the European Parliament and of the Council of 22 September 2010 on the protection of animals used for scientific purposes.

5.2.2 Animals, preparations and measurement conditions

Wild type (C57BL/6J), GCAPs$^{-/-}$, and GCAPs$^{-/-}$ recoverin$^{-/-}$ mice (kindly provided by J. Chen, University of Southern California, Los Angeles, CA; Mendez et al., 2001) of both sexes were used in these studies. Mice were housed at 24 °C and kept under 12/12 hour light-dark cycle. They were dark-adapted overnight before the experiment day, and euthanized by CO_2 inhalation and cervical dislocation 4 – 6 hours after the usual time of light onset. The eyes were enucleated and bisected along the equator with micro-scissors, and the eyecups were placed in a cooled nutrition solution. The retina was isolated from one eyecup under a microscope with the help of micro-scissors and forceps. The isolated retina was placed in a recording chamber inside a light protective Faraday cage while the other eyecup was stored (to be used later on the same day) at +7 °C in a light-tight container filled with a nutrition solution. All procedures were conducted under dim red light.

The recording chamber allowed stimulation and perfusion of the retina, and the recording of TERG and LERG simultaneously or individually. The recording chamber was developed based on the specimen holder introduced in (Donner *et al.*, 1988). The recording chamber for LERG recordings contained a passage for two microelectrodes into the retina and optical pathway for visualization of the retinal surface with a bottom view microscope. The isolated retina was placed on a filter paper photoreceptors facing upwards, and the retina was held in place by gently clamping the rim of the retina between two accurately fitted polycarbonate pieces. The electrical connection around the edges of the retina was minimized with a rubber seal and vacuum grease.

The photoreceptor side of the retina was perfused with a constant flow of nutrition solution (*ca*. 3 ml/min). The retina was perfused either with HEPES buffered or bicarbonate buffered solutions. The composition of the HEPES buffered solution was (mM): Na^+, 133.4; K^+, 3.3; Mg^{2+}, 2.0; Ca^{2+}, 1.0; Cl^-, 143.2; glucose, 10.0; EDTA, 0.01; HEPES, 12.0. The composition of the bicarbonate buffered solution was (mM) Na^+, 124.3; K^+, 3.3; Mg^{2+}, 2.0; Ca^{2+}, 1.0; Cl^-, 133.6; glucose, 10.0; EDTA, 0.01; HEPES, 10.0; NaOH, 4.8; $NaHCO_3$, 20. Both solutions contained 0.72 mg/ml Leibovitz culture solution L-15 to improve the viability of the retina. Synaptic transmission to bipolar cells was blocked with 20 µM APB in bicarbonate-buffered solution and with 2 mM sodium aspartate in HEPES-buffered solution (Nymark *et al.*, 2005). The slow PIII component arising from Müller cells was abolished by adding 50 µM $BaCl_2$ to the solutions (Bolnick *et al.*, 1979; Nymark *et al.*, 2005). These substances had little or no effect on the LERG signal at the concentrations used (see Paper II). To examine the effect of calcium on photoresponses, a solution with extremely low calcium ion concentration, referred to as a low Ca^{2+} solution, was prepared. The total calcium concentration was adjusted to 100 µM (including 66 µM calcium from the 0.72 mg/ml L-15 supplement), and the free calcium concentration was dropped to

~20 nM with 3.4 mM EGTA calculated with an "EGTA calculator". (Portzehl *et al.*, 1964; Vinberg *et al.*, 2015*a*). The pH of all solutions was adjusted to 7.5 with 5.8 mM NaOH. In addition, phototransduction was manipulated with PDE6 inhibitors: sildenafil, zaprinast, and 3-isobutyl-1-methylxanthine (IBMX). All chemicals used in these studies were purchased from Sigma-Aldrich (Espoo, Finland).

Recordings were conducted at physiological temperature 37 ± 1 °C. The recording chamber was placed on top of a heat exchanger whose temperature could be controlled with a water circulating heat bath (LTD6G; Grant Instruments Ltd, Shepreth, Royston, UK). The temperature was monitored with a calibrated thermistor (30K6A309I; BetaTHERM; Measurement Specialties, Inc., Hampton, VA, USA). The perfusion solution was connected to the signal ground through a 4.7 µF capacitor, which let high-frequency noise pass to the ground.

5.2.3 Recordings and light stimulation

Transretinal electroretinography

Transretinal voltage was recorded across the whole retina with Ag/AgCl pellet electrodes (EP2; WPI). The proximal side of the retina was connected to the electrode space through a small hole under the retina and the filter paper. The electrode space on the distal side of the retina was connected to the perfusion solution channel, and hence to the photoreceptor side of the retina, through a narrow passage. Both electrode spaces were filled with a chloride solution containing 115 mM Na^+, 122.3 mM Cl^-, 3.3 mM K^+, and 2.0 mM Mg^{2+}.

Local electroretinography

Local electroretinography entailed recording across the photoreceptor outer segment layer or across the whole photoreceptor layer with microelectrodes (as described in Paper II). Microelectrodes were pulled from glass capillaries (WPI TW100-6; EP2; World Precision Instruments Ltd [WPI], Hitchin, UK) with a micropipette puller (Model P-97; Shutter Instrument Co., Novate, CA, USA), filled with 5.3 w% sodium chloride solution, and connected to an Ag/AgCl pellet electrode (EP2; WPI). The reference electrode (tip size ~ 30 µm) was moved to the proximity of the surface of the retina with a micromanipulator (MR 471843; Carl Zeiss AG, Oberkochen, Germany). The recording electrode (tip size 2 – 5 µm) was inserted to a depth of 20 – 30 µm in the retina in LERG-OS recordings and to a depth of ~ 100 µm in LERG-PR recordings with a micromanipulator (MC-35A, 0.2 µm resolution; Narishige International Ltd., London, UK) in an angle of 30° to the retinal surface. The surface of the retina was identified visually or from the voltage change in the oscilloscope when the electrode penetrated the retina. Simultaneous TERG was recorded along with LERG to monitor the general viability of the photoreceptors and the retina.

Light stimulation

The stimulus light arrived in the recording chamber parallel to the axis of photoreceptor cells. The stimulation was accomplished either with two laser sources: 532 nm laser diode module (IQ5C (532-100)L74; Power Technology Inc., Little Rock, AR, USA) and 633 nm HeNe laser (25 LHR 151; Melles Griot, Carlsbad, CA, USA) or with two similar LED light sources (Luxeon Rebel LXML-PM01-0100, λmax = 532 nm; Lumileds, Amsterdam, the Netherlands). The stimulus illu-

minated the whole retina homogeneously, which was verified with a camera-based beam profiler (Model SP503U; Spiricon Laser Beam Diagnostics, Ophir-Spiricon Inc., Logan, UT, USA). The absolute light intensity incident on the retina was measured with a calibrated photodiode (FDS100-cal; Thorlabs GmbH, Newton, NJ, USA, or with HUV-1000B; EG&G, URS Corporation, Gaithersburg, MD, USA). The number of rhodopsin photoisomerizations in rod photoreceptors (R^*rod^{-1} or $R^*rod^{-1}s^{-1}$) caused by the stimulus was calculated based on the rod outer segments dimensions (Ø = 1.4 µm, l = 24 µm), the LED/laser emission spectrum, the photodiode spectral sensitivity curve, and the pigment template (Govardovskii *et al.*, 2000) as described in (Heikkinen *et al.*, 2008).

Additionally, a proportional-integral-derivative (PID) controlled feedback loop from the recorded voltage signal to the light source was developed for cGMP clamp experiments (see Paper IV). In cGMP clamp, the PID controller keeps the recorded signal constant by adjusting background light strength after the introduction of the PDE6 inhibitor to the retina. This closed-loop light control was carried out digitally in LabVIEW. The PID controlled background light feedback was utilized in Papers IV and V.

5.2.4 Data collection

Data acquisition and light stimulus controls were handled with a data acquisition card (PCIe-6351 or PCI-6024E; National Instruments, Austin, TX, USA) and custom made LabVIEW or LabWindows software. The recorded DC signals were amplified 1000-fold and sampled at 1000 Hz in one or two recording channels. Signals were first low-pass filtered with f_c = 500 Hz (8-pole Bessel filter) and, in most cases, filtered digitally with f_c = 100 Hz afterward to increase the signal-to-noise ratio.

5.3 Modeling

This thesis aimed to develop and modify existing phototransduction models to determine phototransduction parameters, and to investigate the effect of PDE6 inhibitors and calcium concentration on LERG-OS photoresponses. The models were constructed based on the theoretical background introduced and discussed thoroughly in (Pugh & Lamb, 2000). The following section describes the framework of the utilized models and introduces new insights and examines their validity.

5.3.1 Activation model

The Lamb and Pugh activation model quantifies the activation steps in phototransduction, and it can be used to determine the overall gain in the phototransduction cascade (Lamb & Pugh, 1992). The model assumes that at times considerably after the time constant for rhodopsin activation (0.1 ms, Penn & Hagins, 1972), the number of activated rhodopsin molecules R* in a rod photoreceptor increases stepwise after a brief stimulus with a flash strength of Φ. The molecules in the rod disk membrane are in constant Brownian motion resulting in molecular encounters. Rhodopsin activates transducin molecules at an approximately constant rate. The activated transducins bind to PDE6 γ-subunits, each assumed to activate one of the two catalytic PDE6 subunits. The rate constant by which rhodopsin activation leads to the activation of

PDE6 is denoted ν_{RE}. The number of activated PDE6 subunits after a flash stimulus can be expressed by a ramp function

$$PDE6^*(t) = \Phi\nu_{RE}(t - t_{RGE}), \tag{7}$$

where t_{RGE} denotes the combined time delay from rhodopsin activation to the activation of PDE6. The activated PDE6 enzyme starts to hydrolyze its substrate molecules, cGMPs. In the total cytoplasmic space, the cGMP concentration decreases according to Michaelis-Menten relation

$$\frac{d[cGMP](t)}{dt} = -PDE6^*(t)\frac{½k_{cat}}{N_A V_{cyto} B_{cGMP}} \cdot \frac{[cGMP](t)}{[cGMP](t)+K_M} \tag{8}$$

where $½k_{cat}$ is the average turnover rate of one activated PDE6 subunit, N_A is Avogadro's number, V_{cyto} is the rod outer segment cytoplasmic volume, B_{cGMP} is the cGMP buffer capacity in rod outer segments, and K_M is the Michaelis constant for the cGMP hydrolysis by PDE6 (Pugh & Lamb, 2000).

The Lamb and Pugh activation model assumes that cytoplasmic $cGMP$ concentration is always substantially smaller than K_M. With this assumption, Eq. 8 simplifies to

$$\frac{d[cGMP](t)}{dt} = -PDE6^*(t)\frac{½k_{cat}/K_M}{N_A V_{cyto} B_{cGMP}}[cGMP](t). \tag{9}$$

The implication of this assumption is considered in Section 5.3.6 and in the supplementary material of Paper V. Eq. 9 can be presented in the form

$$\frac{d[cGMP](t)}{dt} = -PDE6^*(t)\beta_{sub}[cGMP](t), \tag{10}$$

where β_{sub} is the average rate of cGMP hydrolysis catalyzed by one active PDE6 subunit. This equation simplifies further to

$$\frac{d[cGMP](t)}{dt} = -\beta_{light}[cGMP](t). \tag{11}$$

where β_{light} presents the light-induced PDE6 activity.

In addition to light-activated PDE6, cGMP concentration is regulated by the rate of cGMP synthesis α and the hydrolysis by basal PDE6 activity β_{dark},

$$\frac{d[cGMP](t)}{dt} = \alpha - \left(\beta_{dark} + \beta_{light}\right)[cGMP](t). \tag{12}$$

During times early enough after a flash stimulus, the cGMP concentration and the rate of cGMP synthesis are still unmodulated from their dark-adapted values, $[cGMP]_{dark}$ and α_{dark}, respectively. Additionally, the cGMP synthesis is in balance with the rate of cGMP hydrolysis in darkness

$$\alpha_{dark} = \beta_{dark}[cGMP]_{dark}. \tag{13}$$

At these times, Eq. 12 simplifies to Eq. 11, which has the following solution:

$$\frac{[cGMP](t)}{[cGMP]_{dark}} = e^{-½\Phi\nu_{RE}\beta_{sub}(t-t_{RGE})^2}. \quad (14)$$

The cation current through the CNG channels in the rod outer segment is directly proportional to the number of open CNG channels. Hence, CNG channel current obeys the same Hill equation as in Eq. 1 for channel open probability

$$\frac{J_{cG}}{J_{cG,max}} = \frac{[cGMP]^{n_{cGMP}}}{[cGMP]^{n_{cGMP}} + K_{cGMP}{}^{n_{cGMP}}}. \quad (15)$$

Here J_{cG} denotes the current through CNG channels, $J_{cG,max}$ denotes the maximal current when all the CNG channels are open, and n_{cGMP} represents the cooperativity of the cGMP binding sites in the CNG channels (Lamb & Pugh, 1992). The value of n_{cGMP} is considered to be close to 3 in vertebrate rod photoreceptors (Pugh & Lamb, 2000; Gross *et al.*, 2012*a*; Lamb & Kraft, 2016). The cGMP concentration leading to half-maximal channel opening, K_{cGMP}, is always substantially larger than the cGMP level in physiological conditions (Pugh & Lamb, 2000). Thereby, Eq. 15 simplifies to

$$\frac{J_{cG}(t)}{J_{dark}} \approx \left(\frac{[cGMP](t)}{[cGMP]_{dark}}\right)^{n_{cGMP}}, \quad (16)$$

where J_{dark} is the value of circulating current through the CNG channels in darkness. The circulating current $J_{cG}(t)$ follows the Ohmic relation with the voltage drop in the extracellular space across the rod outer segments. The LERG-OS signal amplitude, $r(t)$, normalized by the LERG-OS signal saturation level, r_{max}, can be considered to follow

$$\frac{r(t)}{r_{max}} \approx 1 - \left(\frac{[cGMP](t)}{[cGMP]_{dark}}\right)^{n_{cGMP}}. \quad (17)$$

Combining Eqs. 14 and 17 yields the Lamb and Pugh activation model that can be used to quantify the phototransduction amplification constant from LERG-OS responses.

$$\frac{r(t)}{r_{max}} = 1 - e^{-½\Phi A(t-t_d)^2}, \quad (18)$$

where the amplification constant, A, is

$$A = \nu_{RE}\beta_{sub}n_{cGMP} \quad (19)$$

and t_d is the combined delay from the recording equipment and from the phototransduction (t_{RGE}).

The Lamb and Pugh activation model does not consider the deactivation reactions of phototransduction. Hence, the model fits only the early phase of the responses after a flash stimulus.

5.3.2 Model for response onset including deactivation of rhodopsin and PDE6

In mouse rods, the average lifetime of activated rhodopsin has been estimated to be 40 ms (Gross & Burns, 2010). Assuming first-order deactivation kinetics, the number of activated rhodopsin molecules has decreased by 10% already at 4 ms after the flash stimulus. The difference between the photoresponse trace and the activation model fit increases the further

the two are compared after the moment of the flash stimulus. An expanded form of the activation model, developed in this thesis, takes into account the deactivation of activated rhodopsin and PDE6 in order to increase the valid time range for the fit. The model assumed that the number of activated rhodopsins decay with first-order reaction kinetics

$$R^*(t) = \Phi e^{-\frac{t}{\tau_R}}, \tag{20}$$

where Φ is the number of activated rhodopsins produced by the stimulus flash and τ_R is the average lifetime of activated rhodopsin. Also, PDE6 activation can be assumed to decay with first-order reaction kinetics and thus, the total PDE6 activity due to a light stimulus can be solved from a convolution

$$PDE6^*(t) = \Phi e^{-\frac{t}{\tau_R}} * \nu_{RE} e^{-\frac{t}{\tau_{PDE}}} \tag{21}$$

where τ_{PDE} is the average lifetime of activated PDE6 subunit. Adding the terms from the deactivation of activated rhodopsin and PDE6 to Eq. 10, the light-induced change in the cGMP hydrolysis is

$$\frac{dcGMP(t)}{dt} = -\beta_{light} cGMP(t) = -\Phi e^{-\frac{t}{\tau_R}} * \nu_{RE} e^{-\frac{t}{\tau_{PDE}}} \beta_{sub} cGMP(t). \tag{22}$$

By taking the deactivation reactions into account, the range of model validity can be extended in order to estimate the amplification constant A and the activated rhodopsin lifetime τ_R in mouse rods without foreknowledge on basal PDE6 or guanylate cyclase activity. Eq. 22 can be solved numerically and converted to relative LERG-OS voltage according to Eq. 17. The lifetime of activated PDE6, τ_{PDE}, can be determined from the flash responses by Pepperberg analysis (Pepperberg *et al.*, 1992; Krispel *et al.*, 2006; Invergo *et al.*, 2013).

5.3.3 Model for the entire flash responses

Eq. 12 takes into account the basal and the light-induced rate of cGMP hydrolysis and the rate of cGMP synthesis. To model the entire flash response trace, the relative change in the cGMP concentration can be solved from Eq. 12 numerically, and the result can be converted to LERG-OS voltage change according to Eq. 17. β_{light} can be calculated based on the Eq. 22. This thesis disregarded the calcium-mediated modulations of phototransduction in the modeling. Hence, the model is valid for flash responses with insignificant or abolished calcium-mediated modulation. Papers IV and V modeled entire dim flash responses recorded using LERG-OS from GCAPs$^{-/-}$ and GCAPs$^{-/-}$ recoverin$^{-/-}$ mouse retinas where the calcium regulation during flash responses should play only a minor role (Burns *et al.*, 2002).

5.3.4 Inhibition of light-activated and spontaneously activated PDE6

Paper III describes novel methods to determine the inhibition constants against naturally occurring activated forms of PDE6, both light-activated PDE6 ($K_{I,light}$) and spontaneously active PDE6 ($K_{I,dark}$), using electroretinography from intact isolated mouse retinas. These inhibition constants were further used in the cGMP clamp paradigm (Papers IV and V).

Inhibition of light-activated PDE6

The determination of $K_{I,light}$ is based on the ability of PDE6 inhibitors to decrease the hydrolytic rate of light-activated PDE6. When a competitive PDE6 inhibitor, I, is introduced to the retina, it will reduce the hydrolytic rate of cGMP according to the equation

$$\beta_{sub,I} = \frac{\beta_{sub}}{1+\frac{[I]}{K_{I,light}}}, \tag{23}$$

where $\beta_{sub,I}$ is the rate constant of cGMP hydrolysis in the presence of the inhibitor. The reduction of the PDE6 hydrolytic activity leads to a decrease in molecular amplification of phototransduction, which can be quantified as a decrease in the amplification constant.

$$A_I = \nu_{RE}\beta_{sub,I}n_{cGMP} = \nu_{RE}\left(\frac{\beta_{sub}}{1+\frac{[I]}{K_{I,light}}}\right)n_{cGMP}. \tag{24}$$

The ratio of amplification constants without ($A_{control}$) and in the presence of the inhibitor (A_I) gives a linear equation that can be used to determine the inhibition constant for PDE6 inhibitors against light-activated PDE6

$$\frac{A_{control}}{A_I} = \frac{[I]}{K_{I,light}} + 1. \tag{25}$$

Inhibition of spontaneously activated PDE6

In addition to light-activated PDE6, the introduction of a PDE6 inhibitor reduces the basal PDE6 activity. The decreased basal level of cGMP hydrolysis causes an increase in the intracellular cGMP concentration. In wild type animals, the increase in the cGMP concentration will lead to an increase in calcium influx into the rod outer segment, which in turn will decrease the guanylate cyclase activity through GCAPs. The resulting reduction in the rate of cGMP synthesis will largely compensate for the inhibitor-induced decrease in cGMP hydrolysis (Zhang *et al.*, 2005). However, in GCAPs$^{-/-}$ mice, the guanylate cyclase activity is locked to its dark value α_{dark} and no such compensation can arise. For GCAPs$^{-/-}$ mouse rods in steady-state in darkness,

$$\frac{d[cGMP]}{dt} = \alpha_{dark} - \beta_{dark}[cGMP]_{dark} = \alpha_{dark} - \beta_{dark,I}[cGMP]_{dark,I} = 0. \tag{26}$$

For a competitive PDE6 inhibitor, solving Eq. 26 gives

$$\frac{[cGMP]_{dark,I}}{[cGMP]_{dark}} = \frac{\beta_{dark}}{\beta_{dark,I}} = 1 + \frac{[I]}{K_{I,dark}}. \tag{27}$$

The relative change in the extracellular voltage across the rod outer segment layer is proportional to the relative change in the intracellular cGMP concentration raised to the power of the Hill coefficient for CNG channels, as shown in Eq 17. Hence, $K_{I,dark}$ can be determined from the relation

$$\left(\frac{r_{max,I}}{r_{max,control}}\right)^{1/n_{cGMP}} = 1 + \frac{[I]}{K_{I,dark}}, \tag{28}$$

where $r_{max,control}$ and $r_{max,I}$ presents the maximal LERG-OS voltage suppressible by light in the absence and the presence of the inhibitor, respectively. Hence, Eq. 28 provides a way to determine the $K_{I,dark}$ by recording the inhibitor-induced increase in maximal LERG-OS response amplitudes.

5.3.5 cGMP clamp

The introduction of a PDE6 inhibitor can decrease the basal PDE6 activity, which should manifest itself as an elevation in the intracellular cGMP concentration. The elevation can be compensated by increasing PDE6 activity with light. By adding just the right amount of light, the circulating current and the cGMP concentration can be clamped to their dark values. Hence, in the presence of the PDE6 inhibitor and the compensating amount of light, one can derive

$$\frac{d[cGMP]}{dt} = \alpha_{dark} - \left(\frac{\beta_{dark}}{1+\frac{[I]}{K_{I,dark}}} + \frac{\beta_{light}}{1+\frac{[I]}{K_{I,light}}} \right) [cGMP]_{dark} = 0, \quad (29)$$

where the $1/\left(1+\frac{[I]}{K_I}\right)$ denotes the decrease of PDE6 activity due to the introduction of competitive PDE6 inhibitor, and β_{light} stands for the increment in the PDE6 activity due to compensating light. $[I]$ is the inhibitor concentration, and $K_{I,dark}$ and $K_{I,light}$ are the inhibition constants against spontaneously active and light-activated PDE6, respectively. Combining Eqs. 26 and 29 gives a formula, that can be used to determine the value for β_{dark}

$$\beta_{dark} = \beta_{light} \frac{1+\frac{K_{I,dark}}{[I]}}{1+\frac{[I]}{K_{I,light}}}. \quad (30)$$

If $K_{I,dark}$ and $K_{I,light}$ are equal, the Eq. 30 simplifies to a form

$$\beta_{dark} = \beta_{light} \frac{K_I}{[I]}. \quad (31)$$

β_{light} in the presence of steady light can be calculated using the derived phototransduction parameters and the amount of light Φ_{BG} needed to clamp [cGMP] to its dark state value

$$\beta_{light} = \Phi_{BG} \frac{A\tau_R\tau_{PDE}}{n_{cGMP}}. \quad (32)$$

5.3.6 Modeling assumptions and their justifications

The models used in this thesis are based on the assumption that activated rhodopsin and PDE6 deactivate through first-order reactions. In addition, the hydrolytic activity of PDE6 is assumed to behave linearly in relation to intracellular cGMP concentration, while the CNG channel open probability assumed to be proportional to the third power cGMP concentration. The reacting molecules are thought to be thoroughly mixed and diffusing freely in the rod outer segment disk membranes and in the rod cytoplasm. The concentrations of the reacting molecules, excluding cGMP, are not expected to change significantly during the photoresponses. These simplifications are not all accurate, but they allow reducing the number of free parameters in the models. The next section considers the implications and justification of these assumptions.

Exponential deactivation of rhodopsin

According to first-order reaction kinetics, rhodopsin activity decays exponentially, and the deactivation occurs without intermediate states. After the average rhodopsin lifetime, τ_R, each of the activated rhodopsin molecules has e^{-1} (~37%) probability of being still active. However, there is convincing evidence that the probability for arrestin binding and complete deactivation of rhodopsin increases stepwise with rhodopsin phosphorylations (Wilden *et al.*, 1986; Xu *et al.*, 1997; Gibson *et al.*, 2000; Mendez *et al.*, 2000; Arshavsky, 2002; Hamer *et al.*, 2003; Doan *et al.*, 2006; Vishnivetskiy *et al.*, 2007; Gross *et al.*, 2012*b*; Berry *et al.*, 2016). Additionally, the phosphorylation of rhodopsin seems to decrease rhodopsin activity in a graded fashion (explained in more detail in Section 3.3.3). The assumption of graded rhodopsin shut-off leads to a near exponential decline in total rhodopsin activity (see Fig. 2 from Lamb & Kraft, 2016 and Fig. S2C from Gross *et al.*, 2012*b*). Therefore, the assumption that the rhodopsin deactivation follows first-order reaction kinetics should not cause a substantial error in the modeling of flash responses. However, Lamb and Kraft (2016) suggested an alternative model to explain their experimental results with arrestin and rhodopsin kinase mutant mice (Lamb & Kraft, 2016). In the model, rhodopsin has to enter a low-activity state before it can bind arrestin and deactivate. Rhodopsin stays fully active until several phosphorylations cause an abrupt decline in its activity. This results in a delay before rhodopsin activity starts to decline in contrast to the exponential model, where deactivation starts immediately (see Fig. 4 in Lamb & Kraft, 2016). If the latter model is more accurate, using the exponential model might cause a small overestimation of the number of rhodopsin activations or the phototransduction gain when modeling flash responses. The impact of assuming the first-order deactivation of rhodopsin on response modeling and cGMP clamp is discussed further in Paper IV.

Assumption: $K_{cGMP} >> [cGMP]$

The opening probability of the CNG channels can be assumed to be proportional to the intracellular cGMP concentration raised to the power of the Hill coefficient for the CNG channels (see Eq. 1). This assumption holds when ${K_{cGMP}}^{n_{cGMP}} \gg [cGMP]^{n_{cGMP}}$. The estimates for cGMP concentration leading to a half-maximal CNG channel opening (K_{cGMP}) vary between 30 and 165 µM (see Section 3.2) and the value of 20 µM has been previously used for modeling (Pugh & Lamb, 2000; Shen *et al.*, 2010; Lamb *et al.*, 2018). With K_{cGMP} of 20 µM, n_{cGMP} of 3 and $[cGMP]$ of 4 µM, ${K_{cGMP}}^{n_{cGMP}} = 125[cGMP]^{n_{cGMP}}$. Hence, the error from this approximation should be insignificant.

Assumption: $K_M >> [cGMP]$

The assumption that PDE6 hydrolytic activity depends linearly from the cGMP concentration in physiological cGMP concentrations ($K_M >> [cGMP]$, compare Eqs. 8 and 9) is widely used in the modeling of photoresponses (e.g., in Lamb & Pugh, 1992; Pugh & Lamb, 2000; Hamer *et al.*, 2005; Caruso *et al.*, 2005; Gross *et al.*, 2012*a*; Reingruber *et al.*, 2013; Invergo *et al.*, 2014; Lamb & Kraft, 2016; Lamb *et al.*, 2018). The estimates of the rod intracellular cGMP concentrations in darkness vary from 2 – 4 µM (see Section 2.3.1). The impact of the approximation in 4 µM cGMP concentration with different K_M values is illustrated in Fig. 7, which plots the hydrolytic rates ($d[cGMP]/dt$) of a single active PDE6 subunit with the catalytic activity of $½k_{cat}$ = 2200 s^{-1} without the assumption (Eq. 8) and with the assumption (Eq. 9) when K_M values range from 10 to 100 µM. The error in the hydrolytic rate due to the approximation is

less than 10% with K_M values of 40 µM or higher. However, with K_M estimates of 10 µM (Leskov *et al.*, 2000), the approximation becomes questionable.

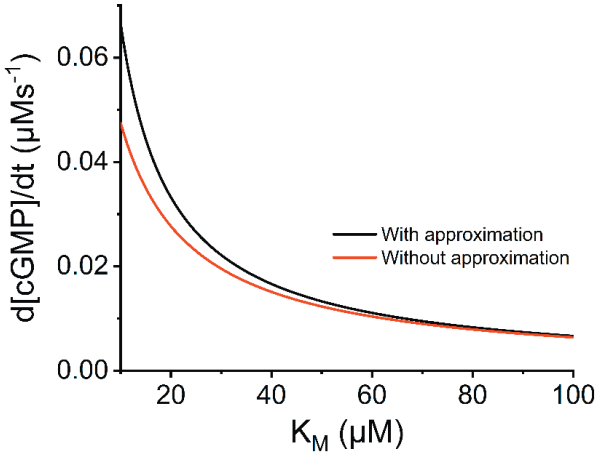

Figure 7. Rate of cGMP hydrolysis by one active PDE6 subunit with $½k_{cat}$ of 2200 s^{-1} calculated with the approximation K_M >> [cGMP] (Eq. 8, black line) and without the approximation (Eq. 9, red line). $[cGMP]_{dark}$ = 4 µM, V_{cyto} = 11 fl, B = 2, N_A = 6.022·10^{23}.

The catalysis of cGMP hydrolytic reaction by PDE6 can be denoted with the following expression

$$PDE6^* + cGMP \rightleftharpoons_{k_r}^{k_f} PDE6^*cGMP \xrightarrow{½k_{cat}} PDE6^* + GMP, \quad (33)$$

where $PDE6^*$ and $cGMP$ presents active PDE6 subunits and cGMP molecules, respectively. k_f is the rate of the PDE6 and cGMP encounters and k_r is the rate constant for the dissociation of the enzyme-substrate complex. Recent studies indicate that the PDE6 enzyme approaches catalytic perfection meaning that the catalytic rate of PDE6 is limited by the encounter rate of cGMP and PDE6, and not by the catalytic power of PDE6 (Reingruber & Holcman, 2008, 2009; Reingruber *et al.*, 2013). This implies that the enzyme-substrate complex decomposes quickly after it is formed ($PDE6^*cGMP \approx 0$). As a result, k_f can be assumed to be the rate-limiting factor in the reaction and the reverse reaction back from the enzyme-substrate complex can be assumed to be negligible. With these assumptions, the Eq. 33 simplifies to

$$PDE6^* + cGMP \xrightarrow{k_f} PDE6^* + GMP \quad (34)$$

and the hydrolytic rate of cGMP can be expressed as

$$\frac{dcGMP(t)}{dt} \approx -k_f PDE6^*(t) cGMP(t) \text{ (Reingruber \& Holcman, 2008).} \quad (35)$$

Thus, the hydrolytic rate of PDE6 depends linearly on cGMP concentration and on the diffusion-defined encounter rate of the substrate and the enzyme. Noteworthy is that Eq. 35 is analogous with the Eq. 10, which uses the approximation K_M >> $[cGMP]$ and it can substitute the Eq. 10 in modeling of photoresponses. In order for the reaction to be purely diffusion-limited, the total rate of cGMP encounters with PDE6 subunit in one disk compartment ($k_f N_{cGMP/comp.}$) should be substantially smaller than $½k_{cat}$ for PDE6 (Reingruber & Holcman,

2008). However, the diffusion-limited encounter rate of cGMP and PDE6 in mouse rods disk compartment is estimated to be k_f = 61 s^{-1} (Reingruber *et al.*, 2013). If there are approximately 33 cGMP molecules in one mouse rod compartment in darkness (4 µM cGMP dark concentration, 11 fl cytoplasmic rod outer segment volume and 810 compartments, $N_{cGMP/comp.} \approx 33$), $k_f N_{cGMP/comp.}$ is close to 2000 s^{-1}. The value is only slightly smaller than the catalytic rate of cGMP hydrolysis by PDE6 subunit (½k_{cat} = 2200 s^{-1}, Leskov *et al.*, 2000) or by the fully active dimer (~ 5000 s^{-1}, Dumke *et al.*, 1994; Mou & Cote, 2001; Muradov *et al.*, 2010), which questions the validity of Eq. 35, at least with the estimated 4 µM cGMP concentration.

Overall, if the reaction rate is diffusion-limited, as suggested by (Reingruber & Holcman, 2008, 2009; Reingruber *et al.*, 2013), or if the K_M value is closer to 100 µM than it is to 10 µM, the approximation K_M >> $[cGMP]$ is acceptable. In other cases, Michaelis-Menten kinetics for cGMP hydrolysis without the assumption should be preferred. The effect of this approximation is analyzed in more detail in the supplementary part of Paper V.

Thoroughly mixed and abundant molecules in free diffusion

According to the current understanding, the phototransduction molecules are not thoroughly mixed in the rod disk membranes, and neither can they diffuse freely. Novel studies have revealed the organization of rhodopsin to dimer lattices, which form tracks to support, e.g., collisions with transducin (Fotiadis *et al.*, 2003, 2004; Govardovskii *et al.*, 2009; Gunkel *et al.*, 2015). Also, PDE6 has been shown to concentrate mostly on the rim regions of the discs instead of being evenly distributed in the lateral space of the discs (Muradov *et al.*, 2009, 2010). The disk membranes themselves serve as diffusion barriers that divide the intracellular space to somewhat separate compartments. These findings give ground for questioning the assumed free diffusion of thoroughly mixed molecules in the rod disk membranes and cytoplasm. However, most of the current phototransduction models use these assumptions while still accurately describing averaged rod photoresponses of both amphibians and rodents under various stimulation paradigms. (Leskov *et al.*, 2000; Nikonov *et al.*, 2000; Hamer *et al.*, 2005; Invergo *et al.*, 2014; Lamb *et al.*, 2018). Nevertheless, inaccurate model presumptions can create some bias in the derived model parameters.

Within the independent compartments, the diffusion distances are relatively small, and the total time from photon absorption to PDE6 activation is short concerning the overall kinetics of the rod photoresponse (peaking around in 150 ms in WT mouse rods). The pooled delay from photon absorption to PDE6 activation is determined to be less than 2 ms mammalian rods in body temperature (Breton *et al.*, 1994; Pugh & Lamb, 2000). Considering more sophisticated models for molecular diffusion would affect only the very beginning of the model responses before factors, like rhodopsin deactivation, start to affect the signal shape. Hence, investigating complex molecular diffusion might not be practical with tools such as ERG, and assuming free diffusion of well-mixed molecules should offer a solid basis for photoresponse modeling.

The number of activable phototransduction proteins decreases upon light absorption. However, the protein concentrations in the rod compartments are high. PDE6 is the most sporadic of the molecules involved in phototransduction activation. Poisson statistics can describe the probability that a certain amount of photoisomerizations will occur in one disk membrane (see, e.g., equation 2.10 from Lamb *et al.*, 2018). The models in this thesis were used with

stimulus strengths causing less than 200 isomerizations per rod per one flash, which causes less than 0.25 isomerizations per rod disk membrane on average. The probability that two or more isomerizations would occur in one disk is thus less than 3%. The isomerization of single rhodopsin causes on average activation of 10 – 50 PDE6 subunits while there are around 200 PDE6 molecules in one rod disk (see Sections 3.3.2 and 4.1). Therefore, there are plenty of PDE6 molecules available with stimulus strengths producing less than 200 R^*rod^{-1}. Hence, the depletion of the phototransduction molecules should not be a significant factor in photoresponse modeling with subsaturating stimulus strengths.

Although the compartments function mostly as individual units, they share the same pool of cGMP that can diffuse freely within the rod cytoplasm. Late studies suggest that upon single-photon absorption in one compartment, the cGMP concentration decreases fewer than 20% from its dark level in the vicinity of that compartment (Gross *et al.*, 2012*a*, 2015). When rhodopsin isomerizations happen evenly along the outer segment length, e.g., when using homogenous full-field flash stimuli, the decrease in cGMP level can be assumed to occur evenly within the rod outer segment. However, with intense and uneven light stimulation, the limited rate of cGMP diffusion should be considered in the modeling.

Overall, the assumption that well-mixed phototransduction molecules are abundant and under free diffusion should be valid when modeling dim and subsaturating flash responses, especially in techniques such as ERG, where the rare events average out in the mass potential signal. However, when using intense light stimuli or when harvesting detailed knowledge from diffusion of phototransduction molecules, more complex models should be considered.

6. Results

6.1 Calcium mediates fast light adaptation in mouse rods, but all mechanisms have not been identified (Paper I)

Photoreceptors have accurate control over the intracellular calcium concentration, and the changes in the calcium level mediate fast light adaptation through calcium sensor proteins. GCAP1 and GCAP2 are the dominant mediators of mouse photoreceptor light adaptation, but even after knocking out both GCAPs, some adaptation remains. Paper I characterized the role of recoverin in light adaptation in the absence of the dominant GCAPs-mediated modulation with transretinal *ex vivo* ERG, recorded from isolated GCAPs$^{-/-}$ mouse retinas. We recorded rod responses to flashes and steps of light in normal extracellular calcium concentration (1 mM) and in low free calcium concentration (~ 20 nM), which is expected to drive all the calcium-mediated modulators out of their operational range. In WT mouse photoreceptors, lowering of extracellular calcium causes a substantial increase in maximal flash response amplitudes and non-physiological desensitization of rods due to low Ca^{2+}-induced acceleration of guanylate cyclase activity. However, the study demonstrated that in GCAPs$^{-/-}$ mice, lacking the modulation of guanylate cyclase activity, stable ERG responses can be recorded in low extracellular calcium. The possibility to lower the extracellular calcium allowed us to examine the fully light adapted-like state of rods without using background light. By combining TERG recordings, genetic manipulation, and the low Ca^{2+} approach, the work showed that recoverin mediates a substantial part of the GCAPs-independent light adaptation but not all of it. Even after knocking out both GCAPs and recoverin, rods were still capable of regulating their sensitivity. Paper I investigated the changes in rod sensitivity in relation to the background light intensity in order to clarify the remaining adaptation. In normal Ca^{2+}, the rods still showed significant adaptation to background light illumination in GCAPs$^{-/-}$ recoverin$^{-/-}$ retinas. However, after dropping the extracellular calcium concentration to ~ 20 nM, the rod sensitivity in different background light levels accurately followed the behavior predicted by a model that disregards all light adaption mechanisms. The result indicates that the fast light adaptation of mouse rods is completely mediated by calcium.

6.2 Pharmacologically isolated photoreceptor component of transretinal ERG corresponds well with the ERG registered locally across the rod outer segments (Paper II)

The photoreceptor component of the ERG signal (fast PIII) can be investigated with transretinal *ex vivo* ERG (TERG) from intact mouse retinas, and it gives an insight into the phototransduction mechanisms. However, the isolation of fast PIII component requires pharmacological blocking of the synaptic transmission to the second-order neurons and blocking of potassium channels in Müller cells. These blockers might have some influence on phototransduction, and

imperfect blocking can cause components originating from deeper retinal layers and Müller cells to influence the registered signals. Additionally, the voltage-sensitive channels in the rod inner segment layer are known to modify the TERG signal (Vinberg *et al.*, 2009). Local ERG, on the other hand, can be recorded across the rod outer segment layer alone (LERG-OS) with microelectrodes. Paper II shows that the pharmacological substances commonly used to block the synaptic transmission from photoreceptors to bipolar cells (aspartate and APB) or $BaCl_2$, which blocks the K-channels from Müller cells, do not significantly modify the LERG-OS signal at concentrations sufficient to accomplish blocking (2 mM aspartate or 20 µM APB and 50 µM $BaCl_2$). Moreover, the maximal LERG-OS photovoltage is equal to the dark voltage shift observed when the microelectrode is advanced through the outer segment layer, which verifies that the LERG-OS signal is directly proportional to the changes in the rod outer segments current. These results suggest that the LERG-OS signal can be used as a quantitative indicator of the changes in the outer segment current that reflect changes in phototransduction.

When comparing TERG and LERG-OS with light stimulus paradigms commonly used to examine phototransduction, the study found that the two methods gave very similar results. The activation phases of subsaturated responses were similar with the two methods when the plateau levels were scaled to match, but with stronger flash strengths, a "nose" component emerged in the TERG signal. This "nose" was not present in the LERG-OS. Response recovery was slightly faster, and the time-to-peak and dominant time constant for response turnoff, determined from the Pepperberg plot analysis (Pepperberg *et al.*, 1992), were somewhat smaller as recorded by TERG. However, no differences were observed between the TERG signal and the LERG signal recorded across the whole length of the photoreceptors (LERG-PR). In order to avoid the inner segment contribution to the ERG signal and to get quantitative information about changes in phototransduction, the LERG-OS technique developed in Paper II was further used in the determination of inhibition constants and the cGMP clamp experiments conducted in Papers III, IV and V.

6.3 Inhibition constants for phosphodiesterase-6 inhibitors can be determined with *ex vivo* electroretinography (Papers III, IV and V)

Paper III introduces methods based on *ex vivo* electroretinography for the determination of the inhibition constants of phosphodiesterase-6 (PDE6) inhibitors against the naturally occurring light-activated and spontaneously activated forms of PDE6. We tested the methods with three PDE6 inhibitors: 3-isobutyl-1-methylxanthine (IBMX), sildenafil, and zaprinast. The inhibition of light-activated PDE6 manifested as a decrease in the phototransduction gain and a slowdown of the onset of the flash responses. The phototransduction gain was assessed by determining the amplification constant with the Lamb and Pugh activation model (see Section 5.3.1). The amplification constant decreased linearly with increasing inhibitor concentration with all the tested inhibitors, and it was not sensitive to background light or moderate changes in the cGMP concentration in rods. The inhibition constants against the light-activated PDE6 ($K_{I,light}$) were 13.4 ± 0.7 µM for IBMX (n = 16 retinas), 0.56 ± 0.09 µM for sildenafil (n = 4 retinas), and 0.97 ± 0.07 µM for zaprinast (n = 4 retinas). The relative standard error (RSE) was 5% for IBMX, 16% for sildenafil, and 7% for zaprinast for the $K_{I,light}$ determination.

The inhibition of spontaneously activated PDE6 causes an increase in the intracellular cGMP concentration due to the decrease in the basal rate of cGMP hydrolysis by PDE6. In Paper III, the relative increase in the intracellular cGMP concentration was determined from the cubic root of the relative inhibitor-induced increase in the maximal LERG-OS flash response amplitudes in GCAPs$^{-/-}$ mouse retinas lacking the calcium feedback to guanylate cyclase (see Eq. 17). The inhibition constant against spontaneously activated PDE6 ($K_{I,dark}$) was quantified by determining the slope of the relative increase in the cGMP concentration plotted against the used inhibitor concentration (see Eq. 28). However, the cubic root of the relative increase of maximal LERG-OS amplitudes showed a nonlinear dependence on the inhibitor, which was emphasized towards larger inhibitor concentrations. The behavior manifested as a time-dependent decrease of the maximal LERG-OS amplitude after the introduction of the inhibitor solution to the retina (see Fig. 8A). To correct for the effect of the amplitude decrease, $K_{I,dark}$ values were determined by fitting an exponential model to the data extracted from the steady-state LERG-OS amplitudes and extrapolating the slope in zero inhibitor concentration (see Fig. 8C). The $K_{I,dark}$ was 1.6· $K_{I,light}$for IBMX, 4.0· $K_{I,light}$ for sildenafil, and 9.2· $K_{I,light}$ for zaprinast. 95% confidence bands for the determined $K_{I,dark}$ values were [1.1; 2.0]· $K_{I,light}$, [3.5;4.5]· $K_{I,light}$, [4.5; 14]· $K_{I,light}$, for IBMX, sildenafil, and zaprinast, respectively.

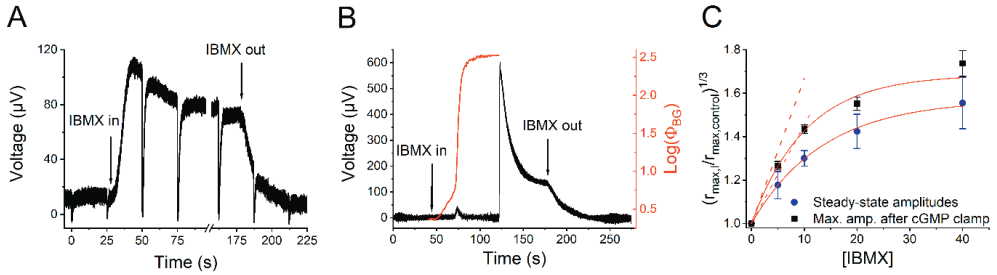

Figure 8. A) Effect of 40 uM IBMX on the LERG-OS voltage in GCAPs$^{-/-}$ mouse retina. The retina was stimulated with saturating flashes at 25 s intervals to determine the change in the maximal LERG-OS amplitude. The arrows indicate the times of introduction and washout of IBMX. B) cGMP clamp run recorded in 1 mM Ca^{2+} with LERG-OS in GCAPs$^{-/-}$ recoverin$^{-/-}$ mouse retina. The black trace illustrates the LERG-OS voltage and red trace the background light strength produced by the closed-loop PID-controlled feedback system to keep the LERG-OS voltage steady after the introduction of 40μM IBMX. After the controller had reached a steady-state, the background light was turned off, causing a rapid increase in the LERG-OS voltage. C) Determination of $K_{I,dark}$ for IBMX. Y-axis shows the cubic root of the IBMX-induced relative increase in LERG-OS amplitude. Error bars represent SEMs. LERG-OS amplitudes were determined using the steady-state amplitudes after the introduction of IBMX (blue circles, see panel A) and using the maximal LERG-OS amplitude increase resulting from the background light turn off after cGMP clamp (black squares, see panel B). The $K_{I,dark}$ values extrapolated from the exponential fit in zero inhibitor concentration (solid red traces illustrate exponential fits and dashed red traces the extrapolated slopes in zero inhibitor concentration) were 22.5 μM (n = 5 GCAPs$^{-/-}$ retinas) and 15.0 μM (n = 9, GCAPs$^{-/-}$ recoverin$^{-/-}$ retinas) when determined using steady-state amplitudes and cGMP clamp-induced amplitude increase, respectively. The figure is modified from Papers III and V.

To conduct the cGMP clamp analysis, $K_{I,dark}$ was probed again for IBMX in Papers IV and V in GCAPs$^{-/-}$ and GCAPs$^{-/-}$ recoverin$^{-/-}$ backgrounds. The decrease of the maximal response amplitude in the inhibitor solution was minimized by evoking the effect of IBMX on the maximal LERG-OS amplitudes as quickly as possible. This was achieved by first introducing the PDE6

inhibitor to the retina and then compensating the decrease of basal PDE6 activity by increasing PDE6 activity with light. The closed-loop feedback-controlled background light kept the total PDE6 activity constant, and after the system had reached a steady-state, the background light was turned off. With this method, the IBMX binding to PDE6 had time to reach equilibrium within rod cells without a change in the cGMP levels or LERG-OS amplitudes. After the light turn off, the cGMP level increased with a rate limited by the deactivation kinetics of light-activated PDE6, which minimized the effect of time-dependent decrease of the maximal LERG-OS amplitudes for $K_{I,dark}$ determination (see Figs. 8B and C). With this method, the study found practically no difference in the inhibition constant of IBMX against the light-activated PDE6 and spontaneously activated PDE6 in the solution containing the 1 mM calcium concentration. However, when the extracellular calcium was lowered from 1 mM to ~ 20 nM, the $K_{I,light}$ value dropped from 13.8 µM to 7.6 µM. Surprisingly, the inhibition constant against spontaneously activated PDE6 shifted in the opposite direction, from 15.0 µM in normal Ca^{2+} to 49.0 µM in low Ca^{2+}.

6.4 cGMP clamp enables the determination of basal phosphodiesterase-6 activity for mammalian rod photoreceptors (Paper IV)

For amphibian photoreceptors, the basal PDE6 activity (β_{dark}) can be determined with an "IBMX jump" method where an individual photoreceptor cell is suddenly exposed to a solution with high IBMX concentration aiming at instantaneous inhibition of the basal PDE6 activity while recording the circulating current with the suction electrode technique (Nikonov *et al.*, 2000; Astakhova *et al.*, 2008). The shutoff of the basal PDE6 activity leads to a rapid increase in intracellular cGMP and in the circulating current. β_{dark} can be determined by quantifying the rate of [cGMP] growth. However, this method is not feasible with the fragile mammalian photoreceptors. Paper IV developed and tested a novel experimental paradigm, cGMP clamp, which allows the determination of basal PDE6 activity in intact retinas of wild type as well as genetically modified mice. The method is based on the ability of PDE6 inhibitors to decrease the catalytic activity of PDE6. A decrease in the basal PDE6 activity can be compensated by introducing a corresponding increase in the PDE6 activity with light, effectively keeping the intracellular cGMP concentration and circulating current at their dark values (cGMP clamp, see Fig. 8B). The basal PDE6 activity can be calculated from the light needed for cGMP clamp, the amplification constant for phototransduction, the Hill coefficient for CNG channel activation, the lifetimes of activated rhodopsin and PDE6, and the inhibition constants $K_{I,dark}$ and $K_{I,light}$ for the used PDE6 inhibitor. To monitor the changes in the intracellular cGMP concentration, we recorded LERG-OS from for WT, $GCAPs^{-/-}$ and $GCAPs^{-/-}$ $recoverin^{-/-}$ mouse retinas. A PID-controlled closed-loop background light feedback from the ERG signal to stimulus light enabled the cGMP clamp procedure. IBMX was used as the PDE6 inhibitor and the inhibition constants were determined as described in Section 6.3. The lifetime of activated PDE6 was determined as the dominant time constant from a Pepperberg plot analysis (Pepperberg *et al.*, 1992; Krispel *et al.*, 2006; Invergo *et al.*, 2013). The amplification constant and the lifetime of activated rhodopsin were determined by modeling the response leading edge (Eq. 22). The average lifetimes of activated rhodopsin were 51 ms for WT, 49 ms for $GCAPs^{-/-}$ and 28 ms for $GCAPs^{-/-}$ $recoverin^{-/-}$ mice, and the amplification constant ranged from 14 to 21 s^{-2} with the used mouse strains. Resolving the necessary parameter values allowed determination of β_{dark}, which was close to 4 s^{-1} for all the mouse strains. The determined β_{dark} values were

very close to that determined earlier from the late recovery of single-photon responses in GCAPs$^{-/-}$ mouse rods (Gross *et al.*, 2012*a*). However, these determinations had utilized the approximation that intracellular cGMP concentration is always substantially smaller than the Michaelis constant K_M for the cGMP hydrolysis. The effect of this assumption was analysed in detail in the supplementary material of Paper V. E.g., with a K_M of 22 µM and $[cGMP\ ]_{dark}$ of 3.7 µM (estimated in the supplementary material of Paper V), the β_{dark} value determined without the approximation was 35% larger than that determined with the approximation. The supplement suggests that, if the approximation K_M >> $[cGMP\ ]$ is omitted, β_{dark} value should be corrected to near 5 s^{-1}.

6.5 Calcium modulates basal PDE6 activity in mouse rods (Paper V)

Paper I discovered a calcium-mediated regulation of rod flash responses, which was present in mouse rods lacking the GCAPs- and recoverin-mediated adaptation pathways. We observed no calcium-mediated change in the activation phase of the responses or in the lifetime of activated PDE6. Additionally, the guanylate cyclase activity and rhodopsin lifetime were constant as the GCAPs- and recoverin-mediated pathways were missing. Hence, the study hypothesized that the novel regulation of flash responses could originate from the modulation of basal PDE6 activity, a crucial effector in setting the rod sensitivity to light. To investigate this, we used the LERG-OS method introduced in Paper II, the method to determine the inhibition constants of PDE6 inhibitors presented in Papers III and IV, and the cGMP clamp paradigm explained in Paper IV. In Paper V, we mimicked the effect of intense background light by lowering the rod extracellular calcium to ~ 20 nM in GCAPs$^{-/-}$ recoverin$^{-/-}$ background. Similarly as shown in Paper I by TERG, LERG-OS recordings in Paper V concluded that lowering of Ca^{2+} causes small desensitization of rods and acceleration of response recovery kinetics. The effects were completely reversible when the low Ca^{2+} solution was changed back to normal Ca^{2+} solution.

The cGMP clamp experiments showed 29% larger basal PDE6 activity in the low Ca^{2+} solution compared to that determined in normal Ca^{2+}. A similar increase in β_{dark} explained the low-Ca^{2+}-induced acceleration of LERG-OS dim flash response recovery kinetics and the decrease in response amplitudes when examined by modeling the dim flash responses recorded in normal and low Ca^{2+} conditions. Taking into account the effect of the common approximation K_M >> $[cGMP\ ]$ (the detailed analysis is found from the supplementary material of the Paper V), the study concluded that the maximal Ca^{2+}-induced increase of β_{dark} is ~ 20 – 30%. This discovered mechanism is a completely new source of calcium-mediated regulation of rod photoresponses, which could explain the GCAPs- and recoverin-independent light adaptation found in Paper I.

7. Discussion

7.1 Transretinal ERG for investigating the retina and the phototransduction

Suction electrode recording (Baylor *et al.*, 1979*b*, 1979*a*) is an established method for examining the phototransduction cascade while corneal ERG is the most widely applied non-invasive electrophysiological method for investigating retinal functions and eye diseases (Whatham *et al.*, 2014; Johnson *et al.*, 2019; McCulloch *et al.*, 2019). *Ex vivo* ERG allows the study of the phototransduction cascade and overall retinal function even from the same retinal preparation providing a competitive technique bridging the gap between the suction electrode and corneal ERG techniques.

Transretinal ERG and the corneal ERG recorded *in vivo* have been compared by several groups (Green & Kapousta-Bruneau, 1999*a*; Heikkinen *et al.*, 2012; Vinberg *et al.*, 2014). These studies emphasized that transretinal recordings are well comparable with corneal ERG recorded from living animals, and the techniques offer very similar qualitative information on the retinal function. Even quantitatively, the size, the sensitivity and the kinetics of the ERG a-wave were found to be comparable between these techniques, although the TERG responses were slightly slower, the b-wave onset delayed, and the oscillatory potential considerably suppressed in the TERG compared to *in vivo* recordings (Heikkinen *et al.*, 2012; Vinberg *et al.*, 2014).

On the other hand, the local ERG across the photoreceptor outer segments accurately reproduces the light-induced changes in the circulating current (discussed in Paper II). In our comparison of the LERG-OS recordings with the published results of suction electrode recordings, photoreceptors appeared more sensitive and response recovery kinetics slightly slower in suction electrode recordings. However, the overall resemblance of responses and the derived parameter values were prominent (see Table 1 in Paper II). Also, the maximal LERG-OS amplitudes (105 µV in bicarbonate solution) matched well with the theoretical expectation (100 µV see Section 5.1.2) calculated based on the extracellular resistivity in the outer segment layer determined from isolated rat retina (Hagins *et al.*, 1970). However, the extracellular resistivity determined from rabbit eyecup preparation (Karwoski & Xu, 1999) gave a 20 times larger estimate for the maximal light-induced extracellular voltage change in the outer segment layer. If the latter estimate is closer to the extracellular resistivity of our isolated mouse retina preparation, a substantial part of the signal must be shunted by a “leaking” ion current via some other pathway than directly from rod inner segments to outer segments. This kind of leakage could also potentially explain the phenomenon described in (Green & Kapousta-Bruneau, 1999*b*), where a reversed miniature version of the transretinal signal superimposed to the local ERG recordings with microelectrodes. A similar phenomenon was sporadically seen in

our experiments, but mostly our LERG-OS responses resembled those recorded with the suction electrode technique, and no other signal components were visible. Another explanation for the observed maximal response amplitude may be the isolation of the retina from the pigment epithelium, decreasing the resistivity in the outer segment layer. The resistivity may further be reduced due to the use of a relatively large recording electrode, which is inserted into the retina (2 – 5 µm tip diameter in our experiments and 1 – 2 µm in Hagins *et al.*, 1970). Reduced extracellular resistivity would be manifest as smaller maximal response amplitudes.

In addition, Paper II concentrated on resolving how well the pharmacologically isolated photoreceptor component of the transretinally recorded ERG corresponds to the signals recorded with the LERG-OS technique in order to examine the usefulness of TERG in quantitative phototransduction research. Excluding the response amplitudes that are substantially larger by TERG than by LERG-OS, the simultaneous recordings with TERG and LERG-OS gave nearly identical results with the conventional light stimulus paradigms used in phototransduction research both in the dark- and light-adapted retinas. The LERG-OS responses were slightly faster than those recorded by LERG-PR or TERG, and the transient nose component that emerged to saturated LERG-PR and TERG responses after strong flash stimuli was never visible in LERG-OS. The nose component is most likely a combination of component arising from the function of HCN1 channels, capacitive component originating in the rod inner segment region, and a small contribution from cones (Heikkinen *et al.*, 2008; Vinberg *et al.*, 2009; Robson & Frishman, 2014). The slightly faster response kinetics by TERG and LERG-PR compared with LERG-OS can be explained by response modulation by voltage-gated channel currents. At least HCN1 channel current is known to speed up the recovery of the membrane potential after a light stimulus (Sothilingam *et al.*, 2016), and it can also contribute to the modulation of TERG and LERG-PR response recovery kinetics. LERG-OS responses, however, should remain unmodulated due to the absence of voltage-gated channels in the outer segment of rods.

Based on our results and those published before, TERG offers a versatile tool for investigating retinal function and the phototransduction cascade. The most significant advantage of TERG compared to single-cell recordings is the unparalleled signal-to-noise ratio and the stability of TERG recordings in long-lasting experiments, and the pooling of the individual cellular variations in the mass potential signal. TERG also allows fast modification of the extracellular solution perfusing the retina, and hence, it enables easy pharmacological manipulation of cells and connections in the intact isolated retina. Paper II demonstrates that TERG is a precise, versatile, and cost-effective technique for quantitative study of the phototransduction machinery and the effects of pharmacological agents on retinal signaling. Still, when investigating changes in the rod circulating current, one should be aware of the signal components arising from the photoreceptor inner segment region.

7.2 Cooperative action of PDE6 γ-subunit and PDE6 inhibitors

Paper III demonstrated that the inhibitory efficacy of PDE6 inhibitors can be substantially different against light-activated, spontaneously activated, and trypsin-activated forms of PDE6. For sildenafil, the inhibition constant against the light-activated form ($K_{I,light}$) was 4 times smaller than against the spontaneously activated form ($K_{I,dark}$) when determined electrophysiologically from isolated mouse retinas. The $K_{I,light}$ of sildenafil was also 50 times larger than the inhibition constant against trypsin-activated form of PDE6 determined biochemically

from purified bovine PDE6 (Zhang *et al.*, 2005). For IBMX, the differences seem to be much smaller ($K_{I,dark} \approx K_{I,light} = 1 - 3 \cdot K_{I,trypsin}$) (Cobbs, 1991; Zhang *et al.*, 2004*a*, 2005 and Paper III & IV of this thesis).

Paper III hypothesizes that the difference between $K_{I,light}$, $K_{I,dark}$ and $K_{I,trypsin}$ is due to the mutual competition of the inhibitory PDE6 γ-subunit, cGMP, and the PDE6 inhibitors for binding to the same catalytic domain in the PDE6 apoenzyme (D'Amours *et al.*, 1999; Zhang *et al.*, 2005). According to our electrophysiological data, the competition for binding to the catalytic site by the PDE6 inhibitor and the PDE6 γ-subunit might be stronger with zaprinast and sildenafil and milder with IBMX judging from the more substantial differences in inhibition constants, $K_{I,dark}$, $K_{I,light}$ and $K_{I,trypsin}$, for sildenafil and zaprinast compared to IBMX. This hypothesis is supported by biochemical evidence for common binding sites for the PDE6 γ-subunit, sildenafil, and zaprinast in the catalytic region of PDE6. The γ-subunit binds to the amino acid residues Met759, Phe778 and Phe782 in the PDE6 αβ-apoenzyme close to the entrance of the catalytic pocket and prevents cGMP from entering the catalytic core (Granovsky & Artemyev, 2001*a*, 2001*b*; Cote, 2004). According to the molecular modeling of the PDE6 catalytic site, in addition to binding to the catalytic core, zaprinast interacts with Met759, and sildenafil with both Met759 and Phe778 (Simon *et al.*, 2006). Due to the competition for the common binding site of sildenafil and zaprinast with the γ-subunit, the inhibitors cannot inhibit the enzyme as effectively as they would in the absence of γ-subunits. This manifests itself as larger $K_{I,dark}$ values compared to those of $K_{I,trypsin}$. Some of this competition might still be present even in the light-activated state of PDE6 leading to differences in $K_{I,light}$ and $K_{I,trypsin}$. In the trypsin-activated state, the PDE6 γ-subunits are disintegrated from the PDE6 body and no interaction between the inhibitors and γ-subunits can arise. IBMX, being the smallest of the tested inhibitors and having no known shared binding sites with the γ-subunit, may completely escape the competition with the γ-subunits, explaining the smaller differences in $K_{I,dark}$, $K_{I,light}$ and $K_{I,trypsin}$, for IBMX.

Interestingly, the inhibition constants of IBMX against light-activated and spontaneously activated PDE6 were similar only with the physiological calcium concentration ($K_{I,dark} \approx K_{I,light}$ = 14 – 15 µM in 1 mM extracellular Ca^{2+}) but differed profoundly in the low Ca^{2+} condition ($K_{I,light}$ = 7.6 µM and $K_{I,dark}$= 49 µM). The result indicates that Ca^{2+} can modify the binding of IBMX to PDE6 by interacting either directly with IBMX or PDE6, or through some indirect pathway. To our knowledge, there is no evidence for an interaction of Ca^{2+} with IBMX, but it is acknowledged that calcium regulates, e.g., the phosphodiesterase-1 group enzymes through calmodulin (Kakkar *et al.*, 1999; Goraya & Cooper, 2005). It is probable that calcium can allosterically regulate the PDE6 enzyme and the binding of IBMX to its catalytic core either directly or indirectly. However, the study cannot provide further evidence on the mechanism of this interaction. It might be that the same mechanism that is causing the calcium-mediated regulation of inhibitor binding to PDE6 is behind the calcium-mediated regulation of basal PDE6 activity found in Paper V.

7.3 Basal PDE6 activity and calcium in sensitivity regulation of mouse rod photoresponses

Paper I reaffirmed that the calcium-dependent modulation of guanylate cyclase activity is the dominant source of fast light adaptation in mouse rod photoreceptors. This modulation is mediated through GCAP1 and GCAP2. Knocking out both GCAPs allowed us to investigate other light adaptation pathways in mammalian rods and to quantify the magnitude of the light adaptation mediated through recoverin, which controls the lifetime of activated rhodopsin and according to recent studies may also modulate the lifetime of activated PDE6 (Chen *et al.*, 2012, 2015). Additionally, a recent study proposes that recoverin might be involved in keeping the basal PDE6 activity high in darkness and decreasing it in background light (Morshedian *et al.*, 2018). In Paper I, knocking out both GCAPs and recoverin allowed the examination of GCAPs- and recoverin-independent regulation of rod photoresponses. Paper I revealed a formerly unknown source of calcium-mediated light adaptation, but the mechanism of the newly identified source of light adaptation in mouse rod photoreceptor cells remained unknown.

The rest of this doctoral thesis delved into examining the source of the unknown sensitivity regulation with a leading hypothesis that basal PDE6 activity might be under calcium-dependent control. The techniques, methods, and paradigms developed to investigate the possible calcium modulation of basal PDE6 activity were introduced in Papers II-IV. Paper V showed with cGMP clamp that calcium can modulate basal PDE6 activity by 20 – 30%. This finding was supported by mathematical modeling of dim flash responses, where similar modulation of basal PDE6 activity could explain the low-Ca^{2+}-induced desensitization of rods as well as the acceleration of response recovery. Additionally, Paper V demonstrated that using a common approximation K_M >> $[cGMP]$ in the determination of phototransduction parameters can lead to a small but significant bias in estimated parameter values. With the current numerical tools available for phototransduction modeling, the approximation is somewhat unnecessary and should be omitted when possible. The supplement to Paper V gives estimates for K_M and $[cGMP]_{dark}$ in mouse rods, but the exact values still need to be confirmed.

Although the cGMP clamp experiments and modeling provide a quantitative estimate for the maximal range of for the Ca^{2+}-dependent modulation of spontaneous PDE6 activity in dark-adapted mouse rods, resolving the exact mechanism for the modulation still needs further research. The Ca^{2+} modulation might be mediated either by the direct interaction of Ca^{2+} with PDE6 or through a calcium sensor protein. In addition to recoverin and GCAPs, at least calmodulin can bind Ca^{2+} with high affinity in rod outer segments, and it is also known to regulate the activity of PDE1 family enzymes (Kakkar *et al.*, 1999; Goraya & Cooper, 2005). However, to our knowledge, a direct interaction of calmodulin with PDE6 has not been demonstrated. Glutamic Acid–Rich Protein-2 (GARP2), on the other hand, can bind Ca^{2+} with low affinity but with high capacity (Haber-Pohlmeier *et al.*, 2007) and at the same time, it can bind PDE6 with high affinity (Pentia *et al.*, 2006). GARP2 concentrates to the rim regions of rod disk membranes (Colville & Molday, 1996; Korschen *et al.*, 1999) together with PDE6 (Muradov *et al.*, 2009, 2010) with relatively similar stoichiometry (Batra-Safferling *et al.*, 2006; Pentia *et al.*, 2006). GARP2 has been shown to regulate phototransduction gain and photoresponse recovery in mouse rods (Sarfare *et al.*, 2014), and basal PDE6 activity in bovine rods (Pentia *et al.*, 2006). It might be possible that GAPR2 is needed to maintain the basal PDE6 activity in darkness and that this interaction is regulated by calcium.

The magnitude of the novel Ca^{2+}-dependent modulation of basal PDE6 activity raises the question about the physiological significance of the effect in the rod photoreceptors. One option is that the primary role of the regulation is not in fast light adaptation. Basal PDE6 activity is the main component in determining the turnover rate of cGMP and the level of dark noise in rods. The turnover rate of cGMP is crucial for setting the photoreceptor response kinetics and amplitude, while the level of dark noise affects the variability of responses and fixes the threshold for light-activity needed for photon detection. Modification of these two factors always leads to a trade-off between absolute visual sensitivity and temporal resolution. The calcium-mediated modulation of the basal level of PDE6 activity might offer a flexible way of tuning the basal turnover rate of cGMP, which could help the animal to adapt to small variations in brightness. Another option is that this modulation of basal PDE6 activity is less significant for rods, but it could be more significant in cone signaling. The dynamic range of mammalian cone-mediated vision exceeds that of rods by several log units (Stockman & Sharpe, 2006; Naarendorp *et al.*, 2010), but the mechanisms of cone light-adaptation are still not fully understood (Sakurai *et al.*, 2011*b*, 2015). As in rods, fast light adaptation in cones in mainly driven by calcium-mediated feedback mechanisms (Matthews *et al.*, 1988; Nakatani & Yau, 1988*b*; Vinberg & Kefalov, 2018). Additionally, in amphibian cone outer segments, the decline in the intracellular calcium concentration is faster, and the dynamic calcium range is at least over three times wider than in rods (Sampath *et al.*, 1998, 1999). Hence, it is likely that a similar mechanism found in this thesis for rods would produce a more significant effect in cones.

8. Conclusions

1. The calcium sensor protein recoverin and a novel mechanism contribute significantly to the fast light adaptation in mouse rods. The fast light-adaptation of mouse rods is completely calcium-mediated.

2. Transretinal *ex vivo* ERG (TERG) enables quantitative examination of photoreceptor signaling after pharmacological blocking the signal transmission to higher-order neurons and Müller cell contribution. Phototransduction parameters extracted from TERG, local ERG across the outer-segment layer (LERG-OS), and suction electrode recordings are closely similar. Still, when investigating the rod phototransduction cascade with TERG, one should take into consideration the ERG components originating in the rod inner segment region.

3. *Ex vivo* ERG offers a potent and versatile tool for investigating phosphodiesterase-6 inhibitors in the natural environment of PDE6. The inhibition constants determined from trypsin-activated, light-activated, and spontaneously activated PDE6 can differ substantially, most likely due to the mutual competition of the PDE6 γ-subunit, the PDE6 inhibitor, and cGMP for common binding sites at the catalytic core of PDE6.

4. A novel experimental paradigm, cGMP clamp, enables the determination of the basal PDE6 activity in the mouse rod photoreceptors. The basal PDE6 activity is approximately 4 – 5 s^{-1} in the wild type, $GCAPs^{-/-}$ and $GCAPs^{-/-}$ $recoverin^{-/-}$ mouse retinas.

5. The basal PDE6 activity is modulated by calcium in mouse rods. Decreasing the extracellular calcium concentration from 1 mM to ~ 20 nM causes roughly ~ 20 – 30% increase in the basal PDE6 activity.

References

Adelson EH (1982). Saturation and adaptation in the rod system. *Vision Res* **22,** 1299–1312.

Ahmad F, Murata T, Shimizu K, Degerman E, Maurice D & Manganiello V (2015). Cyclic nucleotide phosphodiesterases: important signaling modulators and therapeutic targets. *Oral Dis* **21,** e25-50.

Amora TL, Ramos LS, Galan JF & Birge RR (2008). Spectral tuning of deep red cone pigments. *Biochemistry* **47,** 4614–4620.

Angleson JK & Wensel TG (1994). Enhancement of rod outer segment GTPase accelerating protein activity by the inhibitory subunit of cGMP phosphodiesterase. *J Biol Chem* **269,** 16290–16296.

Arden GB (1976). Voltage gradients across the receptor layer of the isolated rat retina. *J Physiol* **256,** 333-360.1.

Arshavsky VY (2002). Rhodopsin phosphorylation: from terminating single photon responses to photoreceptor dark adaptation. *Trends Neurosci* **25,** 124–126.

Arshavsky VY, Dumke CL & Bownds MD (1992). Noncatalytic cGMP-binding sites of amphibian rod cGMP phosphodiesterase control interaction with its inhibitory gamma-subunits. A putative regulatory mechanism of the rod photoresponse. *J Biol Chem* **267,** 24501–24507.

Arshavsky VY & Wensel TG (2013). Timing is everything: GTPase regulation in phototransduction. *Invest Ophthalmol Vis Sci* **54,** 7725–7733.

Artemyev NO, Rarick HM, Mills JS, Skiba NP & Hamm HE (1992). Sites of interaction between rod G-protein alpha-subunit and cGMP-phosphodiesterase gamma-subunit. Implications for the phosphodiesterase activation mechanism. *J Biol Chem* **267,** 25067–25072.

Artemyev NO, Surendran R, Lee JC & Hamm HE (1996). Subunit structure of rod cGMP-phosphodiesterase. *J Biol Chem* **271,** 25382–25388.

Astakhova LA, Firsov ML & Govardovskii VI (2008). Kinetics of turn-offs of frog rod phototransduction cascade. *J Gen Physiol* **132,** 587–604.

Astakhova LA, Samoiliuk E V, Govardovskii VI & Firsov ML (2012). cAMP controls rod photoreceptor sensitivity via multiple targets in the phototransduction cascade. *J Gen Physiol* **140,** 421–433.

Azevedo AW & Rieke F (2011). Experimental protocols alter phototransduction: The implications for retinal processing at visual threshold. *J Neurosci* **31,** 3670–3682.

Azzouni F & Abu samra K (2011). Are phosphodiesterase type 5 inhibitors associated with vision-threatening adverse events? a critical analysis and review of the literature. *J Sex Med* **8,** 2894–2903.

Bader CR, Bertrand D & Schwartz EA (1982). Voltage-activated and calcium-activated currents studied

in solitary rod inner segments from the salamander retina. *J Physiol* **331,** 253–284.

Baehr W, Devlin MJ & Applebury ML (1979). Isolation and characterization of cGMP phosphodiesterase from bovine rod outer segments. *J Biol Chem* **254,** 11669–11677.

Baehr W, Karan S, Maeda T, Luo D-G, Li S, Bronson JD, Watt CB, Yau K-W, Frederick JM & Palczewski K (2007). The function of guanylate cyclase 1 and guanylate cyclase 2 in rod and cone photoreceptors. *J Biol Chem* **282,** 8837–8847.

Barnes S & Kelly MEM (2002). Calcium channels at the photoreceptor synapse. *Adv Exp Med Biol* **514,** 465–476.

Barren B, Gakhar L, Muradov H, Boyd KK, Ramaswamy S & Artemyev NO (2009). Structural basis of phosphodiesterase 6 inhibition by the C-terminal region of the gamma-subunit. *EMBO J* **28,** 3613–3622.

Batra-Safferling R, Abarca-Heidemann K, Korschen HG, Tziatzios C, Stoldt M, Budyak I, Willbold D, Schwalbe H, Klein-Seetharaman J & Kaupp UB (2006). Glutamic acid-rich proteins of rod photoreceptors are natively unfolded. *J Biol Chem* **281,** 1449–1460.

Baumann L, Gerstner A, Zong X, Biel M & Wahl-Schott C (2004). Functional characterization of the L-type Ca2+ channel Cav1.4alpha1 from mouse retina. *Invest Ophthalmol Vis Sci* **45,** 708–713.

Baylor DA, Lamb TD & Yau K-W (1979*a*). Responses of retinal rods to single photons. *J Physiol* **288,** 613–634.

Baylor DA, Lamb TD & Yau K-W (1979*b*). The membrane current of single rod outer segments. *J Physiol* **288,** 589–611.

Baylor DA, Matthews G & Nunn BJ (1984*a*). Location and function of voltage-sensitive conductances in retinal rods of the salamander, Ambystoma tigrinum. *J Physiol* **354,** 203–223.

Baylor DA, Matthews G & Yau K-W (1980). Two components of electrical dark noise in toad retinal rod outer segments. *J Physiol* **309,** 591–621.

Baylor DA & Nunn BJ (1986). Electrical properties of the light-sensitive conductance of rods of the salamander Ambystoma tigrinum. *J Physiol* **371,** 115–145.

Baylor DA, Nunn BJ & Schnapf JL (1984*b*). The photocurrent, noise and spectral sensitivity of rods of the monkey Macaca fascicularis. *J Physiol* **357,** 575–607.

Beech DJ & Barnes S (1989). Characterization of a voltage-gated K+ channel that accelerates the rod response to dim light. *Neuron* **3,** 573–581.

Bender AT & Beavo JA (2006). Cyclic nucleotide phosphodiesterases: molecular regulation to clinical use. *Pharmacol Rev* **58,** 488–520.

Berry J, Frederiksen R, Yao Y, Nymark S, Chen J & Cornwall C (2016). Effect of Rhodopsin Phosphorylation on Dark Adaptation in Mouse Rods. *J Neurosci* **36,** 6973–6987.

Biernbaum MS & Bownds MD (1985). Light-induced changes in GTP and ATP in frog rod photoreceptors. Comparison with recovery of dark current and light sensitivity during dark adaptation. *J Gen Physiol* **85,** 107–121.

Bolnick DA, Walter AE & Sillman AJ (1979). Barium suppresses slow PIII in perfused bullfrog retina. *Vision Res* **19,** 1117–1119.

Boswell-Smith V, Spina D & Page CP (2006). Phosphodiesterase inhibitors. *Br J Pharmacol* **147 Suppl,**

S252-7.

Breton ME, Schueller AW, Lamb TD & Pugh EN (1994). Analysis of ERG a-wave amplification and kinetics in terms of the G-protein cascade of phototransduction. *Invest Ophthalmol Vis Sci* **35,** 295–309.

Bridges CD, Alvarez RA, Fong SL, Gonzalez-Fernandez F, Lam DM & Liou GI (1984). Visual cycle in the mammalian eye. Retinoid-binding proteins and the distribution of 11-cis retinoids. *Vision Res* **24,** 1581–1594.

Bruckert F, Catty P, Deterre P & Pfister C (1994). Activation of phosphodiesterase by transducin in bovine rod outer segments: characteristics of the successive binding of two transducins. *Biochemistry* **33,** 12625–12634.

Burns ME, Mendez A, Chen J & Baylor DA (2002). Dynamics of cyclic GMP synthesis in retinal rods. *Neuron* **36,** 81–91.

Burns ME & Pugh EN (2009). RGS9 concentration matters in rod phototransduction. *Biophys J* **97,** 1538–1547.

Calvert PD, Govardovskii VI, Arshavsky VY & Makino CL (2002). Two temporal phases of light adaptation in retinal rods. *J Gen Physiol* **119,** 129–145.

Cangiano L, Asteriti S, Cervetto L & Gargini C (2012). The photovoltage of rods and cones in the dark-adapted mouse retina. *J Physiol* **590,** 3841–3855.

Capovilla M, Cervetto L & Torre V (1982). Antagonism between steady light and phosphodiesterase inhibitors on the kinetics of rod photoresponses. *Proc Natl Acad Sci U S A* **79,** 6698–6702.

Capovilla M, Cervetto L & Torre V (1983). The effect of phosphodiesterase inhibitors on the electrical activity of toad rods. *J Physiol* **343,** 277–294.

Carter-Dawson LD & Lavail MM (1979). Rods and cones in the mouse retina. I. Structural analysis using light and electron microscopy. *J Comp Neurol* **188,** 245–262.

Caruso G, Khanal H, Alexiades V, Rieke F, Hamm HE & DiBenedetto E (2005). Mathematical and computational modelling of spatio-temporal signalling in rod phototransduction. *Syst Biol (Stevenage)* **152,** 119–137.

Catty P & Deterre P (1991). Activation and solubilization of the retinal cGMP-specific phosphodiesterase by limited proteolysis. Role of the C-terminal domain of the beta-subunit. *Eur J Biochem* **199,** 263–269.

Cervetto L & McNaughton PA (1986). The effects of phosphodiesterase inhibitors and lanthanum ions on the light-sensitive current of toad retinal rods. *J Physiol* **370,** 91–109.

Cheever ML, Snyder JT, Gershburg S, Siderovski DP, Harden TK & Sondek J (2008). Crystal structure of the multifunctional Gbeta5-RGS9 complex. *Nat Struct Mol Biol* **15,** 155–162.

Cheguru P, Zhang Z & Artemyev NO (2014). The GAFa domain of phosphodiesterase-6 contains a rod outer segment localization signal. *J Neurochem* **129,** 256–263.

Chen C-K, Eversole-Cire P, Zhang H, Mancino V, Chen Y-J, He W, Wensel TG & Simon MI (2003). Instability of GGL domain-containing RGS proteins in mice lacking the G protein beta-subunit Gbeta5. *Proc Natl Acad Sci U S A* **100,** 6604–6609.

Chen C-K, Woodruff ML, Chen FS, Chen D & Fain GL (2010*a*). Background light produces a recoverin-dependent modulation of activated-rhodopsin lifetime in mouse rods. *J Neurosci* **30,** 1213–1220.

Chen C-K, Woodruff ML, Chen FS, Chen Y, Cilluffo MC, Tranchina D & Fain GL (2012). Modulation of mouse rod response decay by rhodopsin kinase and recoverin. *J Neurosci* **32,** 15998–16006.

Chen C-K, Woodruff ML & Fain GL (2015). Rhodopsin kinase and recoverin modulate phosphodiesterase during mouse photoreceptor light adaptation. *J Gen Physiol* **145,** 213–224.

Chen C-K, Burns ME, He W, Wensel TG, Baylor DA & Simon MI (2000). Slowed recovery of rod photoresponse in mice lacking the GTPase accelerating protein RGS9-1. *Nature* **403,** 557–560.

Chen C-K, Inglese J, Lefkowitz RJ & Hurley JB (1995). Ca(2+)-dependent interaction of recoverin with rhodopsin kinase. *J Biol Chem* **270,** 18060–18066.

Chen C-K, Woodruff ML, Chen FS, Shim H, Cilluffo MC & Fain GL (2010*b*). Replacing the rod with the cone transducin α subunit decreases sensitivity and accelerates response decay. *J Physiol* **588,** 3231–3241.

Chen J, Woodruff ML, Wang T, Concepcion FA, Tranchina D & Fain GL (2010*c*). Channel modulation and the mechanism of light adaptation in mouse rods. *J Neurosci* **30,** 16232–16240.

Cia D, Bordais A, Varela C, Forster V, Sahel JA, Rendon A & Picaud S (2005). Voltage-gated channels and calcium homeostasis in mammalian rod photoreceptors. *J Neurophysiol* **93,** 1468–1475.

Cideciyan A V & Jacobson SG (1996). An alternative phototransduction model for human rod and cone ERG a-waves: normal parameters and variation with age. *Vision Res* **36,** 2609–2621.

Cobbs WH (1991). Light and dark active phosphodiesterase regulation in salamander rods. *J Gen Physiol* **98,** 575–614.

Cobbs WH & Pugh EN (1985). Cyclic GMP can increase rod outer-segment light-sensitive current 10-fold without delay of excitation. *Nature* **313,** 585–587.

Cobbs WH & Pugh EN (1987). Kinetics and components of the flash photocurrent of isolated retinal rods of the larval salamander, Ambystoma tigrinum. *J Physiol* **394,** 529–572.

Colville CA & Molday RS (1996). Primary structure and expression of the human beta-subunit and related proteins of the rod photoreceptor cGMP-gated channel. *J Biol Chem* **271,** 32968–32974.

Cone RA (1972). Rotational diffusion of rhodopsin in the visual receptor membrane. *Nat New Biol* **236,** 39–43.

Conti M (2004). A view into the catalytic pocket of cyclic nucleotide phosphodiesterases. *Nat Struct Mol Biol* **11,** 809–810.

Conti M & Beavo J (2007). Biochemistry and physiology of cyclic nucleotide phosphodiesterases: essential components in cyclic nucleotide signaling. *Annu Rev Biochem* **76,** 481–511.

Cook NJ & Kaupp UB (1988). Solubilization, purification, and reconstitution of the sodium-calcium exchanger from bovine retinal rod outer segments. *J Biol Chem* **263,** 11382–11388.

Corey DP, Dubinsky JM & Schwartz EA (1984). The calcium current in inner segments of rods from the salamander (Ambystoma tigrinum) retina. *J Physiol* **354,** 557–575.

Cornwall MC & Fain GL (1994). Bleached pigment activates transduction in isolated rods of the salamander retina. *J Physiol* **480 (Pt 2,** 261–279.

Cote R (2006). Photoreceptor Phosphodiesterase (PDE6). In *Cyclic Nucleotide Phosphodiesterases in Health and Disease*, pp. 165–193. CRC Press. Available at: http://www.crcnetbase.com/doi/10.1201/9781420020847.ch8 [Accessed November 15, 2016].

Cote RH (2004). Characteristics of photoreceptor PDE (PDE6): similarities and differences to PDE5. *Int J Impot Res* **16 Suppl 1,** S28-33.

Cote RH, Biernbaum MS, Nicol GD & Bownds MD (1984). Light-induced decreases in cGMP concentration precede changes in membrane permeability in frog rod photoreceptors. *J Biol Chem* **259,** 9635–9641.

Cote RH, Bownds MD & Arshavsky VY (1994). cGMP binding sites on photoreceptor phosphodiesterase: role in feedback regulation of visual transduction. *Proc Natl Acad Sci U S A* **91,** 4845–4849.

Cote RH & Brunnock MA (1993). Intracellular cGMP concentration in rod photoreceptors is regulated by binding to high and moderate affinity cGMP binding sites. *J Biol Chem* **268,** 17190–17198.

Cote RH, Nicol GD, Burke SA & Bownds MD (1986). Changes in cGMP Concentration Correlate with Some, but Not All, Aspects of the Light-regulated Conductance of Frog Rod Photoreceptors. *J Biol Chem* **261,** 12965–12975.

Crescitelli F (1958). the Natural History of Visual Pigments. *Ann N Y Acad Sci* **74,** 230–255.

Curcio C a, Sloan KR, Kalina RE & Hendrickson a E (1990). Human photoreceptor topography. *J Comp Neurol* **292,** 497–523.

D'Amours MR & Cote RH (1999). Regulation of photoreceptor phosphodiesterase catalysis by its non-catalytic cGMP-binding sites. *Biochem J* **340 (Pt 3,** 863–869.

D'Amours MR, Granovsky a E, Artemyev NO & Cote RH (1999). Potency and mechanism of action of E4021, a type 5 phosphodiesterase isozyme-selective inhibitor, on the photoreceptor phosphodiesterase depend on the state of activation of the enzyme. *Mol Pharmacol* **55,** 508–514.

Dauner K, Möbus C, Frings S & Möhrlen F (2013). Targeted expression of anoctamin calcium-activated chloride channels in rod photoreceptor terminals of the rodent retina. *Invest Ophthalmol Vis Sci* **54,** 3126–3136.

Demontis GC, Moroni A, Gravante B, Altomare C, Longoni B, Cervetto L & DiFrancesco D (2002). Functional characterisation and subcellular localisation of HCN1 channels in rabbit retinal rod photoreceptors. *J Physiol* **542,** 89–97.

Dhallan RS, Macke JP, Eddy RL, Shows TB, Reed RR, Yau K-W & Nathans J (1992). Human rod photoreceptor cGMP-gated channel: amino acid sequence, gene structure, and functional expression. *J Neurosci* **12,** 3248–3256.

Dizhoor AM, Olshevskaya E V & Peshenko I V (2010). Mg2+/Ca2+ cation binding cycle of guanylyl cyclase activating proteins (GCAPs): role in regulation of photoreceptor guanylyl cyclase. *Mol Cell Biochem* **334,** 117–124.

Doan T, Mendez A, Detwiler PB, Chen J & Rieke F (2006). Multiple phosphorylation sites confer reproducibility of the rod's single-photon responses. *Science* **313,** 530–533.

Donatien P & Jeffery G (2002). Correlation between rod photoreceptor numbers and levels of ocular pigmentation. *Invest Ophthalmol Vis Sci* **43,** 1198–1203.

Donner K, Firsov ML & Govardovskii VI (1990). The frequency of isomerization-like "dark" events in rhodopsin and porphyropsin rods of the bull-frog retina. *J Physiol* **428,** 673–692.

Donner K, Hemila S & Koskelainen A (1988). Temperature-dependence of rod photoresponses from the aspartate-treated retina of the frog (Rana temporaria). *Acta Physiol Scand* **134,** 535–541.

Dumke CL, Arshavsky VY, Calvert PD, Bownds MD & Pugh EN (1994). Rod outer segment structure influences the apparent kinetic parameters of cyclic GMP phosphodiesterase. *J Gen Physiol* **103,** 1071–1098.

Enright JM, Toomey MB, Sato S, Temple SE, Allen JR, Fujiwara R, Kramlinger VM, Nagy LD, Johnson KM, Xiao Y, How MJ, Johnson SL, Roberts NW, Kefalov VJ, Guengerich FP & Corbo JC (2015). Cyp27c1 Red-Shifts the Spectral Sensitivity of Photoreceptors by Converting Vitamin A1 into A2. *Curr Biol* **25,** 3048–3057.

Essayan DM (1999). Cyclic nucleotide phosphodiesterase (PDE) inhibitors and immunomodulation. *Biochem Pharmacol* **57,** 965–973.

Fain GL, Quandt FN, Bastian BL & Gerschenfeld HM (1978). Contribution of a caesium-sensitive conductance increase to the rod photoresponse. *Nature* **272,** 466–469.

Fawzi AB & Northup JK (1990). Guanine nucleotide binding characteristics of transducin: essential role of rhodopsin for rapid exchange of guanine nucleotides. *Biochemistry* **29,** 3804–3812.

Fesenko EE, Kolesnikov SS & Lyubarsky AL (1985). Induction by cyclic GMP of cationic conductance in plasma membrane of retinal rod outer segment. *Nature* **313,** 310–313.

Fotiadis D, Liang Y, Filipek S, Saperstein DA, Engel A & Palczewski K (2003). Atomic-force microscopy: Rhodopsin dimers in native disc membranes. *Nature* **421,** 127–128.

Fotiadis D, Liang Y, Filipek S, Saperstein DA, Engel A & Palczewski K (2004). The G protein-coupled receptor rhodopsin in the native membrane. *FEBS Lett* **564,** 281–288.

Francis SH, Blount MA & Corbin JD (2011*a*). Mammalian cyclic nucleotide phosphodiesterases: molecular mechanisms and physiological functions. *Physiol Rev* **91,** 651–690.

Francis SH, Conti M & Houslay MD eds. (2011*b*). *Phosphodiesterases as Drug Targets*. Springer Berlin Heidelberg, Berlin, Heidelberg. Available at: http://link.springer.com/10.1007/978-3-642-17969-3 [Accessed November 16, 2016].

Fu Y & Yau K-W (2007). Phototransduction in mouse rods and cones. *Pflugers Arch Eur J Physiol* **454,** 805–819.

Gayet-Primo J, Yaeger DB, Khanjian RA & Puthussery T (2018). Heteromeric KV2/KV8.2 Channels Mediate Delayed Rectifier Potassium Currents in Primate Photoreceptors. *J Neurosci* **38,** 3414–3427.

Gibson SK, Parkes JH & Liebman PA (2000). Phosphorylation modulates the affinity of light-activated rhodopsin for G protein and arrestin. *Biochemistry* **39,** 5738–5749.

Gillespie PG & Beavo JA (1988). Characterization of a bovine cone photoreceptor phosphodiesterase purified by cyclic GMP-sepharose chromatography. *J Biol Chem* **263,** 8133–8141.

Gillespie PG & Beavo JA (1989*a*). cGMP is tightly bound to bovine retinal rod phosphodiesterase. *Proc Natl Acad Sci U S A* **86,** 4311–4315.

Gillespie PG & Beavo JA (1989*b*). Inhibition and stimulation of photoreceptor phosphodiesterases by dipyridamole and M&B 22,948. *Mol Pharmacol* **36,** 773–781.

Goraya TA & Cooper DMF (2005). Ca2+-calmodulin-dependent phosphodiesterase (PDE1): current perspectives. *Cell Signal* **17,** 789–797.

Gordon SE, Downing-Park J & Zimmerman AL (1995). Modulation of the cGMP-gated ion channel in frog rods by calmodulin and an endogenous inhibitory factor. *J Physiol* **486 (Pt 3,** 533–546.

Gorodovikova EN, Senin II & Philippov PP (1994). Calcium-sensitive control of rhodopsin phosphorylation in the reconstituted system consisting of photoreceptor membranes, rhodopsin kinase and recoverin. *FEBS Lett* **353,** 171–172.

Govardovskii VI, Fyhrquist N, Reuter T, Kuzmin DG & Donner K (2000). In search of the visual pigment template. *Vis Neurosci* **17,** 509–528.

Govardovskii VI, Korenyak DA, Shukolyukov SA & Zueva L V (2009). Lateral diffusion of rhodopsin in photoreceptor membrane: a reappraisal. *Mol Vis* **15,** 1717–1729.

Granit R (1933). The components of the retinal action potential in mammals and their relation to the discharge in the optic nerve. *J Physiol* **77,** 207–239.

Granovsky AE & Artemyev NO (2001*a*). Partial reconstitution of photoreceptor cGMP phosphodiesterase characteristics in cGMP phosphodiesterase-5. *J Biol Chem* **276,** 21698–21703.

Granovsky AE & Artemyev NO (2001*b*). A conformational switch in the inhibitory gamma-subunit of PDE6 upon enzyme activation by transducin. *Biochemistry* **40,** 13209–13215.

Granovsky AE, Natochin M, McEntaffer RL, Haik TL, Francis SH, Corbin JD & Artemyev NO (1998). Probing domain functions of chimeric PDE6alpha'/PDE5 cGMP-phosphodiesterase. *J Biol Chem* **273,** 24485–24490.

Gray-Keller MP & Detwiler PB (1996). Ca2+ dependence of dark- and light-adapted flash responses in rod photoreceptors. *Neuron* **17,** 323–331.

Green DG & Kapousta-Bruneau N V. (1999*a*). Electrophysiological properties of a new isolated rat retina preparation. *Vision Res* **39,** 2165–2177.

Green DG & Kapousta-Bruneau N V. (1999*b*). A dissection of the electroretinogram from the isolated rat retina with microelectrodes and drugs. *Vis Neurosci* **16,** 727–741.

Grigoriev II, Senin II, Tikhomirova NK, Komolov KE, Permyakov SE, Zernii EY, Koch K-W & Philippov PP (2012). Synergetic effect of recoverin and calmodulin on regulation of rhodopsin kinase. *Front Mol Neurosci* **5,** 28.

Grimes WN, Baudin J, Azevedo AW & Rieke F (2018). Range, routing and kinetics of rod signaling in primate retina. *Elife*; DOI: 10.7554/eLife.38281.

Gross OP & Burns ME (2010). Control of rhodopsin's active lifetime by arrestin-1 expression in mammalian rods. *J Neurosci* **30,** 3450–3457.

Gross OP, Pugh EN & Burns ME (2012*a*). Spatiotemporal cGMP dynamics in living mouse rods. *Biophys J* **102,** 1775–1784.

Gross OP, Pugh EN & Burns ME (2012*b*). Calcium Feedback to cGMP Synthesis Strongly Attenuates Single-Photon Responses Driven by Long Rhodopsin Lifetimes. *Neuron* **76,** 370–382.

Gross OP, Pugh EN & Burns ME (2015). cGMP in mouse rods: the spatiotemporal dynamics underlying single photon responses. *Front Mol Neurosci* **8,** 6.

Grunwald ME, Yu WP, Yu HH & Yau K-W (1998). Identification of a domain on the beta-subunit of the rod cGMP-gated cation channel that mediates inhibition by calcium-calmodulin. *J Biol Chem* **273,** 9148–9157.

Gunkel M, Schoneberg J, Alkhaldi W, Irsen S, Noe F, Kaupp UB & Al-Amoudi A (2015). Higher-order architecture of rhodopsin in intact photoreceptors and its implication for phototransduction kinetics. *Structure* **23,** 628–638.

Guo L-W, Grant JE, Hajipour AR, Muradov H, Arbabian M, Artemyev NO & Ruoho AE (2005). Asymmetric interaction between rod cyclic GMP phosphodiesterase gamma subunits and alphabeta subunits. *J Biol Chem* **280,** 12585–12592.

Guo L-W, Muradov H, Hajipour AR, Sievert MK, Artemyev NO & Ruoho AE (2006). The inhibitory gamma subunit of the rod cGMP phosphodiesterase binds the catalytic subunits in an extended linear structure. *J Biol Chem* **281,** 15412–15422.

Guo L-W & Ruoho AE (2008). The retinal cGMP phosphodiesterase gamma-subunit - a chameleon. *Curr Protein Pept Sci* **9,** 611–625.

Haber-Pohlmeier S, Abarca-Heidemann K, Korschen HG, Dhiman HK, Heberle J, Schwalbe H, Klein-Seetharaman J, Kaupp UB & Pohlmeier A (2007). Binding of Ca2+ to glutamic acid-rich polypeptides from the rod outer segment. *Biophys J* **92,** 3207–3214.

Hagins WA, Penn RD & Yoshikami S (1970). Dark current and photocurrent in retinal rods. *Biophys J* **10,** 380–412.

Hamer RD, Nicholas SC, Tranchina D, Lamb TD & Jarvinen JLP (2005). Toward a unified model of vertebrate rod phototransduction. *Vis Neurosci* **22,** 417–436.

Hamer RD, Nicholas SC, Tranchina D, Liebman PA & Lamb TD (2003). Multiple steps of phosphorylation of activated rhodopsin can account for the reproducibility of vertebrate rod single-photon responses. *J Gen Physiol* **122,** 419–444.

Hamm HE & Bownds MD (1986). Protein complement of rod outer segments of frog retina. *Biochemistry* **25,** 4512–4523.

He F, Seryshev AB, Cowan CW & Wensel TG (2000*a*). Multiple zinc binding sites in retinal rod cGMP phosphodiesterase, PDE6alpha beta. *J Biol Chem* **275,** 20572–20577.

He W, Cowan CW & Wensel TG (1998). RGS9, a GTPase accelerator for phototransduction. *Neuron* **20,** 95–102.

He W, Lu L, Zhang X, El-Hodiri HM, Chen C-K, Slep KC, Simon MI, Jamrich M & Wensel TG (2000*b*). Modules in the photoreceptor RGS9-1.Gbeta 5L GTPase-accelerating protein complex control effector coupling, GTPase acceleration, protein folding, and stability. *J Biol Chem* **275,** 37093–37100.

Heck M & Hofmann KP (2001). Maximal rate and nucleotide dependence of rhodopsin-catalyzed transducin activation: initial rate analysis based on a double displacement mechanism. *J Biol Chem* **276,** 10000–10009.

Heikkinen H, Nymark S & Koskelainen A (2008). Mouse cone photoresponses obtained with electroretinogram from the isolated retina. *Vision Res* **48,** 264–272.

Heikkinen H, Vinberg F, Pitkänen M, Kommonen B & Koskelainen A (2012). Flash responses of mouse rod photoreceptors in the isolated retina and corneal electroretinogram: Comparison of gain and kinetics. *Investig Ophthalmol Vis Sci* **53,** 5653–5664.

Helten A, Saftel W & Koch K-W (2007). Expression level and activity profile of membrane bound guanylate cyclase type 2 in rod outer segments. *J Neurochem* **103,** 1439–1446.

Hodgkin AL & Nunn BJ (1988). Control of light-sensitive current in salamander rods. *J Physiol* **403,** 439–471.

Van Hook MJ, Nawy S & Thoreson WB (2019). Voltage- and calcium-gated ion channels of neurons in

the vertebrate retina. *Prog Retin Eye Res* **72,** 100760.

Hsu YT & Molday RS (1993). Modulation of the cGMP-gated channel of rod photoreceptor cells by calmodulin. *Nature* **361,** 76–79.

Hu G & Wensel TG (2002). R9AP, a membrane anchor for the photoreceptor GTPase accelerating protein, RGS9-1. *Proc Natl Acad Sci U S A* **99,** 9755–9760.

Hurley JB & Stryer L (1982). Purification and characterization of the gamma regulatory subunit of the cyclic GMP phosphodiesterase from retinal rod outer segments. *J Biol Chem* **257,** 11094–11099.

Ingram NT, Sampath AP & Fain GL (2016). Why are rods more sensitive than cones? *J Physiol* **594,** 5415–5426.

Ingram NT, Sampath AP & Fain GL (2020). Membrane conductances of mouse cone photoreceptors. *J Gen Physiol*; DOI: 10.1085/jgp.201912520.

Invergo BM, Dell'Orco D, Montanucci L, Koch K-W & Bertranpetit J (2014). A comprehensive model of the phototransduction cascade in mouse rod cells. *Mol Biosyst* **10,** 1481–1489.

Invergo BM, Montanucci L, Koch K-W, Bertranpetit J & Dell'orco D (2013). Exploring the rate-limiting steps in visual phototransduction recovery by bottom-up kinetic modeling. *Cell Commun Signal* **11,** 36.

Jeon CJ, Strettoi E & Masland RH (1998). The major cell populations of the mouse retina. *J Neurosci* **18,** 8936–8946.

Johnson MA, Jeffrey BG, Messias AM V & Robson AG (2019). ISCEV extended protocol for the stimulus-response series for the dark-adapted full-field ERG b-wave. *Doc Ophthalmol* **138,** 217–227.

Jones GJ (1995). Light adaptation and the rising phase of the flash photocurrent of salamander retinal rods. *J Physiol* **487 (Pt 2,** 441–451.

Kakkar R, Raju R V & Sharma RK (1999). Calmodulin-dependent cyclic nucleotide phosphodiesterase (PDE1). *Cell Mol Life Sci* **55,** 1164–1186.

Karwoski CJ & Xu X (1999). Current source-density analysis of light-evoked field potentials in rabbit retina. *Vis Neurosci* **16,** 369–377.

Kaupp UB & Seifert R (2002). Cyclic nucleotide-gated ion channels. *Physiol Rev* **82,** 769–824.

Kawai F, Horiguchi M, Suzuki H & Miyachi E (2002). Modulation by hyperpolarization-activated cationic currents of voltage responses in human rods. *Brain Res* **943,** 48–55.

Ke H (2004). Implications of PDE4 structure on inhibitor selectivity across PDE families. *Int J Impot Res* **16 Suppl 1,** S24-7.

Keresztes G, Martemyanov KA, Krispel CM, Mutai H, Yoo PJ, Maison SF, Burns ME, Arshavsky VY & Heller S (2004). Absence of the RGS9.Gbeta5 GTPase-activating complex in photoreceptors of the R9AP knockout mouse. *J Biol Chem* **279,** 1581–1584.

Kerr NM & Danesh-Meyer H V (2009). Phosphodiesterase inhibitors and the eye. *Clin Experiment Ophthalmol* **37,** 514–523.

Khan AS, Sheikh Z, Khan S, Dwivedi R & Benjamin E (2011). Viagra deafness--sensorineural hearing loss and phosphodiesterase-5 inhibitors. *Laryngoscope* **121,** 1049–1054.

Kim J-W, Yang H-J, Oel AP, Brooks MJ, Jia L, Plachetzki DC, Li W, Allison WT & Swaroop A (2016).

Recruitment of Rod Photoreceptors from Short-Wavelength-Sensitive Cones during the Evolution of Nocturnal Vision in Mammals. *Dev Cell* **37,** 520–532.

Knop GC, Seeliger MW, Thiel F, Mataruga A, Kaupp UB, Friedburg C, Tanimoto N & Muller F (2008). Light responses in the mouse retina are prolonged upon targeted deletion of the HCN1 channel gene. *Eur J Neurosci* **28,** 2221–2230.

Koch K-W & Dell'orco D (2013). A calcium-relay mechanism in vertebrate phototransduction. *ACS Chem Neurosci* **4,** 909–917.

Koch K-W & Dell'Orco D (2015). Protein and Signaling Networks in Vertebrate Photoreceptor Cells. *Front Mol Neurosci* **8,** 67.

Koch K-W (1994). Calcium as modulator of phototransduction in vertebrate photoreceptor cells. *RevPhysiolBiochemPharmacol* **125,** 149–192.

Koch K-W & Stryer L (1988). Highly cooperative feedback control of retinal rod guanylate cyclase by calcium ions. *Nature* **334,** 64–66.

Koenig D & Hofer H (2011). The absolute threshold of cone vision. *J Vis* **11,** 1–24.

Koike C, Numata T, Ueda H, Mori Y & Furukawa T (2010*a*). TRPM1: a vertebrate TRP channel responsible for retinal ON bipolar function. *Cell Calcium* **48,** 95–101.

Koike C, Obara T, Uriu Y, Numata T, Sanuki R, Miyata K, Koyasu T, Ueno S, Funabiki K, Tani A, Ueda H, Kondo M, Mori Y, Tachibana M & Furukawa T (2010*b*). TRPM1 is a component of the retinal ON bipolar cell transduction channel in the mGluR6 cascade. *Proc Natl Acad Sci U S A* **107,** 332–337.

Kooragayala K, Gotoh N, Cogliati T, Nellissery J, Kaden TR, French S, Balaban R, Li W, Covian R & Swaroop A (2015). Quantification of Oxygen Consumption in Retina Ex Vivo Demonstrates Limited Reserve Capacity of Photoreceptor Mitochondria. *Invest Ophthalmol Vis Sci* **56,** 8428–8436.

Korenbrot JI (2012). Speed, adaptation, and stability of the response to light in cone photoreceptors: the functional role of Ca-dependent modulation of ligand sensitivity in cGMP-gated ion channels. *J Gen Physiol* **139,** 31–56.

Korschen HG, Beyermann M, Muller F, Heck M, Vantler M, Koch K-W, Kellner R, Wolfrum U, Bode C, Hofmann KP & Kaupp UB (1999). Interaction of glutamic-acid-rich proteins with the cGMP signalling pathway in rod photoreceptors. *Nature* **400,** 761–766.

Koutalos Y, Nakatani K, Tamura T & Yau K-W (1995*a*). Characterization of guanylate cyclase activity in single retinal rod outer segments. *J Gen Physiol* **106,** 863–890.

Koutalos Y, Nakatani K & Yau K-W (1995*b*). The cGMP-phosphodiesterase and its contribution to sensitivity regulation in retinal rods. *J Gen Physiol* **106,** 891–921.

Krispel CM, Chen C-K, Simon MI & Burns ME (2003). Prolonged photoresponses and defective adaptation in rods of Gbeta5-/- mice. *J Neurosci* **23,** 6965–6971.

Krispel CM, Chen D, Melling N, Chen Y-J, Martemyanov KA, Quillinan N, Arshavsky VY, Wensel TG, Chen C-K & Burns ME (2006). RGS expression rate-limits recovery of rod photoresponses. *Neuron* **51,** 409–416.

Krizaj D & Copenhagen DR (2002). Calcium regulation in photoreceptors. *Front Biosci* **7,** d2023–d2044.

Lagnado L & Baylor DA (1994). Calcium controls light-triggered formation of catalytically active rhodopsin. *Nature* **367,** 273–277.

Lamb TD (1994). Stochastic simulation of activation in the G-protein cascade of phototransduction. *Biophys J* **67,** 1439–1454.

Lamb TD, Heck M & Kraft TW (2018). Implications of dimeric activation of PDE6 for rod phototransduction. *Open Biol*; DOI: 10.1098/rsob.180076.

Lamb TD & Kraft TW (2016). Quantitative modeling of the molecular steps underlying shut-off of rhodopsin activity in rod phototransduction. *Mol Vis* **22,** 674–696.

Lamb TD & Pugh EN (1992). A quantitative account of the activation steps involved in phototransduction in amphibian photoreceptors. *J Physiol* **449,** 719–758.

Lamb TD & Pugh EN (2004). Dark adaptation and the retinoid cycle of vision. *Prog Retin Eye Res* **23,** 307–380.

Lee KA, Nawrot M, Garwin GG, Saari JC & Hurley JB (2010). Relationships among visual cycle retinoids, rhodopsin phosphorylation, and phototransduction in mouse eyes during light and dark adaptation. *Biochemistry* **49,** 2454–2463.

Leskov IB, Klenchin V a, Handy JW, Whitlock GG, Govardovskii VI, Bownds MD, Lamb TD, Pugh EN & Arshavsky VY (2000). The gain of rod phototransduction: reconciliation of biochemical and electrophysiological measurements. *Neuron* **27,** 525–537.

Liang Y, Fotiadis D, Maeda T, Maeda A, Modzelewska A, Filipek S, Saperstein DA, Engel A & Palczewski K (2004). Rhodopsin signaling and organization in heterozygote rhodopsin knockout mice. *J Biol Chem* **279,** 48189–48196.

Liebman PA & Entine G (1974). Lateral diffusion of visual pigment in photorecptor disk membranes. *Science* **185,** 457–459.

Liebman PA, Parker KR & Dratz EA (1987). The molecular mechanism of visual excitation and its relation to the structure and composition of the rod outer segment. *Annu Rev Physiol* **49,** 765–791.

Lipton SA, Rasmussen H & Dowling JE (1977). Electrical and adaptive properties of rod photoreceptors in Bufo marinus. II. Effects of cyclic nucleotides and prostaglandins. *J Gen Physiol* **70,** 771–791.

Liu YT, Matte SL, Corbin JD, Francis SH & Cote RH (2009). Probing the catalytic sites and activation mechanism of photoreceptor phosphodiesterase using radiolabeled phosphodiesterase inhibitors. *J Biol Chem* **284,** 31541–31547.

Long JH, Arshavsky VY & Burns ME (2013). Absence of synaptic regulation by phosducin in retinal slices. *PLoS One* **8,** e83970.

Lugnier C (2006). Cyclic nucleotide phosphodiesterase (PDE) superfamily: a new target for the development of specific therapeutic agents. *Pharmacol Ther* **109,** 366–398.

Maeda T, Imanishi Y & Palczewski K (2003). Rhodopsin phosphorylation: 30 years later. *Prog Retin Eye Res* **22,** 417–434.

Makino CL, Dodd RL, Chen J, Burns ME, Roca A, Simon MI & Baylor DA (2004). Recoverin regulates light-dependent phosphodiesterase activity in retinal rods. *J Gen Physiol* **123,** 729–741.

Makino CL, Peshenko I V, Wen X-H, Olshevskaya E V, Barrett R & Dizhoor AM (2008). A role for GCAP2 in regulating the photoresponse. Guanylyl cyclase activation and rod electrophysiology in GUCA1B knock-out mice. *J Biol Chem* **283,** 29135–29143.

Makino CL, Wen X-H, Olshevskaya E V, Peshenko I V, Savchenko AB & Dizhoor AM (2012). Enzymatic relay mechanism stimulates cyclic GMP synthesis in rod photoresponse: biochemical and

physiological study in guanylyl cyclase activating protein 1 knockout mice. *PLoS One* **7,** e47637.

Makino ER, Handy JW, Li T & Arshavsky VY (1999). The GTPase activating factor for transducin in rod photoreceptors is the complex between RGS9 and type 5 G protein beta subunit. *Proc Natl Acad Sci U S A* **96,** 1947–1952.

Matthews HR, Cornwall MC & Fain GL (1996). Persistent activation of transducin by bleached rhodopsin in salamander rods. *J Gen Physiol* **108,** 557–563.

Matthews HR & Fain GL (2001). A light-dependent increase in free Ca2+ concentration in the salamander rod outer segment. *J Physiol* **532,** 305–321.

Matthews HR, Murphy RL, Fain GL & Lamb TD (1988). Photoreceptor light adaptation is mediated by cytoplasmic calcium concentration. *Nature* **334,** 67–69.

Maurice DH, Ke H, Ahmad F, Wang Y, Chung J & Manganiello VC (2014). Advances in targeting cyclic nucleotide phosphodiesterases. *Nat Rev Drug Discov* **13,** 290–314.

McCulloch DL, Kondo M, Hamilton R, Lachapelle P, Messias AM V, Robson AG & Ueno S (2019). ISCEV extended protocol for the stimulus-response series for light-adapted full-field ERG. *Doc Ophthalmol* **138,** 205–215.

Medrano CJ & Fox DA (1995). Oxygen consumption in the rat outer and inner retina: light- and pharmacologically-induced inhibition. *Exp Eye Res* **61,** 273–284.

Melia TJ, Malinski JA, He F & Wensel TG (2000). Enhancement of phototransduction protein interactions by lipid surfaces. *J Biol Chem* **275,** 3535–3542.

Melia TJ, Cowan CW, Angleson JK & Wensel TG (1997). A comparison of the efficiency of G protein activation by ligand-free and light-activated forms of rhodopsin. *Biophys J* **73,** 3182–3191.

Mendez A, Burns ME, Roca A, Lem J, Wu LW, Simon MI, Baylor DA & Chen J (2000). Rapid and reproducible deactivation of rhodopsin requires multiple phosphorylation sites. *Neuron* **28,** 153–164.

Mendez A, Burns ME, Sokal I, Dizhoor AM, Baehr W, Palczewski K, Baylor DA & Chen J (2001). Role of guanylate cyclase-activating proteins (GCAPs) in setting the flash sensitivity of rod photoreceptors. *Proc Natl Acad Sci U S A* **98,** 9948–9953.

Molday RS & Kaupp UB (2000). *Chapter 4 Ion channels of vertebrate photoreceptors*.

Molnar T, Barabas P, Birnbaumer L, Punzo C, Kefalov V & Krizaj D (2012). Store-operated channels regulate intracellular calcium in mammalian rods. *J Physiol* **590,** 3465–3481.

Morgans CW, Brown RL & Duvoisin RM (2010). TRPM1: the endpoint of the mGluR6 signal transduction cascade in retinal ON-bipolar cells. *Bioessays* **32,** 609–614.

Moriondo A, Pelucchi B & Rispoli G (2001). Calcium-activated potassium current clamps the dark potential of vertebrate rods. *Eur J Neurosci* **14,** 19–26.

Morshedian A, Woodruff ML & Fain GL (2018). Role of recoverin in rod photoreceptor light adaptation. *J Physiol* **596,** 1513–1526.

Mou H & Cote RH (2001). The catalytic and GAF domains of the rod cGMP phosphodiesterase (PDE6) heterodimer are regulated by distinct regions of its inhibitory gamma subunit. *J Biol Chem* **276,** 27527–27534.

Mou H, Grazio HJ 3rd, Cook TA, Beavo JA & Cote RH (1999). cGMP binding to noncatalytic sites on

mammalian rod photoreceptor phosphodiesterase is regulated by binding of its gamma and delta subunits. *J Biol Chem* **274,** 18813–18820.

Muradov H, Boyd KK & Artemyev NO (2010). Rod phosphodiesterase-6 PDE6A and PDE6B subunits are enzymatically equivalent. *J Biol Chem* **285,** 39828–39834.

Muradov H, Boyd KK, Haeri M, Kerov V, Knox BE & Artemyev NO (2009). Characterization of human cone phosphodiesterase-6 ectopically expressed in Xenopus laevis rods. *J Biol Chem* **284,** 32662–32669.

Murakami M & Kaneko A (1966). Subcomponents of P3 in cold-blooded vertebrate retinae. *Nature* **210,** 103–104.

Mustafi D, Engel AH & Palczewski K (2009). Structure of cone photoreceptors. *Prog Retin Eye Res* **28,** 289–302.

Naarendorp F, Esdaille TM, Banden SM, Andrews-Labenski J, Gross OP & Pugh EN (2010). Dark light, rod saturation, and the absolute and incremental sensitivity of mouse cone vision. *J Neurosci* **30,** 12495–12507.

Nakatani K, Koutalos Y & Yau K-W (1995). Ca2+ modulation of the cGMP-gated channel of bullfrog retinal rod photoreceptors. *J Physiol* **484 (Pt 1,** 69–76.

Nakatani K & Yau K-W (1988*a*). Calcium and magnesium fluxes across the plasma membrane of the toad rod outer segment. *J Physiol* **395,** 695–729.

Nakatani K & Yau K-W (1988*b*). Calcium and light adaptation in retinal rods and cones. *Nature* **334,** 69–71.

Nathans J (1992). Rhodopsin: structure, function, and genetics. *Biochemistry* **31,** 4923–4931.

Nemargut JP, Zhu J, Savoie BT & Wang G-Y (2009). Differential effects of charybdotoxin on the activity of retinal ganglion cells in the dark- and light-adapted mouse retina. *Vision Res* **49,** 388–397.

Nickell S, Park PSH, Baumeister W & Palczewski K (2007). Three-dimensional architecture of murine rod outer segments determined by cryoelectron tomography. *J Cell Biol* **177,** 917–925.

Nikonov S, Lamb TD & Pugh EN (2000). The role of steady phosphodiesterase activity in the kinetics and sensitivity of the light-adapted salamander rod photoresponse. *J Gen Physiol* **116,** 795–824.

Nikonov SS, Kholodenko R, Lem J & Pugh EN (2006). Physiological features of the S- and M-cone photoreceptors of wild-type mice from single-cell recordings. *J Gen Physiol* **127,** 359–374.

Norton AW, D'Amours MR, Grazio HJ, Hebert TL & Cote RH (2000). Mechanism of transducin activation of frog rod photoreceptor phosphodiesterase. Allosteric interactiona between the inhibitory gamma subunit and the noncatalytic cGMP-binding sites. *J Biol Chem* **275,** 38611–38619.

Nymark S, Heikkinen H, Haldin C, Donner K & Koskelainen A (2005). Light responses and light adaptation in rat retinal rods at different temperatures. *J Physiol* **567,** 923–938.

Oakley B (1977). Potassium and the photoreceptor-dependent pigment epithelial hyperpolarization. *J Gen Physiol* **70,** 405–425.

Oakley B, Katz BJ, Xu Z & Zheng J (1992). Spatial buffering of extracellular potassium by Müller (glial) cells in the toad retina. *Exp Eye Res* **55,** 539–550.

Ohyama T, Hackos DH, Frings S, Hagen V, Kaupp UB & Korenbrot JI (2000). Fraction of the dark current carried by Ca(2+) through cGMP-gated ion channels of intact rod and cone photoreceptors. *J Gen*

Physiol **116,** 735–754.

Okada T, Ernst OP, Palczewski K & Hofmann KP (2001). Activation of rhodopsin: new insights from structural and biochemical studies. *Trends Biochem Sci* **26,** 318–324.

Okawa H, Sampath AP, Laughlin SB & Fain GL (2008). ATP consumption by mammalian rod photoreceptors in darkness and in light. *Curr Biol* **18,** 1917–1921.

Olshevskaya E V, Calvert PD, Woodruff ML, Peshenko I V, Savchenko AB, Makino CL, Ho Y-S, Fain GL & Dizhoor AM (2004). The Y99C mutation in guanylyl cyclase-activating protein 1 increases intracellular Ca2+ and causes photoreceptor degeneration in transgenic mice. *J Neurosci* **24,** 6078–6085.

Ortin-Martinez A, Nadal-Nicolas FM, Jimenez-Lopez M, Alburquerque-Bejar JJ, Nieto-Lopez L, Garcia-Ayuso D, Villegas-Perez MP, Vidal-Sanz M & Agudo-Barriuso M (2014). Number and distribution of mouse retinal cone photoreceptors: differences between an albino (Swiss) and a pigmented (C57/BL6) strain. *PLoS One* **9,** e102392.

Osterberg GA (1935). Topography of the layer of rods and cones in the human retina. *Acta Ophthalmol* **13,** 11–103.

Paglia MJ, Mou H & Cote RH (2002). Regulation of photoreceptor phosphodiesterase (PDE6) by phosphorylation of its inhibitory gamma subunit re-evaluated. *J Biol Chem* **277,** 5017–5023.

Palczewska G, Vinberg F, Stremplewski P, Bircher MP, Salom D, Komar K, Zhang J, Cascella M, Wojtkowski M, Kefalov VJ & Palczewski K (2014). Human infrared vision is triggered by two-photon chromophore isomerization. *Proc Natl Acad Sci U S A* **111,** E5445-54.

Palczewski K (1997). GTP-binding-protein-coupled receptor kinases--two mechanistic models. *Eur J Biochem* **248,** 261–269.

Palczewski K & Benovic JL (1991). G-protein-coupled receptor kinases. *Trends Biochem Sci* **16,** 387–391.

Palczewski K, Polans AS, Baehr W & Ames JB (2000). Ca(2+)-binding proteins in the retina: structure, function, and the etiology of human visual diseases. *Bioessays* **22,** 337–350.

Peet JA (2004). Quantification of the cytoplasmic spaces of living cells with EGFP reveals arrestin-EGFP to be in disequilibrium in dark adapted rod photoreceptors. *J Cell Sci* **117,** 3049–3059.

Peichl L (2005). Diversity of mammalian photoreceptor properties: adaptations to habitat and lifestyle? *Anat Rec A Discov Mol Cell Evol Biol* **287,** 1001–1012.

Pelucchi B, Grimaldi A & Moriondo A (2008). Vertebrate rod photoreceptors express both BK and IK calcium-activated potassium channels, but only BK channels are involved in receptor potential regulation. *J Neurosci Res* **86,** 194–201.

Penn RD & Hagins WA (1969). Signal transmission along retinal rods and the origin of the electroretinographic a-wave. *Nature* **223,** 201–204.

Penn RD & Hagins WA (1972). Kinetics of the photocurrent of retinal rods. *Biophys J* **12,** 1073–1094.

Pentia DC, Hosier S & Cote RH (2006). The glutamic acid-rich protein-2 (GARP2) is a high affinity rod photoreceptor phosphodiesterase (PDE6)-binding protein that modulates its catalytic properties. *J Biol Chem* **281,** 5500–5505.

Pepperberg DR, Cornwall MC, Kahlert M, Hofmann KP, Jin J, Jones GJ & Ripps H (1992). Light-dependent delay in the falling phase of the retinal rod photoresponse. *Vis Neurosci* **8,** 9–18.

Peshenko I V & Dizhoor AM (2004). Guanylyl cyclase-activating proteins (GCAPs) are Ca2+/Mg2+ sensors: implications for photoreceptor guanylyl cyclase (RetGC) regulation in mammalian photoreceptors. *J Biol Chem* **279,** 16903–16906.

Peshenko I V, Olshevskaya E V, Savchenko AB, Karan S, Palczewski K, Baehr W & Dizhoor AM (2011). Enzymatic properties and regulation of the native isozymes of retinal membrane guanylyl cyclase (RetGC) from mouse photoreceptors. *Biochemistry* **50,** 5590–5600.

Poo M & Cone RA (1974). Lateral diffusion of rhodopsin in the photoreceptor membrane. *Nature* **247,** 438–441.

Poo MM & Cone RA (1973). Lateral diffusion of phodopsin in Necturus rods. *Exp Eye Res* **17,** 503–510.

Portzehl H, Caldwell PC & Rüegg JC (1964). The dependence of contraction and relaxation of muscle fibres from the crab Maia squinado on the internal concentration of free calcium ions. *BBA - Spec Sect Biophys Subj* **79,** 581–591.

Pugh EN & Lamb TD (2000). Phototransduction in Vertebrate Rods and Cones: Molecular Mechanisms of Amplification, Recovery and Light Adaptation. In *Handbook of Biological Physics*, ed. Stavenga DG, DeGrip WJ & Pugh EN, pp. 183–254. Elsevier.

Pugh EN, Nikonov S & Lamb TD (1999). Molecular mechanisms of vertebrate photoreceptor light adaptation. *Curr Opin Neurobiol* **9,** 410–418.

Pugh EN, Falsini B & Lyubarsky AL (1998). The Origin of the Major Rod- and Cone-driven Components of the Rodent Electroretinogram and the Effect of Age and Light-rearing History on the Magnitude of These Components. In *Photostasis and Related Phenomena*, ed. Williams TP & Thistle AB.

Pugh EN & Lamb TD (1990). Cyclic GMP and calcium: the internal messengers of excitation and adaptation in vertebrate photoreceptors. *Vision Res* **30,** 1923–1948.

Quandt FN, Nicol GD & Schnetkamp PP (1991). Voltage-dependent gating and block of the cyclic-GMP-dependent current in bovine rod outer segments. *Neuroscience* **42,** 629–638.

Qureshi BM, Behrmann E, Schöneberg J, Loerke J, Bürger J, Mielke T, Giesebrecht J, Noé F, Hofmann KP, Spahn CMT & Heck M (2015). Asymmetric properties of rod cGMP Phosphodiesterase 6 (PDE6): structural and functional analysis. *BMC Pharmacol Toxicol* **16,** A76–A76.

Qureshi BM, Behrmann E, Schöneberg J, Loerke J, Bürger J, Mielke T, Giesebrecht J, Noé F, Lamb TD, Hofmann KP, Spahn CMT & Heck M (2018). It takes two transducins to activate the cGMP-phosphodiesterase 6 in retinal rods. *Open Biol*. Available at: http://rsob.royalsocietypublishing.org/content/8/8/180075.abstract.

Rakshit T, Senapati S, Parmar VM, Sahu B, Maeda A & Park PS-H (2017). Adaptations in rod outer segment disc membranes in response to environmental lighting conditions. *Biochim Biophys acta Mol cell Res* **1864,** 1691–1702.

Ramdas L, Disher RM & Wensel TG (1991). Nucleotide exchange and cGMP phosphodiesterase activation by pertussis toxin inactivated transducin. *Biochemistry* **30,** 11637–11645.

Rebrik TI & Korenbrot JI (1998). In intact cone photoreceptors, a Ca2+-dependent, diffusible factor modulates the cGMP-gated ion channels differently than in rods. *J Gen Physiol* **112,** 537–548.

Reid DM, Friedel U, Molday RS & Cook NJ (1990). Identification of the sodium-calcium exchanger as the major ricin-binding glycoprotein of bovine rod outer segments and its localization to the plasma membrane. *Biochemistry* **29,** 1601–1607.

Reilander H, Achilles A, Friedel U, Maul G, Lottspeich F & Cook NJ (1992). Primary structure and functional expression of the Na/Ca,K-exchanger from bovine rod photoreceptors. *EMBO J* **11,** 1689–1695.

Reingruber J & Holcman D (2008). Estimating the rate constant of cyclic GMP hydrolysis by activated phosphodiesterase in photoreceptors. *J Chem Phys* **129,** 145102.

Reingruber J & Holcman D (2009). Diffusion in narrow domains and application to phototransduction. *Phys Rev E Stat Nonlin Soft Matter Phys* **79,** 30904.

Reingruber J, Pahlberg J, Woodruff ML, Sampath AP, Fain GL & Holcman D (2013). Detection of single photons by toad and mouse rods. *Proc Natl Acad Sci U S A* **110,** 19378–19383.

Reingruber J, Holcman D & Fain GL (2015). How rods respond to single photons: Key adaptations of a G-protein cascade that enable vision at the physical limit of perception. *BioEssays* **37,** 1243–1252.

Reuter T (2011). Fifty years of dark adaptation 1961-2011. *Vision Res* **51,** 2243–2262.

Rieke F & Baylor D (1998). Single-photon detection by rod cells of the retina. *Rev Mod Phys* **70,** 1027–1036.

Rieke F & Baylor DA (1996). Molecular origin of continuous dark noise in rod photoreceptors. *Biophys J* **71,** 2553–2572.

Rieke F & Schwartz EA (1994). A cGMP-gated current can control exocytosis at cone synapses. *Neuron* **13,** 863–873.

Robson JG & Frishman LJ (2014). The rod-driven a-wave of the dark-adapted mammalian electroretinogram. *Prog Retin Eye Res* **39,** 1–22.

Rodieck RW (1999). *The First Steps in Seeing*. Sunderland, Mass. : Sinauer Associates. Available at: http://archopht.jamanetwork.com/article.aspx?doi=10.1001/archopht.117.4.550.

Saari JC (2012). Vitamin A metabolism in rod and cone visual cycles. *Annu Rev Nutr* **32,** 125–145.

Sakurai K, Chen J & Kefalov VJ (2011*a*). Role of guanylyl cyclase modulation in mouse cone phototransduction. *J Neurosci* **31,** 7991–8000.

Sakurai K, Chen J, Khani SC & Kefalov VJ (2015). Regulation of mammalian cone phototransduction by recoverin and rhodopsin kinase. *J Biol Chem* **290,** 9239–9250.

Sakurai K, Young JE, Kefalov VJ & Khani SC (2011*b*). Variation in rhodopsin kinase expression alters the dim flash response shut off and the light adaptation in rod photoreceptors. *Invest Ophthalmol Vis Sci* **52,** 6793–6800.

Sampath AP, Matthews HR, Cornwall MC, Bandarchi J & Fain GL (1999). Light-dependent changes in outer segment free-Ca2+ concentration in salamander cone photoreceptors. *J Gen Physiol* **113,** 267–277.

Sampath AP, Matthews HR, Cornwall MC & Fain GL (1998). Bleached pigment produces a maintained decrease in outer segment Ca2+ in salamander rods. *J Gen Physiol* **111,** 53–64.

Sampath AP, Strissel KJ, Elias R, Arshavsky VY, McGinnis JF, Chen J, Kawamura S, Rieke F & Hurley JB (2005). Recoverin improves rod-mediated vision by enhancing signal transmission in the mouse retina. *Neuron* **46,** 413–420.

Della Santina L, Piano I, Cangiano L, Caputo A, Ludwig A, Cervetto L & Gargini C (2012). Processing of retinal signals in normal and HCN deficient mice. *PLoS One* **7,** e29812.

Sarfare S, McKeown AS, Messinger J, Rubin G, Wei H, Kraft TW & Pittler SJ (2014). Overexpression of rod photoreceptor glutamic acid rich protein 2 (GARP2) increases gain and slows recovery in mouse retina. *Cell Commun Signal* **12,** 67.

Sato S, Jastrzebska B, Engel A, Palczewski K & Kefalov VJ (2019). Apo-Opsin Exists in Equilibrium Between a Predominant Inactive and a Rare Highly Active State. *J Neurosci* **39,** 212–223.

Savchenko A, Barnes S & Kramer RH (1997). Cyclic-nucleotide-gated channels mediate synaptic feedback by nitric oxide. *Nature* **390,** 694–698.

Schnetkamp PP (1986). Sodium-calcium exchange in the outer segments of bovine rod photoreceptors. *J Physiol* **373,** 25–45.

Seeliger MW, Brombas A, Weiler R, Humphries P, Knop G, Tanimoto N & Muller F (2011). Modulation of rod photoreceptor output by HCN1 channels is essential for regular mesopic cone vision. *Nat Commun* **2,** 532.

Senin II, Zargarov AA, Alekseev AM, Gorodovikova EN, Lipkin VM & Philippov PP (1995). N-myristoylation of recoverin enhances its efficiency as an inhibitor of rhodopsin kinase. *FEBS Lett* **376,** 87–90.

Sharpe LT, Fach CC & Stockman A (1992). The field adaptation of the human rod visual system. *J Physiol* **445,** 319–343.

Shen L, Caruso G, Bisegna P, Andreucci D, Gurevich V V, Hamm HE & DiBenedetto E (2010). Dynamics of mouse rod phototransduction and its sensitivity to variation of key parameters. *IET Syst Biol* **4,** 12–32.

Shi L, Chang JY-A, Yu F, Ko ML & Ko GY-P (2017). The Contribution of L-Type Cav1.3 Channels to Retinal Light Responses. *Front Mol Neurosci* **10,** 394.

Sillman AJ, Ito H & Tomita T (1969). Studies on the mass receptor potential of the isolated frog retina. I. General properties of the response. *Vision Res* **9,** 1435–1442.

Simon A, Barabas P & Kardos J (2006). Structural determinants of phosphodiesterase 6 response on binding catalytic site inhibitors. *Neurochem Int* **49,** 215–222.

Skiba NP, Hopp JA & Arshavsky VY (2000). The effector enzyme regulates the duration of G protein signaling in vertebrate photoreceptors by increasing the affinity between transducin and RGS protein. *J Biol Chem* **275,** 32716–32720.

Slaughter MM & Miller RF (1981). 2-amino-4-phosphonobutyric acid: a new pharmacological tool for retina research. *Science* **211,** 182–185.

Smith NP & Lamb TD (1997). The a-wave of the human electroretinogram recorded with a minimally invasive technique. *Vision Res* **37,** 2943–2952.

Soderling SH & Beavo JA (2000). Regulation of cAMP and cGMP signaling: new phosphodiesterases and new functions. *Curr Opin Cell Biol* **12,** 174–179.

Sothilingam V, Michalakis S, Garrido MG, Biel M, Tanimoto N & Seeliger MW (2016). HCN1 channels enhance rod system responsivity in the retina under conditions of light exposure. *PLoS One* **11,** e0147728.

Steinberg RH, Schmidt R & Brown KT (1970). Intracellular responses to light from cat pigment epithelium: Origin of the electroretinogram c-Wave. *Nature* **227,** 728–730.

Stockman A & Sharpe LT (2006). Into the twilight zone: the complexities of mesopic vision and luminous

efficiency. *Ophthalmic Physiol Opt* **26,** 225–239.

Stöhr H, Heisig JB, Benz PM, Schöberl S, Milenkovic VM, Strauss O, Aartsen WM, Wijnholds J, Weber BHF & Schulz HL (2009). TMEM16B, a novel protein with calcium-dependent chloride channel activity, associates with a presynaptic protein complex in photoreceptor terminals. *J Neurosci* **29,** 6809–6818.

Stryer L (1986). Cyclic GMP cascade of vision. *Annu Rev Neurosci* **9,** 87–119.

Tanimoto N, Sothilingam V, Euler T, Ruth P, Seeliger MW & Schubert T (2012). BK channels mediate pathway-specific modulation of visual signals in the in vivo mouse retina. *J Neurosci* **32,** 4861–4866.

Tate RJ, Lochhead A, Brzeski H, Arshavsky V & Pyne NJ (1998). The gamma-subunit of the rod photoreceptor cGMP-binding cGMP-specific PDE is expressed in mouse lung. *Cell Biochem Biophys* **29,** 133–144.

Thoreson WB (2007). Kinetics of synaptic transmission at ribbon synapses of rods and cones. *Mol Neurobiol* **36,** 205–223.

Thoreson WB & Bryson EJ (2004). Chloride equilibrium potential in salamander cones. *BMC Neurosci* **5,** 53.

Thoreson WB, Bryson EJ & Rabl K (2003). Reciprocal interactions between calcium and chloride in rod photoreceptors. *J Neurophysiol* **90,** 1747–1753.

Thoreson WB, Stella SLJ, Bryson EI, Clements J & Witkovsky P (2002). D2-like dopamine receptors promote interactions between calcium and chloride channels that diminish rod synaptic transfer in the salamander retina. *Vis Neurosci* **19,** 235–247.

Tian H, Sakmar TP & Huber T (2017). Measurement of Slow Spontaneous Release of 11-cis-Retinal from Rhodopsin. *Biophys J* **112,** 153–161.

Tsang SH, Woodruff ML, Chen C-K, Yamashita CY, Cilluffo MC, Rao AL, Farber DB & Fain GL (2006). GAP-Independent Termination of Photoreceptor Light Response by Excess Subunit of the cGMP-Phosphodiesterase. *J Neurosci* **26,** 4472–4480.

Tsang SH, Woodruff ML, Lin CS, Jacobson BD, Naumann MC, Hsu CW, Davis RJ, Cilluffo MC, Chen J & Fain GL (2012). Effect of the ILE86TER mutation in the γ subunit of cGMP phosphodiesterase (PDE6) on rod photoreceptor signaling. *Cell Signal* **24,** 181–188.

Uversky VN (2002). Natively unfolded proteins: a point where biology waits for physics. *Protein Sci* **11,** 739–756.

Uversky VN, Permyakov SE, Zagranichny VE, Rodionov IL, Fink AL, Cherskaya AM, Wasserman LA & Permyakov EA (2002). Effect of zinc and temperature on the conformation of the gamma subunit of retinal phosphodiesterase: a natively unfolded protein. *J Proteome Res* **1,** 149–159.

Vinberg F, Chen J & Kefalov VJ (2018*a*). Regulation of calcium homeostasis in the outer segments of rod and cone photoreceptors. *Prog Retin Eye Res*; DOI: 10.1016/j.preteyeres.2018.06.001.

Vinberg F & Kefalov VJ (2018). Investigating the Ca2+-dependent and Ca2+-independent mechanisms for mammalian cone light adaptation. *Sci Rep* **8,** 15864.

Vinberg F, Kolesnikov A V & Kefalov VJ (2014). Ex vivo ERG analysis of photoreceptors using an in vivo ERG system. *Vision Res* **101,** 108–117.

Vinberg F, Peshenko I V, Chen J, Dizhoor AM & Kefalov VJ (2018*b*). Guanylate cyclase-activating protein

2 contributes to phototransduction and light adaptation in mouse cone photoreceptors. *J Biol Chem* **293,** 7457–7465.

Vinberg F, Turunen TT, Heikkinen H, Pitkanen M & Koskelainen A (2015*a*). A novel Ca2+-feedback mechanism extends the operating range of mammalian rods to brighter light. *J Gen Physiol* **146,** 307–321.

Vinberg F, Wang T, De Maria A, Zhao H, Bassnett S, Chen J & Kefalov VJ (2017). The Na(+)/Ca(2+), K(+) exchanger NCKX4 is required for efficient cone-mediated vision. *Elife*; DOI: 10.7554/eLife.24550.

Vinberg F, Wang T, Molday RS, Chen J & Kefalov VJ (2015*b*). A new mouse model for stationary night blindness with mutant Slc24a1 explains the pathophysiology of the associated human disease. *Hum Mol Genet* **24,** 5915–5929.

Vinberg F, Strandman S & Koskelainen A (2009). Origin of the fast negative ERG component from isolated aspartate-treated mouse retina. *J Vis* **9,** 9.1-17.

Vishnivetskiy SA, Raman D, Wei J, Kennedy MJ, Hurley JB & Gurevich V V (2007). Regulation of arrestin binding by rhodopsin phosphorylation level. *J Biol Chem* **282,** 32075–32083.

Wachtmeister L (1998). Oscillatory potentials in the retina: what do they reveal. *Prog Retin Eye Res* **17,** 485–521.

Warren R & Molday RS (2002). Regulation of the rod photoreceptor cyclic nucleotide-gated channel. *Adv Exp Med Biol* **514,** 205–223.

Weitz D, Zoche M, Muller F, Beyermann M, Korschen HG, Kaupp UB & Koch K-W (1998). Calmodulin controls the rod photoreceptor CNG channel through an unconventional binding site in the N-terminus of the beta-subunit. *EMBO J* **17,** 2273–2284.

Wen X-H, Dizhoor AM & Makino CL (2014). Membrane guanylyl cyclase complexes shape the photoresponses of retinal rods and cones. *Front Mol Neurosci* **7,** 45.

Wensel TG & Stryer L (1986). Reciprocal control of retinal rod cyclic GMP phosphodiesterase by its gamma subunit and transducin. *Proteins* **1,** 90–99.

Wensel TG & Stryer L (1990). Activation mechanism of retinal rod cyclic GMP phosphodiesterase probed by fluorescein-labeled inhibitory subunit. *Biochemistry* **29,** 2155–2161.

Whalen MM, Bitensky MW & Takemoto DJ (1990). The effect of the gamma-subunit of the cyclic GMP phosphodiesterase of bovine and frog (Rana catesbiana) retinal rod outer segments on the kinetic parameters of the enzyme. *Biochem J* **265,** 655–658.

Whatham AR, Nguyen V, Zhu Y, Hennessy M & Kalloniatis M (2014). The value of clinical electrophysiology in the assessment of the eye and visual system in the era of advanced imaging. *Clin Exp Optom* **97,** 99–115.

Whitlock GG & Lamb TD (1999). Variability in the time course of single photon responses from toad rods: termination of rhodopsin's activity. *Neuron* **23,** 337–351.

Wilden U, Hall SW & Kuhn H (1986). Phosphodiesterase activation by photoexcited rhodopsin is quenched when rhodopsin is phosphorylated and binds the intrinsic 48-kDa protein of rod outer segments. *Proc Natl Acad Sci U S A* **83,** 1174–1178.

Wimberg H, Janssen-Bienhold U & Koch K-W (2018). Control of the Nucleotide Cycle in Photoreceptor Cell Extracts by Retinal Degeneration Protein 3. *Front Mol Neurosci* **11,** 52.

Woodruff ML, Janisch KM, Peshenko I V, Dizhoor AM, Tsang SH & Fain GL (2008). Modulation of

phosphodiesterase6 turnoff during background illumination in mouse rod photoreceptors. *J Neurosci* **28,** 2064–2074.

Woodruff ML, Rajala A, Fain GL & Rajala RVS (2014). Modulation of mouse rod photoreceptor responses by Grb14 protein. *J Biol Chem* **289,** 358–364.

Woodruff ML, Sampath AP, Matthews HR, Krasnoperova N V, Lem J & Fain GL (2002). Measurement of cytoplasmic calcium concentration in the rods of wild-type and transducin knock-out mice. *J Physiol* **542,** 843–854.

Xu J, Dodd RL, Makino CL, Simon MI, Baylor DA & Chen J (1997). Prolonged photoresponses in transgenic mouse rods lacking arrestin. *Nature* **389,** 505–509.

Xu Y, Dhingra A, Fina ME, Koike C, Furukawa T & Vardi N (2012). mGluR6 deletion renders the TRPM1 channel in retina inactive. *J Neurophysiol* **107,** 948–957.

Yamazaki A, Hayashi F, Tatsumi M, Bitensky MW & George JS (1990). Interactions between the subunits of transducin and cyclic GMP phosphodiesterase in Rana catesbiana rod photoreceptors. *J Biol Chem* **265,** 11539–11548.

Yamazaki M, Li N, Bondarenko VA, Yamazaki RK, Baehr W & Yamazaki A (2002). Binding of cGMP to GAF domains in amphibian rod photoreceptor cGMP phosphodiesterase (PDE). Identification of GAF domains in PDE alphabeta subunits and distinct domains in the PDE gamma subunit involved in stimulation of cGMP binding to GAF domains. *J Biol Chem* **277,** 40675–40686.

Yang RB, Robinson SW, Xiong WH, Yau K-W, Birch DG & Garbers DL (1999). Disruption of a retinal guanylyl cyclase gene leads to cone-specific dystrophy and paradoxical rod behavior. *J Neurosci* **19,** 5889–5897.

Yau K-W & Hardie RC (2009). Phototransduction motifs and variations. *Cell* **139,** 246–264.

Yau K-W & Baylor DA (1989). Cyclic GMP-activated conductance of retinal photoreceptor cells. *Annu Rev Neurosci* **12,** 289–327.

Yau K-W & Nakatani K (1985). Light-suppressible, cyclic GMP-sensitive conductance in the plasma membrane of a truncated rod outer segment. *Nature* **317,** 252–255.

Yue WWS, Silverman D, Ren X, Frederiksen R, Sakai K, Yamashita T, Shichida Y, Cornwall MC, Chen J & Yau K-W (2019). Elementary response triggered by transducin in retinal rods. *Proc Natl Acad Sci U S A* **116,** 5144–5153.

Zang J & Neuhauss SCF (2018). The Binding Properties and Physiological Functions of Recoverin. *Front Mol Neurosci* **11,** 473.

Zhang J, Kuvelkar R, Wu P, Egan RW, Billah MM & Wang P (2004*a*). Differential inhibitor sensitivity between human recombinant and native photoreceptor cGMP-phosphodiesterases (PDE6s). *Biochem Pharmacol* **68,** 867–873.

Zhang KYJ, Card GL, Suzuki Y, Artis DR, Fong D, Gillette S, Hsieh D, Neiman J, West BL, Zhang C, Milburn M V, Kim S-H, Schlessinger J & Bollag G (2004*b*). A glutamine switch mechanism for nucleotide selectivity by phosphodiesterases. *Mol Cell* **15,** 279–286.

Zhang XJ, Cahill KB, Elfenbein A, Arshavsky VY & Cote RH (2008). Direct allosteric regulation between the GAF domain and catalytic domain of photoreceptor phosphodiesterase PDE6. *J Biol Chem* **283,** 29699–29705.

Zhang XJ & Cote RH (2005). cGMP signaling in vertebrate retinal photoreceptor cells. *Front Biosci* **10,**

1191–1204.

Zhang XJ, Feng Q & Cote RH (2005). Efficacy and selectivity of phosphodiesterase-targeted drugs in inhibiting photoreceptor phosphodiesterase (PDE6) in retinal photoreceptors. *Investig Ophthalmol Vis Sci* **46,** 3060–3066.

Zhang XJ, Gao XZ, Yao W & Cote RH (2012). Functional mapping of interacting regions of the photoreceptor phosphodiesterase (PDE6) γ-subunit with PDE6 catalytic dimer, transducin, and regulator of G-protein signaling9-1 (RGS9-1). *J Biol Chem* **287,** 26312–26320.

Zhang Z, He F, Constantine R, Baker ML, Baehr W, Schmid MF, Wensel TG & Agosto MA (2015). Domain organization and conformational plasticity of the G protein effector, PDE6. *J Biol Chem* **290,** 12833–12843.

Aalto-DD 58/2020

ISBN 978-952-60-3832-2 (printed)
ISBN 978-952-60-3833-9 (pdf)
ISSN 1799-4934 (printed)
ISSN 1799-4942 (pdf)

Aalto University
School of Science
Department of Neuroscience and Biomedical Engineering
www.aalto.fi

BUSINESS +
ECONOMY

ART +
DESIGN +
ARCHITECTURE

SCIENCE +
TECHNOLOGY

CROSSOVER

**DOCTORAL
DISSERTATIONS**